ADVANCED STATE ESTIMATION FOR ELECTRIC VEHICLE BATTERIES

ADVANCED STATE ESTIMATION FOR ELECTRIC VEHICLE BATTERIES

BY

SARA SADAT RAHIMIFARD, M.Sc., B.Sc.

A THESIS

SUBMITTED TO THE DEPARTMENT OF MECHANICAL ENGINEERING

AND THE SCHOOL OF GRADUATE STUDIES

OF MCMASTER UNIVERSITY

IN PARTIAL FULFILMENT OF THE REQUIREMENTS

FOR THE DEGREE OF

DOCTOR OF PHILOSOPHY

Doctor of Philosophy (2022) McMaster University

(Department of Mechanical Engineering) Hamilton, Ontario, Canada

TITLE:	Advanced State Estimation for Electric Vehicle Batteries
AUTHOR:	Sara Sadat Rahimifard M.Sc./B.Sc. (Electrical and Computer Engineering), Amirkabir University of Technology, Tehran, Iran/ Shiraz University, Shiraz, Iran
SUPERVISOR:	Dr. Saeid Habibi, and Dr. Gillian Goward
NUMBER OF PAGES:	xxv, 208

Lay Abstract

To address the critical issue of climate change, it is necessary to replace fossil-fuel vehicles with battery-powered electric vehicles. Despite the benefits of electric vehicles, their popularity is still limited by the range anxiety and the cost determined by the battery pack. The range of an electric vehicle is determined by the amount of charge in its battery pack. This is comparable to the amount of gasoline in a gasoline vehicle's tank. In consideration of the need for methods to address range anxiety, it is necessary to develop advanced algorithms for continuous monitoring and control of a battery pack to maximize its performance. However, the amount of charge and health of a battery pack cannot be measured directly and must be inferred from measurable variables including current, voltage and temperature. This research presents several algorithms for detecting the range and health of a battery pack under a variety of operating conditions. With a more accurate algorithm, a battery pack can be monitored closely, resulting in lower long-term costs.

Adaptive methods for determining a battery's state of charge and health in uncertain and noisy conditions have been developed to provide an accurate measure of available charge and capacity. Methods are then extended to improve the determination of state of charge and health for a battery module.

Abstract

Lithium-ion (Li-ion) batteries are amongst the most commonly used types in Electric (EVs) and Hybrid Electric (HEVs) Vehicles due to their high energy and power densities, as well as long lifetime. A battery is one of the most important components of an EV and hence it needs to be monitored and controlled accurately. The safety, and reliability of battery packs must then, be ensured by accurate management, control, and monitoring functions by using a Battery Management System (BMS).

A BMS is also responsible for accurate real-time estimation of the State of Charge (SoC), State of Health (SoH) and State of Power (SoP) of the battery. The battery SoC provides information on the amount of energy left in the battery. The SoH determines the remaining capacity and health of a pack, and the SoP represents the maximum available power. These critical battery states cannot be directly measured. Therefore, they have to be inferred from measurable parameters such as the current delivered by the battery as well as its terminal voltage. Consequently, in order to offer accurate monitoring of SoC, SoH and SoP, advanced numerical estimation methods need to be deployed.

In the estimation process, the states and parameters of a system are extracted from measurements. The objective is to reduce the estimation errors in the presence of uncertainties and noise under different operating conditions. This thesis uses and

provides different enhancements to a robust estimation strategy referred to as the Smooth Variable Structure Filter (SVSF) for condition monitoring of batteries. The SVSF is a predictor-corrector method based on sliding mode control that enhances the robustness in the presence of noise and uncertainties. The methods are proposed to provide accurate estimates of the battery states of operation and can be implemented in real-time in BMS.

To improve the performance of battery condition monitoring, a measurement-based SoC estimation method called coulomb counting is paired with model-based state estimation strategy. Important considerations in parameter and state estimation are model formulation and observability. In this research a new model formulation that treats coulomb counting as an added measurement is proposed. It is shown that this formulation enhanced information extraction, leading to a more accurate state estimation, as well as an increase in the number of parameters and variables that can be estimated while maintaining observability. This model formulation is used for characterizing the battery in a range of operating conditions. In turn, the models are integral to a proposed adaptive filter that is a combination of the Interacting Multiple Model (IMM) concept and the SVSF. It is shown that this combined strategy is an efficient estimation approach that can effectively deal with battery aging. The proposed method provides accurate estimation for various SoH of a battery.

Further to battery aging adaptation, measurement errors such as sensor noise, drift, and bias that affect estimation performance, are considered. To improve the accuracy of battery state estimation, a noise covariance adaptation scheme is developed for the SVSF method. This strategy further improves the robustness of the SVSF in the presence of unknown physical disturbances, noise, and initial conditions.

The proposed estimation strategies are also considered for their implementation on battery packs. An important consideration in pack level battery management is cell-to-cell variations that impact battery safety. This study considers online battery parametrization to update the pack's model over time and to detect cell-to-cell variability in parallel-connected battery cells configurations. Experimental data are used to validate and test the efficacy of the proposed methods in this thesis.

Keywords: Lithium-ion Batteries, Battery Pack, State of Charge, State of Health, State of Power, Parameter Identification, Smooth Variable Structure Filter, Adaptive Filtering.

Acknowledgements

I would like to thank Dr. Saeid Habibi, my Ph.D. supervisor, for his unwavering support and advice during my studies. Without his expertise and knowledge, this thesis would not have progressed as far as it has. Dr. Gillian Goward, my co-supervisor, deserves my gratitude for her constructive feedback. Dr. Jennifer Bauman and Dr. Fengjun Yan, members of my Ph.D. committee, are also to be thanked for their input and suggestions, which helped to strengthen my research.

My thanks also goes to the School of Graduate Studies, the Department of Mechanical Engineering and the Ontario Graduate and Natural Sciences and Engineering Research Council of Canada (NSERC) for their financial support.

I convey my special gratitude to my supervisor at Ford Powertrain Engineering Research and Development Center (PERDC), Dr. Jimi Tjong, and my supervisor at National Research Council of Canada (NRC), Dr. Dean MacNeil, for their technical competence and assistance throughout my internships.

I would like to thank Mr. Cam Fisher for his enduring support and technical insight, as well as all of my colleagues at the Centre for Mechatronics and Hybrid Technologies (CMHT), with special thanks to, Dr. Ryan Ahmed, for his constructive feedback and technical support, and Dr. Marvin Messing, from whom I learned a lot during our theoretical and experimental discussions.

I am truly thankful for the support and encouragements of my family and friends throughout my entire education with special thanks to Keyvan, my best friend and love, who has always been there for me through thick and thin. Without his unending love, support, and motivation, this would not have been possible.

Co-Authorship

This thesis has been prepared in accordance with the regulations for a sandwich thesis format or as a compilation of research papers stipulated by the faculty of graduate studies at McMaster University. This thesis consists of the following papers:

Paper I

Sara Rahimifard, Saeid Habibi, Jimi Tjong. **"Dual Estimation Strategy for New and Aged Electric Vehicles Batteries"**, Published in *2020 IEEE Transportation Electrification Conference & Expo (ITEC), 2020, Pages. 579-583, doi: 10.1109/ITEC48692.2020.9161556.*

Sara Rahimifard conducted literature reviews, conducted experiments, performed simulations, analyzed results. Paper I was written by Sara Rahimifard.

Dr. Habibi and Dr. Tjong provided research advice and revised the paper.

Paper II

Sara Rahimifard, Ryan Ahmed and Saeid Habibi, **"Interacting Multiple Model Strategy for Electric Vehicle Batteries State of Charge/Health/ Power Estimation"**, Published in *IEEE Access, Volume. 9, Pages. 109875-109888, 2021, doi: 10.1109/ACCESS.2021.3102607.*

Sara Rahimifard conducted literature reviews, conducted experiment, performed simulations, analyzed results. Paper II was written by Sara Rahimifard.

Dr. Ahmed provided data and technical guidance.

Dr. Habibi provided research advice and revised the paper.

Paper III

Sara Rahimifard, Saeid Habibi, Gillian Goward, and Jimi Tjong, **"Adaptive Smooth Variable Structure Filter Strategy for State Estimation of Electric Vehicle Batteries"**, Published in *Energies 2021, 14, no. 24: 8560. doi: 10.3390/en14248560.*

Sara Rahimifard conducted literature reviews, designed experiments, conducted experiments, performed simulations, analyzed results. Paper III was written by Sara Rahimifard.

Dr. Habibi, Dr. Goward and Dr. Tjong provided research advice and revised the paper.

Paper IV

Sara Rahimifard, Marvin Messing, Saeid Habibi, Gillian Goward, and Jimi Tjong, **"Robust Estimation Strategy for Parallel-Connected Battery Cells."**

Sara Rahimifard conducted literature reviews, designed experiments, conducted experiments, performed simulations, analyzed results. Paper IV was written by Sara Rahimifard.

Marvin Messing provided technical guidance and assistance on reviewing the paper.

Dr. Habibi, Dr. Goward, and Dr. Tjong provided research advice and revised the paper.

Permission to Use

In presenting this thesis in partial fulfillment of the requirements for a Postgraduate degree from McMaster University, I agree that the Libraries of this University may make it freely available for inspection. I further agree that the permission for copying this thesis in any manner, in whole or in part for scholarly purposes, may be granted by the professors who supervised my thesis work or, in their absence, by the Head of the Department or the Faculty Dean in which my thesis work was conducted. It is understood that any copying or publication or use of this thesis or parts thereof for financial gain shall not be allowed without my written permission. It is also understood that due recognition shall be given to me and McMaster University in any scholarly use which may be made of any material in my thesis. Requests for permission to copy or to make other use of material in this thesis, in whole or part, should be addressed to:

Head of the Department of Mechanical Engineering

McMaster University

Faculty of Engineering

1280 Main Street West

Hamilton, Ontario $L8S\ 4L6$

Canada

Contents

List of Figures

List of Tables

Abbreviations

EV	Electric Vehicle
HEV	Hybrid Electric Vehicle
GHG	Greenhouse Gas
BMS	Battery Management System
Li-ion	Lithium-ion
EIS	Electrochemical Impedance Spectroscopy
SEI	Solid Electrolyte Interphase
CE	Coulombic Efficiency
SoC	State of Charge
SoH	State of Health
SoP	State of Power
RUL	Remaining Useful Life
SoF	State of Function

DoD	Depth of Discharge
OCV	Open Circuit Voltage
CC	Constant Current
CV	Constant Voltage
CCCV	Constant Current Constant Voltage
RPT	Reference Performance Test
HPPC	Hybrid Pulse Power Characterization
EPA	US Environmental Protection Agency
UDDS	Urban Dynamometer Driving Schedule
HWFET	Highway Fuel Economy Test
US06	Supplemental Federal Test Procedure (high acceleration aggressive driving schedule)
ECM	Equivalent Circuit Model
GA	Genetic Algorithm
LS	Least Square
RLS	Recursive Least Square
KF	Kalman Filter
EKF	Extended Kalman Filter

AKF	Adaptive Kalman Filter
VSC	Variable Structure Control
SMC	Sliding Mode Control
SMO	Sliding Mode Observer
SBL	Smoothing Boundary Layer
VBL	Variable Boundary Layer
VSF	Variable Structure Filter
EVSF	Extended Variable Structure Filter
SVSF	Smooth Variable Structure Filter
ASVSF	Adaptive Smooth Variable Structure Filter
MM	Multiple Model
GPB	Generalized Pseudo-Bayesian
IMM	Interacting Multiple Model
RMSE	Root Mean Square Error

Chapter 1: Introduction

Global warming poses a threat to humanity, and no one is immune to its consequences. Environmental degradation, natural disasters, extreme weather conditions, food and water shortages, and economic disruption are all symptoms of climate change. Environmental changes adversely affect competition for resources such as land, food, and water, increasing the likelihood of conflicts and forced migrations. As a result, the continuation of Greenhouse Gas (GHG) emissions with our current lifestyles is not sustainable. Given the irreversible costs of climate change, it is imperative to take concerted effort to fight it.

Massive amounts of carbon dioxide are released into the atmosphere every year as a result of coal, oil, and gas production and consumption. The transportation sector is a major source of air pollution. In urban areas, the air pollution caused by vehicles is increasing due to an increased population density. Driving less, combining trips to make them more efficient, or taking public transport are ways that could help reduce the GHG emissions. However, this by no means, is enough. Although, climate change has been impacted by advances in technology such as the discovery of fossil fuels, new and efficient technologies can also contribute to the reduction of GHG emissions and creation of a cleaner economy.

Switching to clean, regenerative energy is a necessary first step towards ending our reliance on fossil fuels. The goal of combating climate change is to minimize GHG emissions, and Electric Vehicles (EVs) play a vital part in achieving this global goal. Consumers are becoming more interested in EVs even though public transport has been piloting them for a while. Automobile manufacturers intend to introduce more

EVs in the future as EVs become more popular.

Batteries are the main form of energy storage system in EVs. A battery pack in an EV contains hundreds of battery cells that are connected in parallel and series to generate the power that the vehicle requires. These batteries must be monitored and controlled continuously to ensure safety and reliability. A battery pack is controlled by a Battery Management System (BMS). In general, a BMS ensures that the battery cells are in a safe operating region and prevents them from being overly-charged or discharged. As a result, the BMS' role is to protect the battery from conditions that may damage or shorten its lifespan. The BMS also performs cell balancing and temperature regulation. In order to monitor the battery pack more accurately, a BMS must be able to estimate the battery pack's critical parameters, such as its State of Charge (SoC), State of Health (SoH), and State of Power (SoP). Monitoring and controlling these parameters impact the battery's longevity, safety and operational range.

By combining a robust and adaptive estimation strategy with an accurate, reliable battery model, the BMS will be able to estimate the battery's SoC, SoH, and SoP, at various levels of state of life, power demand, and temperature. It is also vital to establish an algorithm that can function in a range of circumstances. This thesis considers the use of state estimation for monitoring of EV batteries under a range of operating conditions. It specifically contributes to improved state estimation of battery cells and packs by introducing different adaptive strategies. In this chapter, the background material is covered in Sections 1.1 through 1.7, including introductions to battery management system, Lithium-ion batteries, battery testing, battery modeling, estimation theory, and system observability. Section 1.8 describes a technical

introduction to this thesis, the research hypotheses and contributions. Section 1.9 provides the outline of this thesis.

1.1 Battery Management System

In recent years, as concern about climate change has grown, extensive research and development on Electric Vehicles (EVs) has been conducted. One of the main component of an EV, is the battery pack, that is critical to the EV's performance, and initial and operating costs. To meet the power and energy requirements of EVs, a battery pack typically has hundreds of battery cells connected in series and parallel. An effective Battery Management System (BMS) is responsible for ensuring a safe and reliable operation by continuously monitoring and controlling the battery pack. Although a BMS can be used on any portable electronic device, as the number of cells increases, it becomes more complicated. In batteries, temperatures that are too high or too low, as well as over-charging and over-discharging, may accelerate the rate of degradation and cause safety issues. Cell protection, thermal management, cell balancing, modeling, state and parameter estimation, and fault detection are all functions of a BMS, as presented in Figure 1.1 [1].

With an accurate BMS, safety concerns can be addressed, performance maximized, and longevity increased. To achieve high battery pack performance, the state of a battery pack including State of Charge (SoC), State of Health (SoH), State of Power (SoP), State of Function (SoF), and Remaining Useful Life (RUL) must be constantly monitored. Temperature can affect the capacity and power of a battery pack. Temperatures above a certain threshold can result in accelerated degradation or thermal runaways, both of which can be very dangerous to users. Therefore,

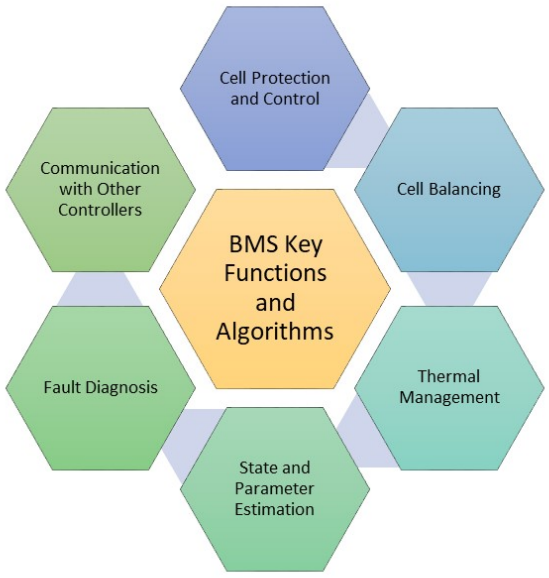

Figure 1.1: Battery management system key functionalities.

temperature should be considered and emphasized in modeling and state estimation. The BMS is also responsible for detecting cell-to-cell variations, as they may differ in their states while operating. Cell balancing is provided by a BMS to equalize the charge in cells. A BMS should provide safety features for all types of batteries [1, 2]. A BMS is made up of numerous circuits, components, power electronics, sensors, and safety devices that are all controlled by sophisticated algorithms. It is necessary to create efficient algorithms in a BMS [3].

1.2 Lithium-ion Batteries

The utilization of Lithium-ion (Li-ion) batteries has been increasing steadily in different applications due to their energy and power densities, and longevity. Li-ion

batteries solve a variety of design challenges in EVs due to their high energy and power densities in comparison to other types of batteries. Despite their numerous advantages, the cost of the Li-ion battery technology remains high when compared to other internal combustion engines [4, 5].

Li-ion batteries employ oxidation-reduction reactions to convert chemical and electrical energies in a reversible manner. All batteries have four major components including a positive (cathode) and a negative (anode) electrode, an electrolyte, and a separator as shown in Figure 1.2. The positive and negative electrodes are separated by the electrolyte and separator. As ions move from the cathode to the anode, the electrolyte acts as a catalyst, charging and vice versa discharging the battery. A layered structure in the electrode allows lithium atoms to move between layers. However, this movement inside a battery has no effect on the battery's degradation. In a Li-ion battery cell, graphite is the dominant material for the anode and a form of lithium transition metal oxide is used for the cathode. Electrons move from the cathode to the anode when a battery cell is charged. When the battery is charged, the lithium containing graphite and the lithium transition metal oxide with missing lithium become extremely reactive. As a result, they react with the electrolyte solution by which they come into contact. Fortunately, these reactions are stable, and a passivating film forms to prevent further electrolyte decomposition. This passivating surface allows the battery to function for a long time [6, 7].

Despite the presence of passivating film formation, parasitic reactions continue to occur slowly during normal operation and storage, leading to battery degradation. The formed passivation layer on electrode surface is called the Solid Electrolyte Interphase (SEI). Figure 1.3 represents the formation of SEI in the negative electrolyte

surface over time which leads to battery degradation [8].

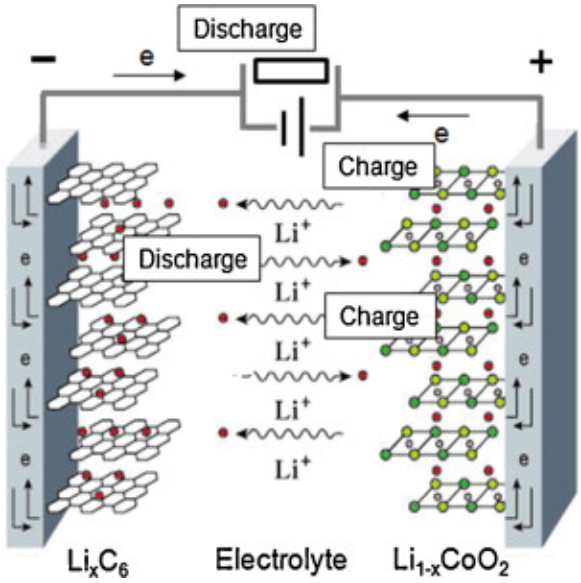

Figure 1.2: Illustration of lithium-ion battery cell [9].

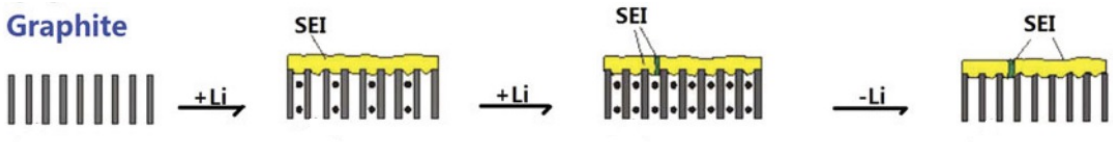

Figure 1.3: SEI formation [10].

1.2.1 Aging Factors

Battery degradation and capacity loss are caused by various reactions inside the Li-ion battery, such as SEI formation. Although a battery's internal reactions cannot be controlled while it is in use, the external factors can be monitored and controlled to extend its lifetime. These factors include operating temperature, charge or discharge rate (C-rate), operating voltage range, and Depth of Discharge (DoD) [11]. This section explains these factors and their impact on the aging process.

Charge/discharge C-rate

The C-rate is the rate at which a battery is charged or discharged in relation to its capacity. A battery's capacity is commonly expressed as 1C, which means that a battery takes one hour to fully charge. When a battery operates at a high C-rate, different reactions happen inside the battery such as uneven lithium deposition, irreversible loss of Li-ions, and increase of SEI formation resulting in capacity loss. When a Li-ion battery is operated at a high C-rate, it reaches its critical point or the end of life in a faster rate than when it is functioned at a low C-rate. Although accelerated aging is used in research facilities to reach the battery's end of life faster, it should be restricted in real-time applications to enhance the performance of the battery [11].

Depth of Discharge

The battery's Depth of Discharge (DoD) indicates how much of the battery has been discharged compared to its overall capacity. The DoD is the complement of the battery's SoC which means as one increases, the other decreases. This factor has a major impact on the battery's lifetime, however, this varies a lot depending on the cathode materials [11]. When DoD is limited to 20%–80%, batteries degrade at a slower rate than when DoD is set to 0%–100%. To slow the rate of battery degradation caused by DoD, battery manufacturers suggest an optimal value to improve the battery's performance. In order to extend the battery pack's longevity, car manufacturers limit the battery's usable range based on the battery's optimal DoD [12].

Operating Temperature

Temperature has the most significant impact on battery aging. The standard operating temperature for a battery is at room temperature ($25°C$), however, this is not always the case in realistic conditions. The operating range of temperature for EVs and HEVs can change between $-30°C$ to $+50°C$. The effect of low and high temperature is different as it relates to battery aging. The capacity degradation caused by cathode degradation increases at high temperatures. Lithium plating, on the other hand, at low temperatures has a negative impact on battery safety. Therefore, it is critical to provide an accurate thermal management system for the battery pack in order to keep it within an acceptable range of temperature and prevent accelerated aging [11, 12].

Operating Voltage Range

A battery should be used within its optimal voltage range. Over-charging or discharging a battery may cause a significant increase in temperature and pressure inside the battery, which can lead to fire, cell damage and short circuits. As a consequence, the battery life is reduced. The range of operation in a battery should be limited by a BMS to avoid battery aging caused by over-charging or discharging [12].

1.3 Battery Testing

Laboratory tests are needed in order to assess the performance of battery cells, modules, and packs under different operating conditions [13]. The data collected from

these tests can be used to validate battery models, which are required for state estimation. Standard tests are performed to provide a common foundation for battery manufacturers [13, 14, 15]. Battery test procedures are categorized in different groups including: characterization, aging, and reference performance tests, [15].

1.3.1 Characterization Tests

Characterization tests provides information about the performance of a battery cell such as its internal resistance, capacity, and time constants. Static capacity, pulse charge/discharge, Open Circuit Voltage (OCV) characterization, self-discharge, cold cranking, thermal performance, and efficiency tests are categorized in this group [15, 16]. Some of these tests that have been considered in this study are as follows,

1. **Static capacity test** determines the capacity of a battery cell. A standard capacity test can be defined as follows,
   (a) The battery is charged in a Constant Current Constant Voltage (CCCV) mode at a standard C-rate (usually 1C, provided in the datasheet). The battery is fully charged when it reaches the maximum voltage and the end point current (usually about $0.02C$, provided in the datasheet).
   (b) The battery is left to rest for one hour to reach its steady state condition.
   (c) The battery is discharged in a standard Constant Current (CC) mode using a standard C-rate (usually 1C) until it reaches the minimum voltage.
   (d) The battery is left to rest for one hour to reach its steady state condition.
2. **OCV characterization test** is performed to identify the nonlinear relationship between the OCV and the battery SoC. A standard OCV characterization test

can be defined as follows,

(a) The battery is discharged in a CC mode with a standard C-rate (usually 1C) to its minimum voltage.

(b) The current accumulator is reset to zero to provide zero SoC.

(c) The battery is charged in a CCCV mode using a very small C-rate (usually $C/15$ or $C/20$) until the battery is fully charged.

(d) The battery is left to rest for one hour.

(e) The battery is discharged in a CC mode using the same C-rate (usually $C/15$ or $C/20$) until the battery hits the minimum voltage.

(f) The battery is left to rest for one hour.

The relationship between the OCV and SoC can be achieved using an average of the charge and discharge curve. The obtained OCV-SoC curve could change for a battery at different temperatures and states of life.

3. **Pulse charge/discharge tests** are used to characterize the parameters of an equivalent circuit model for a range of SoCs. The pulse discharge test can be defined as follows,

(a) The battery is charged in a CCCV mode using a standard C-rate (usually 1C) until it is fully charge.

(b) The battery is left to rest for one hour.

(c) For the SoC in the range of 100% to 90%, the battery is discharged at 1C with pulses of 1% capacity of the battery.

(d) For the SoC in the range of 90% to 10%, the battery is discharged at 1C with pulses of 5% capacity of the battery.

(e) For the SoC in the range of 10% to 0%, the battery is discharged at 1C with pulses of 1% capacity of the battery.

(f) The battery is left to rest for 2 hours between pulses for the whole range of SoC.

Similar steps should be followed for pulse charge test [16].

1.3.2 Aging Test

Aging tests demonstrate the effect of aging on a battery. There are two ways in which a battery can age; the first being that a battery ages after multiple charges and discharges, known as cycle life, the second being that it is possible to cause by storing a battery, known as calendar aging. The study of battery characteristics necessitates the consideration of various types of aging [15, 17]. A battery's performance can be quickly evaluated with accelerated aging. The aging study considered in this study is based on the cycle life which can be divided into two groups as follows,

1. **Standard charge/discharge cycling**

   This method performs continuous charging and discharging usually at a high C-rate and an elevated temperature. This method is relatively fast; however, it cannot provide the realistic conditions that exists in EVs. The following steps are considered for this test,

   (a) The battery is charged in CCCV mode until the battery is fully charged.

(b) The battery is discharged in CC mode with its maximum discharge C-rate (provided in the datasheet) until it reaches the minimum voltage of the battery.

(c) The battery is left to rest for 5 minutes.

(d) The battery is charged in CCCV mode with its maximum charge C-rate (provided in the datasheet) until the battery is fully charged.

(e) Steps b to d are repeated until capacity hits the expected value (usually 80%).

Characterization tests are considered at about every 50 cycles to investigate the behavior of the battery at different states of life.

2. **Drive cycle aging**

Standardized drive cycles can be used to simulate battery aging more realistically. The US Environmental Protection Agency (EPA) provides standard drive cycles for different driving scenarios [18]. The drive cycles considered in this study include an Urban Dynamometer Driving Schedule (UDDS), a light duty drive cycle for high speed and high load (US06), and a Highway Fuel Economy Test (HWFET). The UDDS cycle can depict the driving habits of a typical city driver. The US06 simulates aggressive driving habits, while the HWFET simulates highway driving conditions. The speed vs. time data, provided by EPA, should be converted to the current demand of a battery pack. A simulated EV model can be used to determine the current consumed by a battery pack. This can be scaled down based on the number of batteries connected in parallel and series in a battery pack to determine the amount of current for a cell or a

module [16].

1.3.3 Reference Performance Test

Reference performance tests (RPTs) are usually performed after a certain number of cycle life tests to measure the capacity and investigate battery degradation. These tests include static capacity tests at different C-rates, OCV characterizations, pulse charge/discharge and driving cycles for a whole range of SoC [13]. These tests are useful to provide ECM model for different SoHs as explained in Chapter 3.

1.4 Key States of a Battery

The most important operating variables and states of a battery are introduced in this section. The estimation of these states is critical in order to perform better management of the battery pack.

1.4.1 State of Charge

State of Charge (SoC) is an important consideration for a battery that should be estimated accurately in a BMS. As the name implies, SoC indicates the amount of charge remaining in the battery pack, which can be influenced by a variety of factors such as charge/discharge rate, temperature, and battery age. It is necessary to employ a robust and adaptive strategy for its estimation in order to develop an effective solution for energy management of EVs. Since there is no sensor that can directly measure the battery's SoC, it must be estimated by using measurements such as terminal voltage, temperature, and current. There are various strategies for

estimating the SoC of a battery. These methods are classified into two types including measurement-based methods and indirect methods [12, 19].

Measurement-based methods use direct measurements from a battery including terminal voltage, impedance, and current for its SoC estimation. These methods are commonly based on open circuit voltage, terminal voltage, internal resistance and conventional coulomb counting. Coulomb counting is the most common technique for SoC estimation and it is popular in the automotive industry as a baseline for SoC estimation. The coulomb counting method calculates the SoC by integrating the current consumed by the battery and is defined as follows,

$$SOC(t) = SOC_0 - \frac{1}{C_n} \int_0^t \eta i(\tau) d\tau \tag{1.1}$$

where SOC_0 is the initial value of the battery SoC, η is the cell Coulombic Efficiency (CE) and C_n is the nominal capacity. This method is impacted by sensor noise, uncertainty in the initial value of SoC, and the battery's SoH over time. The strategy can be adjusted to achieve a balance of simplicity and accuracy. The SoC of a battery can also simply be calculated by considering the relationship between the OCV and the battery SoC as shown in Figure 1.4. However, the method cannot provide an accurate estimation as it only applies to a battery that is in a state of rest as well as being affected by the SoH, and temperature. The long rest time required for relaxation of the battery before using the OCV for SoC estimation make this method impractical to be used onboard of a BMS [12].

Although indirect methods are more complex, they are more reliable for real-time use. The indirect methods can be divided into two categories: model-driven and

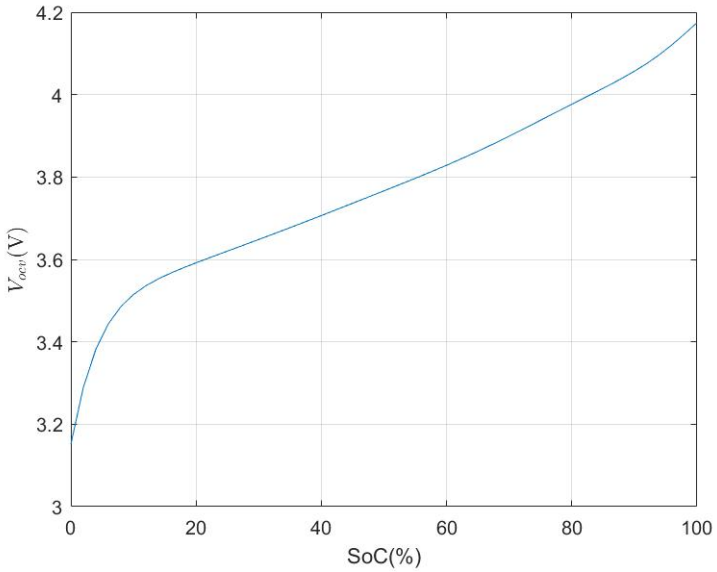

Figure 1.4: Example of OCV-SOC curve for a Li-ion battery.

data-driven. The data-driven methods use advanced machine learning techniques to predict the battery SoC from the provided data. However, a large volume of data is required for initial training. Further, their accuracy depends on diversity, quality and amount of data that is available [20, 21]. In cases where the internal dynamics of the system are easily characterized, such as in batteries, it is more practical to use a model-based strategy. More details on different model-based approaches are provided throughout this research. This thesis looks for advanced model-based estimation strategies to be used on a battery under different operating conditions.

1.4.2 State of Health

During the life cycle of a battery, its dynamic behavior changes. State of Health (SoH) of a battery provides a gauge for its life span. It is important to provide an indicator for estimating this key element, as it can affect the accuracy of SoC estimation. The

battery SoH can be obtained through estimating the change in different parameters of the battery including its internal resistance, capacity, impedance, cycle count, or self-discharge. A combination of these different factors should be considered to provide an accurate estimate of the SoH. Similarly to the battery SoC, SoH can be obtained by using different algorithms categorized into two groups: measurement-based and indirect methods. Measurement-based algorithms include but are not limited to Electrochemical Impedance Spectroscopy (EIS), current pulses, discharge test to obtain the impedance, internal resistance, and the capacity of the battery, respectively. The SoH can also be found by comparing the battery's cycling history to previous data. Although, these methods require low computational efforts and could be easy to implement, their accuracy is not enough [12, 22].

By determining the internal resistance (R_{in}) and the available capacity (C) of the battery cells, the SoH of a battery can be investigated. These two variables reflect the energy and power potential of a battery, respectively. The SoH, based on the internal resistance and the available capacity, can be determined as follows,

$$SOH_C = \frac{C}{C_n} \times 100\% \tag{1.2}$$

$$SOH_R = \frac{R_{EOL} - R_{in}}{R_{EOL} - R_{new}} \times 100\% \tag{1.3}$$

where C_n is the nominal capacity of the battery, R_{EOL} is the internal resistance at the end of battery life, R_{new} is the internal resistance of a new battery.

Adaptive filters are developed to estimate SoH using parameter estimation techniques [22]. The accuracy of SoH estimation can be affected by the robustness and

adaptability of the estimation algorithm or filter and the SoC. The research presented here provides advanced strategies for state and parameter estimation that are applicable to different modes of operation.

1.4.3 State of Power

The State of Power (SoP) indicates the power capability of a battery. It is essential that a battery's SoP be accurately estimated in order to operate in a safe region. This along with the current limitation could protect a battery pack from over-charging and over-discharging. In a similar manner to the SoC and SoH of a battery, this key element cannot be measured directly. Hybrid Pulse Power characterization method (HPPC) is commonly used to calculate the peak charge/discharge power based on the provided range of the battery's terminal voltage and current. Despite the simplicity of this method, however, it is not suitable for real-time applications. Different methodologies have been presented within the literature for calculating SoP by considering the terminal voltage, SoC, current limitation, and internal resistance of a battery. The SoP can be calculated by taking into account the available current at a given voltage, as well as the limiting factors for current supply that are typically determined by the BMS [23, 24, 25]. The accuracy of estimation for the states and parameters is imperative for SoP estimation using this method. The estimation accuracy could affect the performance of the battery pack and can be mitigated by providing improved state estimation for the battery's parameters. The maximum available charge/discharge power of a battery, by us ing this method, can be determined as,

$$P_{max}^{cha} = I_{max}^{cha}(V_{ocv} + I_{max}^{cha}R_{in}) \tag{1.4}$$

$$P_{max}^{dch} = I_{max}^{dch}(V_{ocv} - I_{max}^{dch}R_{in}) \tag{1.5}$$

where $I_{max,cur}^{cha}$ and $I_{max,cur}^{dch}$ are the charge and discharge current thresholds, respectively, which can be calculated as follows,

$$I_{max}^{cha} = min(I_{max,vol}^{cha}, I_{max,cur}^{cha}) \tag{1.6}$$

$$I_{max}^{dch} = min(I_{max,vol}^{dch}, I_{max,cur}^{dch}) \tag{1.7}$$

where $I_{max,vol}^{cha}$ and $I_{max,vol}^{dch}$ are the maximum available charge and discharge current under the terminal voltage limits and can be calculated as follows,

$$I_{max,vol}^{cha} = \frac{V_{max} - V_{ocv}}{R_{in}} \tag{1.8}$$

$$I_{max,vol}^{dch} = \frac{V_{ocv} - V_{min}}{R_{in}} \tag{1.9}$$

The V_{max} and V_{min} denote the voltage limits, and V_{ocv} is obtained by the SoC estimation results using a look-up table. The formulation shows that accurate estimation of the internal resistance and the SoC could lead to an accurate estimate of the battery's SoP.

1.5 Battery Modeling

To estimate the states of a battery, a suitable model is needed. The model should be able to capture the key characteristics of both steady-state and transient reactions, under different operating conditions. Battery models can be categorized into three groups including Electrochemical Model, empirical model and Equivalent Circuit Models (ECMs). An electrochemical model can represent the interior chemistry and physics of a battery cell. However, using them with estimation algorithms and in real-time is difficult due to their high computational complexity. ECMs, on the other hand, may be easily parameterized using system identification techniques and experimental data. Despite the fact that the parameters of ECM models do not match the actual reaction within a battery cell, the accuracy of estimated SoC is adequate to be used onboard of a BMS within restricted working region. Empirical models use mathematical expressions to represent the characteristics of a battery. Similar to ECMs, they can be easily implemented and be used in real-time. To provide an accurate model for a battery cell, the number of parameters in empirical models should be increased [12, 26, 27].

1.5.1 Electrochemical Models

Partial differential equations are used to explain both the electrochemical reaction between the electrodes and the electrolyte in this type of model. In comparison to equivalent-circuit based models, electrochemical models are more sophisticated and need more computing resources. Despite their complexity, these models are preferred due to their physical significance. Previous research has looked at two

types of electrochemical models: Pseudo Two-Dimensional (P2D) and Single Particle Models (SPM). To improve the accuracy of SPM in high C-rate, a few Extended SPM (E-SPM) have been reported. According to the structure of electrochemical models in a battery management system, model reduction is required to lower the model's complexity. Furthermore, electrochemical models necessitate the measurement of multiple parameters, making modeling more complex. With one input called cell current and one output called terminal voltage, full-order electrochemical models should be defined which includes four partial differential equations that represent the internal interactions within a battery cell. As a result, in order to estimate SoC and SoH in a BMS, a reduced-order form of electrochemical model can be considered [28, 29].

1.5.2 Empirical Models

Empirical battery models use various mathematical formulation to define the relationship between the terminal voltage of the battery with its current, and SoC. The parameters of these model can be found by using experimental data. Empirical models include the Shepherd model, the Nernst model, the enhanced self-correcting model, the zero-state hysteresis model, and black-box models [12, 30]. Although these models employ simple expressions and efficient computation, they have some limitations in terms of describing the terminal voltage. Empirical models can be simple while still delivering a reliable model, however, they are limited to a specific range of conditions. This can be improved by increasing the number of parameters in the model or by providing larger data-set [26].

1.5.3 Equivalent Circuit Models

Equivalent Circuit Models (ECMs) replicate the charging and discharging behavior of Li-ion batteries using simple elements, including resistors and capacitors. These models have a basic structure as shown in Figure 1.5, making them simple to implement and computationally efficient. The relationship between the terminal voltage and the input is defined as follows,

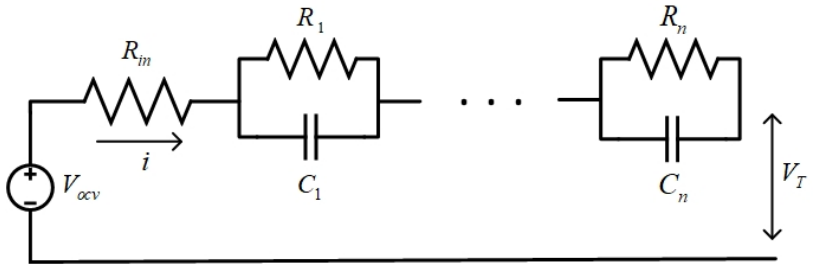

Figure 1.5: ECM battery model of order n.

$$V_{j,k+1} = (1 - \frac{\Delta T}{R_j C_j})V_{j,k} + \frac{\Delta T}{C_j} i_k, \quad j = 1, ..., n \tag{1.10}$$

$$SOC_{k+1} = SOC_k - \frac{\eta \Delta T}{C_n} i_k \tag{1.11}$$

$$V_{T,k} = V_{ocv}(SOC_k) - \sum_{j=1}^{n} V_{j,k} - R_{in} i_k \tag{1.12}$$

where V_T is the cell terminal voltage, V_j is the voltage across the jth RC branch, V_{ocv} is the OCV (nonlinear function of SoC), C_n is the cell's nominal capacity, η is the cell Coulombic Efficiency (CE), and i is the current flowing across the cell.

There is no physical meaning to ECMs, even though they reflect the electrical relationship between the battery's terminal voltage, current, SoC, and temperature. This could restrict the model for SoH and SoP estimation [28, 31]. Different techniques, such as parameter estimation and model selection, can be used to modify these models and change the model parameters for different operational circumstances. This study proposes a number of changes to ECMs in order to achieve a balance between complexity and accuracy. Further, these changes can offer indicators for SoH and SoP in order to estimate the entire key states of a battery.

1.5.4 Model Parameters Identification

Battery models differ not only in their structure, but also in the methods for estimating their parameters. The model's parameters, which include physical and electrical quantities, determine the battery's characteristics. To estimate the parameters of the battery models, different techniques are used. Parameters identification methods are divided into two categories: offline and online. This section presents an overview of these methods [12, 32].

Offline Parameter Identification

Parameters of a battery model can be identified by using different test procedures such as continuous and pulse charging/discharging, and Electrochemical Impedance Spectroscopy (EIS). Since the parameters of a battery model are affected by temperature, current, SoH, and SoC, the tests should be repeated under different conditions to provide a more accurate model. The provided data are then used to identify the parameters of the battery model by optimizing an objective function such as the

mean square error. Model fitting methods include Genetic Algorithms (GAs), Particle Swarm Optimizations (PSOs), and Levenberg-Marquardt. Offline parameter identification methods provide accurate battery models through laboratory tests, ensuring a reliable battery state estimate. However, these methods are highly dependent on a large number of tests [32, 33].

Online Parameter Identification

The objective of online parameter identification is to identify the model's parameters based on real-time observations, resulting in an accurate battery model under a wide range of operating conditions. An accurate battery model indicates the internal characteristics of the battery and is essential for improved state estimate. Filtering methods such has Kalman Filter (KF), and Least Square (LS) methods are commonly used for online parameter identification. Although these methods provide an accurate model for real-time applications, they can be affected by measurement errors such as sensor noise, and bias in the measured current and terminal voltage. This can lead to inaccurate identification. Advancements of these strategies such as the Recursive Least Square (RLS) with forgetting factor can be used to address this issue [34, 35].

Recursive Least Square with Forgetting Factor

A Recursive Least Square (RLS) is a real-time parameter estimation method. RLS with a forgetting factor helps to capture the slow variations of the parameters of a system in real-time. A linear regression, conducted from the system model equations, is used for this method.

$$V_k = \theta^T \Phi_k \tag{1.13}$$

where Φ_k is the regressor of the known signals and θ is the parameter vector. The loss function of the RLS method can be defined as follows [36],

$$V(\hat{\theta}, k) = \frac{1}{2} \sum_{i=1}^{k} \lambda^{k-i} (y_i - \hat{\theta}_k^T \Phi_i) \tag{1.14}$$

Here, λ is called the forgetting factor and can be chosen as $0 < \lambda < 1$. This loss functions is used to obtain, the parametric vector (θ) as follows,

$$\hat{\theta}_k = \hat{\theta}_{k-1} + L_k (y_k - \hat{\theta}_{k-1}^T \Phi_k) \tag{1.15}$$

$L(k)$ and $P(k)$ are the gain and covariance matrix, that are updated as follows,

$$L_k = P_{k-1} \Phi_k (\lambda + \Phi_k^T P_{k-1} \Phi_k)^{-1} \tag{1.16}$$

$$P_k = (I - L_k \Phi_k^T) P_{k-1} \frac{1}{\lambda} \tag{1.17}$$

Equations 1.13 through 1.17 summarize the RLS process, and is repeated iteratively.

1.6 Estimation Theory

Physical modeling of a system is used for capturing its dynamic behavior. Prior knowledge and empirical characterization are two sources of information for constructing a system model. Once model is obtained, model-based estimation is the process of extracting the dynamic states and on a more limited basis some parameters associated with the model from measurements. The goal of the estimating process is to reduce state and parameter estimation errors in the presence of uncertainties and noise under different operating conditions. Filtering, smoothing, and prediction are the three types of estimation processes. Filtering is used to extract an accurate value of the states at a current time from prior measurements, including the current point. An estimation process can be model-based; the form taken into consideration in this study [37, 38, 39].

Since the fifteenth century, there have been numerous contributions to estimation theory. As the field's first important contributor, Thomas Bayes proposed the Bayesian rule which provided the bases of the Bayesian estimator [40]. Later, Gauss introduced the least square estimation approach for nonlinear problems [41]. Based on statistics and probability methodologies, the Markov process and Markov chain theories were introduced in [42]. Many studies have been conducted using the methodologies described [43]. Norbert Wiener invented the Wiener filter, which can be utilized in signal processing applications to solve estimation challenges [29]. Based on previous research, Rudolf Kalman introduced a new estimation approach for linear systems called the Kalman Filter (KF). The KF, has been one of the most powerful and popular approaches in estimation theory [39]. Numerous improvements have

been made on the KF.

Furthermore, other types of optimal filters have been introduced based on sliding mode control and variable structure control called Sliding Mode Observers (SMO). Because of their robustness in the presence of uncertainties and disturbances, these filters can be employed in fault detection and signal reconstruction [43]. This section briefly describes different type of filters considered in this research.

1.6.1 Kalman-Based filtering

The KF is an optimal Bayesian filter. This method is reliant on a few assumptions, including the availability of a known linear system model and presence of only white noise, both of which are not guaranteed in real-time applications. The KF's precision, on the other hand, is quite appropriate for a linear system. A KF works in a predictor-corrector way, meaning each cycle of the KF consists of two steps: prediction and correction. In the prediction step, the KF finds the state estimates of the current time step by using the state estimates from the previous time step. In the correction step, the current measurement is combined with a-priori prediction to find an updated a-posteriori state estimate. A continuous version of the KF, known as the Kalman-Bucy filter was later introduced by Kalman and Bucy. Enhancements such as the Extended Kalman filter (EKF) was also presented to deal with nonlinear system [39, 44, 45].

Although there are some drawbacks to employing the KF, it does have certain advantages, such as giving a real-time unbiased and low variance state estimates. However, when both the process and the measurement have very small noise covariance matrices, the error covariance drops quickly, which can lead to instability. To solve the numerical instability problem of KF, enhancements have been presented

based on the KF such as the Robust Kalman Filter (RKF). Other enhancements presenting a trade-off between performance, robustness and computational complexity include the Unscented Kalman filter (UKF), Mixture Kalman filter (MKF), Quadrature Kalman filter (QKF), Cubature Kalman filter (CKF), Sigma Point Kalman Filter (SPKF), Monte Carlo Kalman filter (MCKF), and Adaptive Kalman Filter (AKF). These can improve the capability of estimation for different applications in presence of non-linearity, uncertainties and noise [39, 43, 46]. Furthermore, to deal with fractional order models, an extension of the KF filter is presented in [47, 48].

1.6.2 Sliding Mode Based Filtering

In 1940, variable structure theory was introduced for systems with discontinuities in their differential equations. The discontinuity hyperplane divides the state space into regions with continuous dynamic equations. These systems are known as variable structure systems. Variable Structure Control (VSC) is a technique that changes the control gain based on the state space region in which the state trajectory is located. As a consequence, the control input is discontinuous. The Sliding Mode Control (SMC) is a special form of VSC where it uses the discontinuous control input to force the state trajectory to converge and remain close to a sliding hyperplane. In 1985, the discrete forms of the VSC and SMC were presented. The discrete SMC's stability conditions were then provided, and it is now widely used in the design of discrete controllers [37]. While SMC is generally robust in terms of uncertainties, it suffers from high frequency chattering. This effect can be mitigated by employing a Smoothing Boundary Layer (SBL), which calculates the control signal based on the distance of the states from the sliding hyperplane. The duality of control and observer

theories have led to the development of estimation techniques based on the VSC and the SMC [37, 49]. This section briefly introduces these techniques.

Sliding Mode Observer

Sliding Mode Observers (SMOs) were created in 1980 as a robust way to dealing with uncertainties and nonlinearities. VSC and SMC are used by these observers to perform their tasks. In the face of uncertainties and disturbances, the SMC is remarkably resilient. The SMO has been presented based on SMC due to the duality of observers and controllers. The SMO defines a hyperplane, known as the sliding surface, and performs a discontinuous force to the estimates in terms of reaching to the sliding surface. The estimates are brought to the sliding surface by the SMO from their initial conditions in a phase known as the reachability. Later in the sliding phase, the estimates are forced to remain on the sliding surface. The SMO is affected by the gain that is chosen. A small gain leads to a slow response and the estimates may not converge to the sliding surface. A large gain provides more robustness, however, the observer is more sensitive to the measurement noise [37, 50]. Because the SMO is robust to nonlinearities, disturbances, and uncertainties, it may be applied to a variety of applications including fault detection, signal processing, and state estimation. Observers can be employed to estimate system parameters as well as states [43].

The Variable Structure Filter

In 2003, a new estimation method so-called the Variable Structure Filter (VSF) was proposed for state estimation of linear systems. Although this method defines a sliding surface to force the estimates to go back and forth across their actual value, it has a different structure than the SMO. This method has a predictor-corrector form [51]. The VSF filter is able to increase stability and convergence when there are higher degrees of modeling or parametric uncertainties. The performance of other filters such as Kalman-based filters degrade or may lead to instability in these situations. However, the stability of VSF can be guaranteed in the presence of bounded uncertainties using the variable structure system's concept. The control input in sliding mode control involves a discontinuous term, which is defined as a function of the state variables in the following manner [43, 52],

$$u(x,t) = \begin{cases} u^{+}(x,t) & s(x) > 0 \\ u^{-}(x,t) & s(x) < 0 \end{cases} \tag{1.18}$$

where $u^{+}(x,t)$ and $u^{-}(x,t)$ are continuous functions. Using this theory, the VSF gain is defined based on the upper bounds of uncertainties and noise. This method can only be used for observable linear systems. Lyapunov's second law of stability is used to demonstrate the VSF's stability. In [53], an Extended Variable Structure Filter (EVSF) with the same structure and the capacity to be used for nonlinear systems was presented.

The Smooth Variable Structure Filter

The Smooth Variable Structure Filter (SVSF), a more flexible version of the VSF, was introduced in 2007 [54]. The SVSF is a robust model-based prediction-corrector filter that works with both linear and nonlinear systems that are differentiable and observable. The Smoothing Boundary Layer (SBL) and the existence boundary layer are the two separate boundary layers connected to the SVSF idea. The SBL is a function of the upper bound of uncertainties and disturbances and could be different from the existence boundary layer. The existence boundary layer's width is unknown, as it is a function of disturbances and uncertainties. The SBL width has to be greater than the existence subspace for the smoothing action to eliminate chattering. The SVSF's switching action ensures that the estimates converge to the vicinity of their actual values. The switching features enable stability in the face of unknowns and disturbances. Further to an initial guess based on a-priori information, the estimated state trajectory is pushed to a neighborhood of the system's true trajectory referred to as the existence subspace. Once they enter this subspace, the corrective switching action forces the estimated state trajectory to stay within it. Modeling uncertainties, measurement noise, and disturbances all influence the width of the existence subspace [54]. The concept of the SVSF state estimation is shown in Figure 1.6. Assuming the following typical model,

$$\begin{aligned} x_{k+1} &= f(x_k, u_k, w_k), \\ z_k &= h(x_k, u_k, v_k) \end{aligned} \tag{1.19}$$

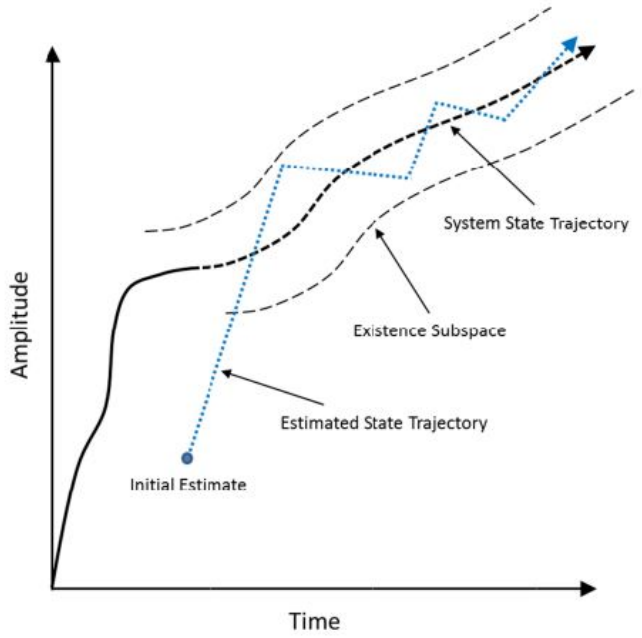

Figure 1.6: An overview of the SVSF estimation concept [54].

where v_k is the measurement noise and w_k is the system noise and they are uncorrelated white noise with the following mean and covariance,

$$E[w_k] = 0, \quad E[w_k w_k^T] = Q_k \tag{1.20}$$

$$E[v_k] = 0, \quad E[v_k v_k^T] = R_k \tag{1.21}$$

The SVSF method can be described as follows [51],

- Prediction: The a-priori state estimate is obtained by using an estimated model.

$$\hat{x}_{k+1|k} = f(\hat{x}_{k|k}, u_k), \tag{1.22}$$

$$\hat{z}_{k+1|k} = \hat{H}\hat{x}_{k+1|k} \tag{1.23}$$

$$e_{z_{k+1|k}} = z_{k+1} - \hat{z}_{k+1|k} \tag{1.24}$$

where $e_{z_{k+1|k}}$ is the a-priori measurement error vector.

- Correction: The updated state is obtained by using a gain to refine the a-priori estimate into its a-posteriori form.

$$\hat{x}_{k+1|k+1} = \hat{x}_{k+1|k} + K_k^{SVSF} e_{z_{k+1|k}},$$

$$\hat{z}_{k+1|k+1} = \hat{H}\hat{x}_{k+1|k+1} \tag{1.25}$$

$$e_{z_{k+1|k+1}} = z_{k+1} - \hat{z}_{k+1|k+1} \tag{1.26}$$

where $e_{z_{k+1|k+1}}$ is the a-posteriori measurement error vector.

The SVSF's gain K_{SVSF_k} is a function of the a-priori and a-posteriori measurement error vectors $e_{z_{k+1|k}}$ and $e_{z_{k+1|k+1}}$, the SBL widths (ψ), and the SVSF memory or convergence (γ) with elements $0 < \gamma_{ii} \leq 1$, defined as follows,

$$K_k^{SVSF} = \hat{H}^{+}\big[diag\big(|e_{z_{k|k-1}}| + \gamma|e_{z_{k-1|k-1}}|\big).sat(\frac{e_{z_{k|k-1}}}{\psi})\big][diag(e_{z_{k|k-1}})]^{-1} \tag{1.27}$$

Equations 1.22 through 1.27 summarize the SVSF process, and is repeated iteratively. The estimation process is proven to be stable and converges to the existence subspace if the following condition is satisfied [54],

$$|e_{k|k}|_{Abs} > |e_{k+1|k+1}|_{Abs} \tag{1.28}$$

The $|e|_{Abs}$ is the absolute value of the vector e, and is equal to $|e|_{Abs} = e.sign(e)$.

Theorem 1 (see [54]). *On the stability of the SVSF strategy, if the system is stable, consecutive bijective (or completely observable and completely controllable in the case of linear systems), then the SVSF corrective gain K_k that would satisfy the stability condition of Equation 1.28 is subject to the following conditions,*

$$|e_{k+1|k}|_{Abs} \leqslant |K_{k+1}|_{Abs} < |e_{k+1|k}|_{Abs} + |e_{k|k}|_{Abs} \tag{1.29}$$

The corrective gain K_k of the SVSF as Equation 1.27 satisfies this condition [54]. A great deal of research have been done to improve the SVSF's performance [52]. A revised form of the SVSF with a covariance derivation was presented in [55, 56] where the a-priori ($P_{k+1|k}$) and a-posteriori ($P_{k+1|k+1}$) error covariance matrices are defined as follows,

$$P_{k+1|k} = \hat{A} P_{k|k} \hat{A}^T + Q_k \tag{1.30}$$

$$P_{k+1|k+1} = (I - K_{k+1}^{SVSF} \hat{H}) P_{k+1|k} (I - K_{k+1}^{SVSF} \hat{H})^T + K_{k+1}^{SVSF} R_{k+1} K_{k+1}^{SVSF,T} \tag{1.31}$$

Using a covariance, which is a function of state estimation error, can provide a derivation for an optimal gain. An optimal form of the SVSF referred to as the SVSF with Variable Boundary Layer (SVSF-VBL) was presented by considering an optimal time-varying SBL [57] defined as follows,

$$S_{k+1} = \hat{H} P_{k+1|k} \hat{H}^T + R_{k+1} \tag{1.32}$$

$$E_{k+1} = |e_{z_{k+1|k}}| + \gamma |e_{z_{k|k}}| \tag{1.33}$$

$$\psi_{k+1} = (\bar{E}_{k+1}^{-1} \hat{H} P_{k+1|k} \hat{H}^T S_{k+1}^T)^{-1} \tag{1.34}$$

where S_{k+1} is the innovation covariance matrix, E_{k+1} is the combination of measurement error vectors, and ψ_{k+1} is the SBL width.

Therefore, the optimal SVSF gain for the case when $\psi_{k+1} \geqslant \psi_{lim}$ is defined as follows,

$$K_{k+1}^{SVSF} = \hat{H}^{-1} \bar{E}_{k+1} sat(e_{z_{k+1|k}} \psi_{k+1}^{-1}) \bar{e}_{z_{k+1|k}}^{-1} \tag{1.35}$$

where ψ_{lim} is the upper limit for the boundary layer. For the case with $\psi_{k+1} < \psi_{lim}$, the method uses the standard SVSF gain as obtained in Equation 1.27.

In [58], the SVSF's covariance formulation was modified to a general form. Furthermore, a generalized form of VBL was presented in [58]. Figure 1.7 provides an overview of the research on SVSF over the past decade. This research provides some improvements on SVSF including IMM-SVSF-VBL, Dual estimation strategy based on SVSF-VBL, and Adaptive SVSF-VBL for battery applications.

1.6.3 Adaptive Filtering

All prior methods assume that the input and measurement noise statistics, as well as system characteristics, are known; this is not the case in real-world situations.

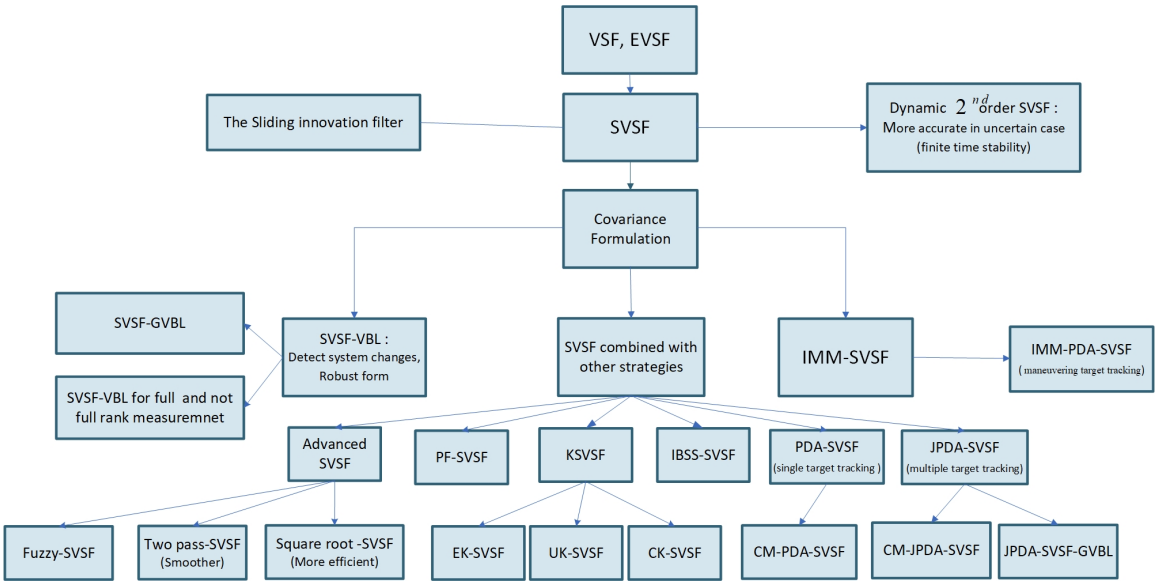

Figure 1.7: A general overview of VSF-based filters.

Physical parameters, noise characteristics, and initial conditions all have some uncertainties or inaccuracies. Estimating the unclear factors and conditions throughout the estimation process is one answer to these challenging scenarios. This mechanism is referred to as adaptation and, the associated methods are called adaptive filtering. Adaptive filters come in a variety of forms, including multiple model filters and filter tuning [43].

Multiple Model Methods

Multiple Model (MM) approaches are well-known adaptive filters that use a finite number of models to characterize a system's behavior [39]. The MM methods work based on a Bayesian framework. In these methods, the prior probability and likelihood functions of the models are used. The static MM method and the dynamic MM methods are two commonly used types of MM methods. In the static MM algorithm, the closest model is chosen at the start of the process, and the system follows a single

fixed model during the filtering phase. As a result, there is no need to switch between models. Conversely, the dynamic MM filters automatically switch between many models to determine the best accurate approximation depending on the operating conditions [39]. The Generalized Pseudo-Bayesian (GPB) and Interacting Multiple Model (IMM) are considered in this group because of their moderate computational complexity. This research proposes a method using the IMM concept for state estimation of EV batteries. A finite number of models based on the SoH of a battery are considered. Chapter 3 provides more details on this algorithm.

Interacting Multiple Model Concept

The Interacting Multiple Model (IMM) approach assumes that a system's behavior can be represented using a finite number of models. These models can capture various system structures and parameters. Therefore, the IMM method uses r number of models associated with filters to operate in parallel. A mixed initial condition based on the previous step is used to initialize the individual filters. The output of each filter includes its state estimate, error covariance matrix, and likelihood function. The likelihood function of each filter, which is a function of the a-priori measurement error and innovation covariance, quantifies its estimation error as well as the model's applicability. The mode probabilities, which represent how close the filter model is to the true system model, are then evaluated using likelihood functions of the filters. The mode probabilities represent the best model for capturing the system's dynamics at time k. In comparison to other dynamic MM methods, it is shown that the IMM method is more effective and computationally efficient at capturing a system's changing dynamics [39, 59].

The IMM concept consists of five main steps: calculation of mixing probabilities;

mixing stage; mode-matched filtering; mode probability update; and calculation of the a-posteriori state estimate and covariance matrix. Figure 1.8 shows an overview of the IMM concept using two parallel filters. The algorithm is demonstrated as follows,

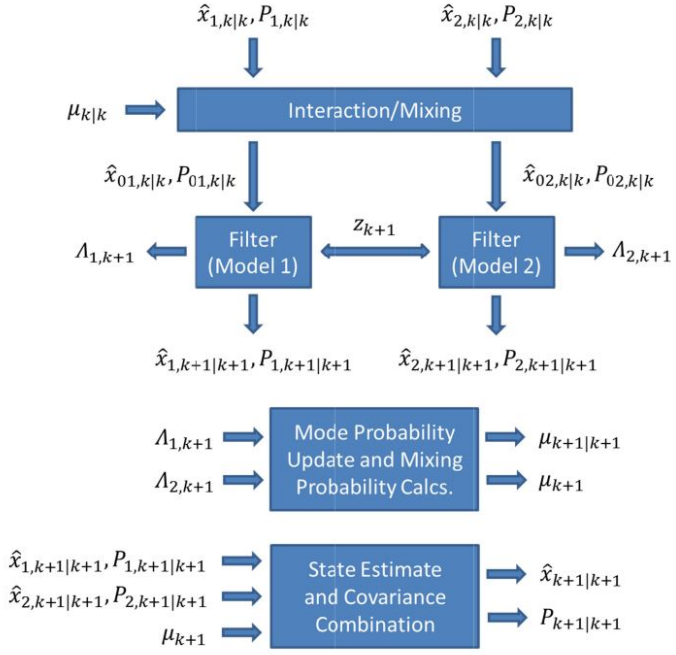

Figure 1.8: An overview of the IMM concept[59].

1. Calculation of the mixing probabilities $(i, j = 1, ..., r)$. The mixing probably $(\mu_{i|j})$ is the probability of the system that was in mode i given that it is now in mode j. This can be calculated as follows,

$$\mu_{i|j}(k|k) = \frac{1}{\bar{c}_j} p_{ij} \mu_{i|j} \quad i, j = 1, ..., r \tag{1.36}$$

where the probability mass function prediction ($\bar{c}_j$) and the transition probability matrix (p_{ij}) are defined as follows,

$$\bar{c}_j = \sum_{i=1}^{r} p_{ij}\mu_i \qquad j = 1, ..., r \tag{1.37}$$

$$p_{ij} \triangleq P\{M_i(k)|M_j(k), Z^k\} \tag{1.38}$$

2. Mixing ($j = 1, ..., r$). The Mixing step determines the mixed initial conditions of the state vectors ($\hat{x}^{0j}$) and state error covariance matrices (P^{0j}) for the filters by using the calculated mixing probabilities, the previous mode-matched states ($\hat{x}^i(k|k)$), and covariances ($P^i(k|k)$) as follows,

$$\hat{x}^{0j}(k|k) = \sum_{i=1}^{r} \hat{x}^i(k|k)\mu_{i|j}(k|k) \quad j=1, ..., r \tag{1.39}$$

$$P^{0j}(k|k) = \sum_{i=1}^{r} \mu_{i|j}(k|k)\{P^i(k|k) + [\hat{x}^i(k|k) - \hat{x}^{0j}(k|k)][\hat{x}^i(k|k) - \hat{x}^{0j}(k|k)]^T\}$$

$$j=1, ..., r \tag{1.40}$$

3. Mode-matched filtering ($j = 1, ..., r$). In this step, one iteration of the filter evaluates in mode j to produce a new state estimate based on the state and covariance values obtained by the mixing step. Following that, the likelihood

functions of filters (Λ_j) in mode j are calculated as follows,

$$\Lambda_j(k+1)=\mathcal{N}[z(k+1);\hat{z}^j[k+1|k;\hat{x}^{0j}(k|k)],S^j[k+1;\hat{P}^{0j}(k|k)]] \quad j=1,...,r \tag{1.41}$$

The likelihood function of each filter, provided in Equation 1.41, can be solved as follows,

$$\Lambda_j(k+1) = \frac{1}{\sqrt{|2\pi S_{j,k+1}|_{Abs}}} \exp(\frac{-\frac{1}{2}e^T_{j,k+1|k}e_{j,k+1|k}}{S_{j,k+1}}) \tag{1.42}$$

where S_j is the innovation covariance matrix, and $e_{j,k+1|k}$ is the a-priori measurement error vector of filter j.

4. Mode probability update ($j=1,...,r$). Mode probability (μ_j) takes into account the likelihoods of all the models and can be updated as follows,

$$\mu_j(k+1)=\frac{1}{c}\Lambda_j(k+1)\bar{c}_j \qquad j=1,...,r \tag{1.43}$$

where the normalizing constant (c) is defined as,

$$c=\sum_{j=1}^{r}\Lambda_j(k+1)\bar{c}_j \tag{1.44}$$

5. Estimate and covariance combination. The algorithm outputs are then computed by combining the a-posteriori estimated states ($\hat{x}^j(k+1|k+1)$) and covariances ($P^j(k+1|k+1)$) from each filter by their mode probability ($\mu_j(k+1)$).

$$\hat{x}(k+1|k+1) = \sum_{j=1}^{r} \hat{x}^j(k+1|k+1)\mu_j(k+1) \tag{1.45}$$

$$P(k+1|k+1) = \sum_{j=1}^{r} \mu_j(k+1)\{P^j(k+1|k+1) + [\hat{x}^j(k+1|k+1) - \hat{x}(k+1|k+1)][\hat{x}^j(k+1|k+1) - \hat{x}(k|k)]^T\} \tag{1.46}$$

Equations 1.36 through 1.46 summarize the steps for the IMM method. It should be noted that Equations 1.45 and 1.46 are only used to obtain the algorithm outputs and do not take part in its recursions. Different filters can be paired with the IMM strategy to be used for different applications. This thesis provides an IMM technique paired with SVSF-VBL for state estimation of batteries under different operating conditions. Chapter 3 provides more details on this algorithm.

Filter Tuning

Filter tuning methods can be categorized into two groups including noise adaptation, and parameter tuning. In parameter tuning methods, the parameters are tuned based on measurements. Recent research has proposed dual and joint filtering strategies for estimating both the parameters and the states of a system at the same time. These strategies are useful for applications when parameters are changing in time such as in the case of batteries. In joint filtering, a model-based filter is applied to an augmented system created by combining the states and parameters dynamics [60, 61].

Although, these techniques are widely used for parameter tuning, the observability of the system cannot be ensured. Dual strategies, on the other hand, estimate the parameters and the states using separate filters [62]. This study proposes a dual and combined estimation strategy across a wide range of battery operations. Chapter 2 presents a dual estimation strategy to update the battery model as the battery ages. Joint estimation methods are also included in this thesis to estimate the parameters and measurement biases including SoC bias, current sensor bias, and voltage sensor bias.

For model-based filters, noise statistics are needed. Most filters assume that the noise is white, Gaussian, and has a zero mean. The filter's performance diminishes if this assumption is not met. Noise characterization have sparked ample amounts of interest in a range of applications as a result of this. A wide range of studies have been conducted on the features, benefits, and drawbacks of noise adaptation techniques. Feedback methods and feedback-free methods are two types of noise covariance estimation approaches. Feedback approaches allow for simultaneous estimation of states and noise covariance matrices. Covariance matching and Bayesian procedures are examples of these techniques. In contrast, estimated noise covariances are not necessary for state estimation with feedback-free approaches. Correlation and maximum-likelihood approaches are two examples of statistical procedures [63, 64]. Chapter 4 presents an adaptive version of the SVSF-VBL strategy to tune the level of noise measurement and modeling uncertainties (R and Q) to improve the performance of the filter for noisy conditions. The proposed strategy is used to improve the state estimate of a battery.

1.7 System Observability

An observable system is one in which its states can be determined from knowledge of its outputs. The observability of a system model should be assessed before employing an estimation method. For a linear time-invariant system defined by a state-space representation, an observability matrix with a full rank can ensure the global observability. However, determining whether a nonlinear system is observable can be more challenging. The state-space form of a nonlinear system can be defined as follows,

$$x_{k+1} = f(x_k) + g(x_k)u_k, \tag{1.47}$$

$$y_k = h(x_k, u_k) \tag{1.48}$$

For a nonlinear system, the local observability can be analyzed. Several concepts must be introduced for analyzing the observability of a nonlinear system.

Definition 1 (see [65]). *For a system represented by equations 1.47 and 1.48,* x_0 *and* x_1 *are declared to be distinguishable states if there exists an input function* $u(.)$ *such that*

$$y(k, x_0, u) \neq y(k, x_1, u) \tag{1.49}$$

for a finite time. The system is locally observable at $x_0 \in X$ *if there exists a neighborhood* N *of* x_0 *such that every* $x \in N$ *excluding* x_0 *is distinguishable from* x_0*. Therefore, the system is called locally observable if it is locally observable at each* $x \in X$*.*

A system is globally observable if every pair of states (x_0, x_1) with $x_0 \neq x_1$ is distinguishable. It can be demonstrated that two states are distinguishable for a linear system if $y(k, x_0, u) \neq y(k, x_1, u)$ condition holds for any u. Furthermore, it can be proven that for a linear system, local observability leads to global observability. However, this is not guaranteed for a nonlinear system. The observability of a nonlinear system can be illustrated using extended Lie-derivative.

Definition 2 (see [66]). *Suppose the output* $h(x,u) = \begin{bmatrix} h_1 & h_2 & ... & h_m \end{bmatrix}^T$ *is a m-dimensional vector function on* x *and* u*. The gradient of* $h_j, j = 1, ..., m$ *denoted by* dh_j *is a form of,*

$$dh_j = \begin{bmatrix} \frac{\partial h_j}{\partial x_1} & \frac{\partial h_j}{\partial x_2} & ... & \frac{\partial h_j}{\partial x_n} \end{bmatrix} \tag{1.50}$$

Then the extended Lie-derivative of h *with respect to* f *is,*

$$\mathcal{L}_f h(x,u) = dh(x,u)f(x) + \sum_{i=0}^{i=\infty} \frac{\partial h(x,u)}{\partial u^i} u^{i+1} \tag{1.51}$$

The Lie-derivatives for higher order than one are obtained as,

$$\mathcal{L}_f^j h(x,u) = d\mathcal{L}_f^{j-1} h(x,u)f(x) + \sum_{i=0}^{i=\infty} \frac{\partial \mathcal{L}_f^{j-1} h(x,u)}{\partial u^i} u^{i+1} \tag{1.52}$$

The following theorem provides a sufficient condition for a nonlinear system's local observability based on the given definitions.

Theorem 1 (see [65]). *For a system described by Equation 1.47 and 1.48 with the*

assumption of given $x_0 \in X$. *Consider the form,*

$$(d\mathcal{L}_{z_s}\mathcal{L}_{z_{s-1}}...\mathcal{L}_{z_1}h_j), s \geqslant 0, z_i \in \{f, g_1, ..., g_p\} \tag{1.53}$$

evaluated at x_0 *where* $i = 1, ..., s$, $j = 1, ..., m$ *and for* $s = 0$ *the expression is equal to* $dh_j(x_0)$. *Suppose there are n linearly independent row vectors in this set. Then the system is locally observable around* x_0.

Theorem 1 can also be used to derive the observability condition for a linear system. Based on theorem 1, the observability matrix for a general nonlinear system can be defined as,

$$\mathcal{O}_I(x,u) = \begin{bmatrix} dh(x,u) \\ \mathcal{L}_f h(x,u) \\ \mathcal{L}_g h(x,u) \\ \mathcal{L}_f^2 h(x,u) \\ \mathcal{L}_g^2 h(x,u) \\ . \\ . \\ . \end{bmatrix} \tag{1.54}$$

Therefore, the model described by equations 1.47 and 1.48 is locally observable if the observability matrix ($\mathcal{O}_I(x,u)$) has n linearly independent row vectors. In Chapter 3, the observability of the battery model is demonstrated prior to implementing the proposed estimation method.

1.8 Research Contributions

Estimation of the battery's State of Charge (SoC), State of Health (SoH), and State of Power (SoP), which cannot be measured directly, is critical for its energy management system. This thesis focuses on improving the estimation accuracy of a battery's states of operation under different operating conditions. Despite the fact that battery state estimation continues to be a frequently debated topic of research, there are still gaps in the literature. This thesis proposes advanced estimation strategies for battery cells and packs to address the existing issues.

The first challenge with estimation strategies is their reliance on an accurate mathematical battery model. A proper model should describe the behavior of a battery under a variety of conditions such as temperature, and current level. Furthermore, the impact of battery degradation and SoH should be considered. Different strategies have been introduced for model adjustment of a system. Adaptive techniques such as online parameter estimation are widely used to improve the battery performance by adjusting the model to changing conditions. A dual estimation method using two cooperating filters is firstly introduced in this thesis. To mitigate the impact of modeling errors and uncertainties, a robust filter is required. The robustness of the filter is critical since the parameters of the battery model are changing with SoC and SoH. These changes could lead to instability or divergence of the filter. Therefore, the SVSF method is used for state estimation of the battery. A Recursive Least Square with a Forgetting factor is also considered to capture the changes in parameters of a third-order ECM. The RLS strategy is numerically stable and its computational efficiency is well known. Furthermore, the dual estimation of RLS with the SVSF-VBL

provides higher accuracy in comparison to the well known EKF method. However, the full dual estimation strategy (RLS-SVSF) considering a third-order battery model is computationally intensive. The RLS method uses a regression model to obtain the parametric vector. The parameters of the battery model are then calculated by solving a system of nonlinear equations which is computationally heavy for the third-order ECM.

Model selection strategy is therefore proposed in this thesis to ensure adaptation stability and computation efficiency. Three predefined models, each for a different state of life of the battery cell, are considered in the concept of IMM as shown in Figure 1.8, to effectively deal with battery aging. The IMM strategy is combined with the SVSF-VBL method to reduce the effect of modeling errors and uncertainties. The SVSF-VBL provides an accurate estimate while ensuring that the estimate is stable. The SVSF-VBL filters' error covariance represents the estimation error and thus the applicability of each of these parallel filters in the IMM concept. The error covariances are used to determine the mode probabilities as defined in Equation 1.43. This demonstrates how close the filter model for a specific SoH is to the true age of the battery. The mode probability indicates the suitable model that captures the SoH of the battery.

The coulomb counting method, defined in Equation 1.1, is commonly regarded as the base technology for obtaining the actual SoC, which is then compared to the model-based state estimation strategy such as the IMM-SVSF-VBL. However, due to the inaccurate initial value of the battery SoC, current sensor bias, and the available capacity limited by age, a bias in the calculated SoC may exist. To address this problem, the coulomb counting method is used in conjunction with the proposed

model-based state estimation strategy (IMM-SVSF-VBL). Coulomb counting is regarded as an additional measurement in the formulation of the predefined ECMs, described in Equation 1.12, to improve the performance of the battery state estimation. Furthermore, the number of parameters that can be estimated while remaining observable is increased. As a result, the SoC bias and the internal resistance of the battery cell are estimated in addition to its states. The internal resistance is an indicator for the SoH of the battery as defined in Equation 1.3 which is then combined with the SoH obtained from the mode probability to provide an accurate measure of the battery's SoH. The estimated internal resistance and SoC are then used to quantify the battery's SoP, which provides a complete estimation of the battery's operating states.

Although the proposed strategy provides accuracy for estimating the states of a battery cell, obtaining the same result in a battery pack is limited due to cell-to-cell variations. Variations in the SoC and SoH of batteries over time can accelerate the degradation of the battery pack, and should therefore be taken into account. In series-connected cells, balancing methods are used to detect cell inconsistencies. In parallel-connected battery cells, however, it is impractical and costly to measure the current of individual cells. Therefore, a robust strategy is required to estimate the states of the module with respect to the existing sensors. Parallel-connected battery cells are commonly modelled as a single cell, with all cells consuming the same amount of current which may not be the case in presence of an aged cell in the module. A RLS is considered for real-time parameterization of parallel-connected battery cells. A first-order model is used and considered to provide a computationally effective method for use on a BMS for a module. The effect of the weakest cell in the

battery module model is determined using the online parameter identification. To improve the performance of the state estimation, the proposed strategy of combining the coulomb counting method with the model-based state estimation strategy (SVSF-VBL) is therefore implemented for the parallel-connected battery module. The new ECM formulation is then used to estimate the terminal voltage bias in order to provide a more accurate result in terms of cell inconsistencies for state estimation. The proposed dual estimation strategy provides robustness in presence of a faulty cell in a parallel-connected battery module.

Model-based filters proposed for state and parameter estimation assume that the input functions and the noise statistics (Equations 1.20 and 1.21), are largely known. However, this may not be the case in all applications and may need to be remedied through noise adaptation. In battery applications, measurement errors such as sensor noise, drift, and bias affect the performance of the state estimation and therefore the BMS. Noise covariance adaption approaches help estimation algorithms to perform more accurately. In addition, a more effective approach should also consider sensor bias estimation, as well as noise. To mitigate this issue, this thesis proposes a noise covariance adaptation method for the SVSF-VBL algorithm to improve its robustness for state estimation of a battery in presence of unknown physical disturbances, noise, and initial conditions.

The rest of this section summarizes the main hypotheses and contributions of this thesis.

1.8.1 Hypotheses

The hypotheses that formed the foundation for this thesis are as follows:

Hypothesis 1. *The accuracy of SoC estimation can be improved by combining state estimation and coulomb counting.*

Coulomb counting method needs regular calibration as a result of measurement errors and noise. It also requires knowledge of the initial SoC as well as the capacity of the battery. Treating coulomb counting as an extra measurement with a revised battery model provides a new formulation for state estimation. The updated formulation ensures the model's observability for estimating added parameters that lead to higher accuracy for SoC estimation at the cell and pack levels.

Hypothesis 2. *The IMM strategy can be used to improve SoC and SoH estimation by considering a number of predefined models each for a different SoH.*

The IMM strategy employs a finite number of independent models to capture the changing dynamics of a system. An ECM accurately represents the characteristics of a battery model when the battery is at its early stage. However, as a battery ages, the parameters of the ECM should be updated. In addition, a higher order model should be considered to simulate the characteristics of the battery. Hence, a single ECM structure is insufficient for all stages of a battery's life cycle, necessitating the real-time updating of the model's parameters. The MM strategy with different battery models, each assigned to a specific SoH, can improve the performance of state estimation significantly.

Hypothesis 3. *Adjusting the system and measurement noise covariances enhances the performance of the SVSF for state estimation of a battery.*

For accurate state and parameter estimation, knowledge of the system model is required. A stable filter requires the characterization of noise statistics in addition to

the dynamic model. If this information is incorrect, the designed filter may perform significantly worse and result in divergence. It is especially important for batteries that operate over a wide range of conditions, such as different C-rates and temperatures. The SVSF algorithm can use noise covariance adaptation to update these parameters during the estimation process.

1.8.2 Contributions

An overview of the contributions of this thesis is shown in Figure 1.9. The contributions of this research are published as journal and conference papers. The main contributions of the work, which are published as journal papers, are marked with red in Figure 1.9. Conference papers are highlighted green. This work's primary and secondary contributions are summarized below.

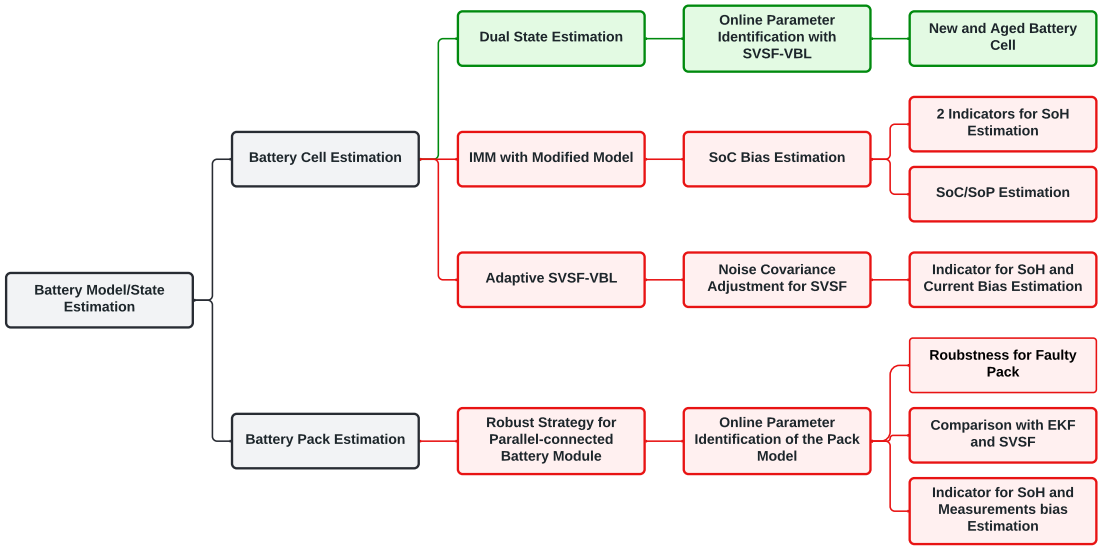

Figure 1.9: Research Contributions Flowchart.

Primary Contributions

The primary contributions of this research are:

1. Development of a new SoC estimation strategy by combining state estimation with coulomb counting (Chapters 3 and 5).

   Battery state estimation should aim to strike a balance between accuracy and complexity. The proposed strategies in Chapters 3 and 5 significantly reduce estimation error rates without overly increasing complexity.

2. Development of an adaptive method for state estimation of a battery based on the IMM concept using SVSF-VBL filters (Chapter 3).

   The second contribution is based on research into combining different models to be able to provide an accurate estimation for SoC as well as SoH. This contribution is further to Hypothesis 2 and can determine SoC within an error of 2%. Chapter 3 proposes a method for real-time capture of the SoC, SoH, and SoP of a battery.

3. Development of an adaptive method based on the SVSF to adjust the process and noise covariances (Chapter 4).

   Battery SoC estimation shows higher errors in presence of noise and bias in measurements. The performance could worsen at higher C-rates. The goal of Chapter 4 is to demonstrate the effect of noise on estimation methods and to develop an adaptive strategy for compensating changes in noise statistics.

4. Development of a robust strategy for state estimation of parallel-connected battery cells (Chapter 5).

As part of this research, the proposed estimation methods are extended from the cell level to module level. Chapter 5 introduces a robust strategy for estimating the states of parallel-connected battery cells in the absence of balancing without any additional sensors.

Secondary Contributions

The secondary contributions of this research are:

1. Online parameter estimation of a third-order ECM along with a robust strategy for state estimation of a battery at different SoH (Chapter 2).

   Online parameter estimation provides a higher accuracy for state estimation. An updated battery model according to the battery's SoH enhances the performance of estimation. Chapter 2 provides a dual state and parameter estimation strategy for a battery using a SVSF.

2. An investigation into the observability of a modified battery model with additional measurement is undertaken (Chapter 3).

   System observability must be considered in state estimation. Chapter 3 looks into the observability of a battery model when there are extra states to be estimated. The specific conditions that must be met for filter stability and performance are investigated.

3. Identification of the current bias to provide adaption for a filter for state estimation of a battery (Chapter 4).

   The estimation of the SoC and SoH must be robust and reliable despite noise, uncertainty and sensor biases. Chapter 4 provides an adaptation scheme for

estimating the sensor bias in current measurements. This could increase the performance of the state estimation especially at higher C-rates.

4. Identification of the terminal voltage bias to improve state estimation of parallel-connected battery module in presence of a faulty cell (Chapter 5).

   Identification of the terminal voltage bias is an important consideration. Chapter 5 investigates how the terminal voltage bias estimation could improve the state estimation of a parallel-connected battery module in presence of a faulty cell. A significant improvement is shown on SoC estimation in comparison to other strategies.

5. Online parameter estimation of a battery module's model along with its state estimation (Chapter 5).

   Parallel-connected battery cells can be regarded as a single cell with higher capacity. Online parameter estimation of an ECM for a battery pack enhances the performance of state estimation significantly. Combination of online parameter identification with a robust method shows a higher accuracy in comparison to other methods in Chapter 5.

1.9 Thesis Outline

Chapter 2 provides a review of the literature on the effect of online parameter identification, with a focus on the battery SoH. To estimate the battery SoC using an updated model, a dual estimation method is proposed. The results show how model parameters can change for batteries with varying SoH.

Chapter 3 provides a literature review of estimation strategies with applications to batteries. A novel estimation strategy is proposed by combining a measurement-based strategy with a model-based method. The IMM strategy with SVSF-VBL is presented to obtain an accurate estimation for SoC, SoH and SoP. Finally, the results are presented to demonstrate how the filter performs under various operating conditions.

Chapter 4 provides a literature review on the use of the noise covariance adaptation for state estimation. In this chapter, an adaptive version of the SVSF-VBL is proposed, which is combined with online current bias estimation. Along with the SoC estimation, an indicator of SoH is also presented. The results show how the filter reacts in the presence of noise and uncertainties in the measurements and battery model.

Chapter 5 provides an overview of SoC estimation techniques with a particular emphasis on parallel-connected battery cells. To improve the accuracy of state estimation at the module level, a robust strategy is considered. A dual strategy for state estimation of a parallel-connected battery module is introduced. The results are presented showing the significant improvement of the proposed method for SoC and SoH estimation of a battery module.

Chapter 6 contains the conclusions and summary of this work. This chapter also includes a discussion of future work.

Chapter 2: Dual Estimation Strategy for New and Aged Electric Vehicles Batteries

Sara Rahimifard, Saeid Habibi, Jimi Tjong

Department of Mechanical Engineering, McMaster University, Hamilton, ON, Canada, Ford Motor Company, Windsor, ON, Canada

This paper is published in 2020 IEEE Transportation Electrification Conference and Expo (ITEC), 2020, pp. 1-6, doi: 10.1109/ITEC48692.2020.9161556. This paper is republished here with permission.[1]

Abstract: The use of Hybrid (HEVs) and Electric (EVs) Vehicles has become more prevalent around the world in the last decade. These vehicles commonly use lithium-ion (Li-ion) batteries due to their high energy density. They also utilize Battery Management Systems (BMSs), which rely on continuous real-time monitoring and control, to ensure safe operation. The BMS acquires accurate State of Charge (SoC) and State of Health (SoH) estimates. For these, battery models that are identified and updated at various states of life from new to aged are required. In this paper, a dual strategy for both parameters and SoC estimation is proposed using a third-order equivalent circuit-based battery model (OCV-R-3RC). The strategy

[1]In reference to IEEE copyrighted material which is used with permission in this thesis, the IEEE does not endorse any of McMaster's products or services. Internal or personal use of this material is permitted. If interested in reprinting/republishing IEEE copyrighted material for advertising or promotional purposes or for creating new collective works for resale or redistribution, please go to `http://www.ieee.org/publications_standards/publications/rights/rights_link.html` to learn how to obtain a License from RightsLink.

employs a Recursive Least Squares (RLS) method with a forgetting factor to identify the parameters related to SoC. The Smooth Variable Structure Filter (SVSF) is then used as an estimation strategy for obtaining the battery's SoC. The efficacy of the proposed algorithm is verified by applying it to experimental data from an extensive aging test.

2.1 Introduction

Batteries are a particularly important component in Electric Vehicles (EVs) requiring accurate control and monitoring. All the challenges faced in the production of electric vehicles such as cost, range anxiety, safety and reliability originate in batteries. Therefore, accurate management, control and monitoring are essential to guarantee safety, and reliability of battery packs [23]. The BMS is responsible for providing a real-time estimate of the SoC and SoH of the battery. The battery SoC is a critical indicator for the driver on the amount of energy left in the battery. Since SoC and SoH are not directly measurable, a reliable and accurate estimation strategy is needed for the BMS [67].

Different methods proposed in the past to calculate the battery SoC have included strategies using coulomb counting, impedance measurement, fuzzy logic, artificial neural network and model-based estimation methods. One of the popular approaches used to estimate the battery SoC, even with an unknown initial SoC, is the Kalman Filter (KF) and its Extended version (EKF) [68]. However, in practice, the use of EKF has some shortcomings related to the characterization of noise and uncertainties that could result in instability [69]. More robust strategies include the Variable Structure Filter (VSF) [51] and Smooth Variable Structure Filter (SVSF) [54]. A comparison

of robustness between the performance of the EKF, the Particle Filter (PF), the Quadrature KF (QKF), and the SVSF shows the better robustness of the SVSF in the estimation of the SoC of lithium-ion (Li-ion) batteries [70].

The above methods rely on having a mathematical model for the battery. In [71], a comparison between different battery model is provided. However, a proper battery model should describe the behavior of the battery in a wide range of circumstances and also consider the effects of aging and degradation [16, 23]. In [28, 29], a reduced-order electrochemical model is proposed for aged batteries and used for SoC estimation. In [62], Plett proposed two approaches to estimate both parameters and states simultaneously: I) Joint estimation II) Dual estimation. The joint estimation method augments the state vector with model parameters and estimates these using an EKF. The dual estimation method employs two cooperating EKFs where one estimates the states and the other estimates the parameters.

In [72], a parameter identification strategy using Least Square (LS) is applied to an equivalent circuit-based model for estimating the parameters of the model and SoC. A genetic-algorithm-based multi-objective optimization is proposed in [73] to identify the parameters of an equivalent circuit-based battery model. In [68], an Adaptive Unscented KF (AUKF) is considered for battery model parameters identification. A dual estimation of an EKF for parameter estimation and a PF for SoC estimation is proposed in [74]. A Recursive Least Square (RLS) and an EKF are proposed for parameters and state estimation in [75, 76].

This paper considers a RLS with a forgetting factor to estimate the model parameters of a battery. The SVSF, is combined with online parameter identification to create an accurate SoC estimation. The proposed strategy demonstrates robustness

to model uncertainties, sensor noise and unknown initial SoC. Its performance has been verified using an extensive aging test with real-world driving cycle. These tests were conducted over a 12-month period and involved accelerated testing of a battery lifetime [16, 77]. A third-order equivalent circuit-based battery model (OCV-R-3RC) is used for this study as it provides an accurate model for real-time implementation on a BMS, especially as the battery ages.

The outline of the paper is as follows: Section II presents the battery model, and the proposed online parameter estimation method. The estimation of SoC and experimental results are presented in Section III. Section IV contains the conclusions of the work.

2.2 Battery Modeling and Parameter Estimation

A third-order equivalent circuit model is considered in this study as shown in Figure 2.1 and according to the following equations.

$$V_{1,k} = a_1 V_{1,k-1} + b_1 I_{L,k-1} \tag{2.1}$$

$$V_{2,k} = a_2 V_{2,k-1} + b_2 I_{L,k-1} \tag{2.2}$$

$$V_{3,k} = a_3 V_{3,k-1} + b_3 I_{L,k-1} \tag{2.3}$$

$$V_{T,k} = V_{oc} + c I_{L,k} + V_{1,k} + V_{2,k} + V_{3,k} \tag{2.4}$$

where the parameters $a_i = e^{-T_s/\tau_i}$, $b_i = R_i(1 - e^{-T_s/\tau_i})$, $c = R_0$ and $\tau_i = R_i C_i, i = 1, 2, 3$.

To estimate the battery model parameters, a suitable model needs to be developed for the battery that can describe the salient features of both steady-state and transient

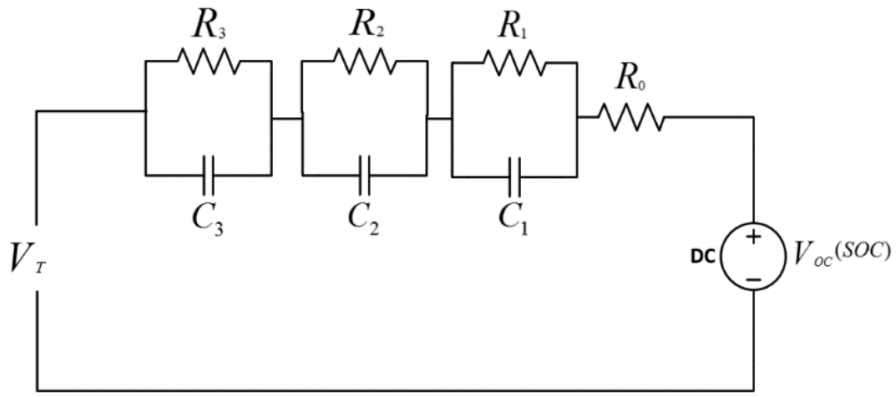

Figure 2.1: OCV-R-3RC Model [78].

responses. The following equation relates the load current (I_L) to the battery terminal voltage (V_T) in the z-domain.

$$V_T(z) = (\frac{b_1}{z-a_1} + \frac{b_3}{z-a_3} + \frac{b_3}{z-a_3})I_L(z) + cI_L(z) + V_{ocv} \tag{2.5}$$

Since the open circuit voltage (V_{ocv}) is just a function of SoC, it can be considered as a parameter and a linear regression model can be constructed based on the OCV-R-3RC model. The linear regression model can be compactly written as the inner product as follows from the inverse z-transform of (2.5) [79, 80],

$$V_{T,k} = \theta^T \Phi_k \tag{2.6}$$

where,

$$\Phi_k = [I_{L,k-3} \quad ... \quad I_{L,k} \quad V_{T,k-3} \quad V_{T,k-2} \quad V_{T,k-1} \quad 1]^T$$

is a regressor consisting of known signals and $\theta = [\theta_1 \quad ... \quad \theta_8]^T$ is the parameter vector

which is defined as follows:

$$\begin{aligned}
\theta_1 &= -ca_1a_2a_3 + b_1a_2a_3 + b_2a_1a_3 + b_3a_2a_3 \\
\theta_2 &= c(a_1a_2 + a_2a_3 + a_1a_3) - b_1(a_2 + a_3) \\
&\quad - b_2(a_1 + a_3) - b_3(a_1 + a_2) \\
\theta_3 &= b_1 + b_2 + b_3 - c(a_1 + a_2 + a_3) \\
\theta_4 &= c \\
\theta_5 &= a_1a_2a_3 \\
\theta_6 &= -(a_1a_2 + a_2a_3 + a_1a_3) \\
\theta_7 &= a_1 + a_2 + a_3 \\
\theta_8 &= (1 - (\theta_5 + \theta_6 + \theta_7))V_{ocv}
\end{aligned} \tag{2.7}$$

A RLS algorithm with a forgetting factor is then employed to the regression model [36]. The RLS algorithm is known for its computational efficiency and stability. Since the RLS algorithm guarantees a positive-definite and symmetric covariance matrix, it is numerically stable [36]. In order to track the variation of parameters, a forgetting factor is considered in the RLS. The battery electrical parameters are then generated from the output of this algorithm. The parameters $c, a_i, b_i, i = 1, 2, 3$ can be calculated from the estimated θ by solving eq.2.7 . Then, the battery electrical parameters $R_0, R_i, C_i, i = 1, 2, 3$ and V_{ocv} can be obtained from these parameters. In the next section, the obtained parameters are employed to estimate the SoC with the SVSF strategy.

2.3 SoC Estimation And Experimental Results

2.3.1 SoC Estimation Using SVSF

This section presents the combination of the RLS method for parameter estimation with the SVSF strategy for SoC estimation. The SVSF approach is a predictor-corrector method [54]. The SVSF can be utilized for observable and differentiable systems for the following class of systems:

$$\begin{aligned} x_{k+1} &= f(x_k, u_k, w_k), \\ z_k &= Hx_k + v_k \end{aligned} \tag{2.8}$$

The SVSF method can be described as follows [51]:

- Prediction: The a-priori state estimate is obtained by using an estimated model.

$$\hat{x}_{k+1|k} = f(\hat{x}_{k|k}, u_k),$$

$$\hat{z}_{k+1|k} = \hat{H}\hat{x}_{k+1|k} \tag{2.9}$$

$$e_{z_{k+1|k}} = z_{k+1} - \hat{z}_{k+1|k} \tag{2.10}$$

- Correction: The updated state is obtained by using a gain to refine the a-priori estimate into its a-posteriori form.

$$\hat{x}_{k+1|k+1} = \hat{x}_{k+1|k} + K_{SVSF_k} e_{z_{k+1|k}},$$

$$\hat{z}_{k+1|k+1} = \hat{H}\hat{x}_{k+1|k+1} \tag{2.11}$$

$$e_{z_{k+1|k+1}} = z_{k+1} - \hat{z}_{k+1|k+1} \tag{2.12}$$

The SVSF's gain K_{SVSF_k} is defined as follows [54]:

$$K_{SVSF_k} = \hat{H}^{+} diag\big[|e_{z_{k|k-1}}| + \gamma |e_{z_{k-1|k-1}}|\big).sat(\frac{e_{z_{k|k-1}}}{\psi})]diag(e_{z_{k|k-1}}), \tag{2.13}$$

The RLS online parameter identification method is combined with SVSF to calculate the battery parameters and SoC over time. Figure 2.2 shows an overview of the proposed algorithm. The RLS method provides updated parameters to the SVSF at each time step. The SVSF is then used to estimate the battery SoC.

2.3.2 Experimental Results

This study used a mixture of the following three driving schedules: an Urban Dynamometer Driving Schedule (UDDS), a light duty drive cycle for high speed and high load (US06) and a Highway Fuel Economy Test (HWFET) driving cycle. The driving schedule includes currents of up to 10 C across the entire SoC range of 20% to 90%. The aging data is experimental and has been collected for both new and aged battery cells [16]. Figure 2.3 shows the current, the measured terminal voltage and the battery SoC for new and aged battery cells. The difference SoC estimates

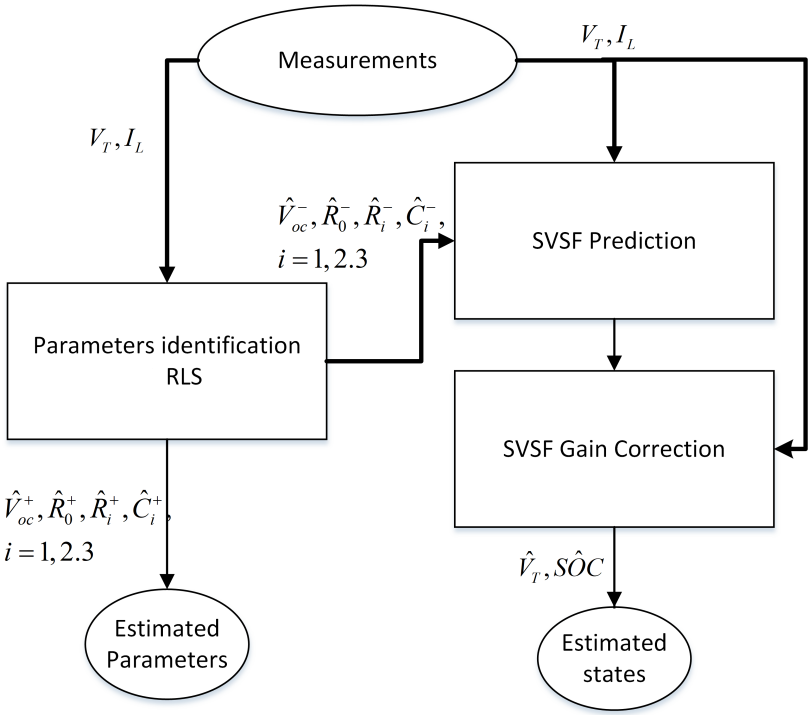

Figure 2.2: The proposed dual estimation algorithm.

for the aged versus new battery cells shows the importance of updating the model parameters as the battery ages. The proposed algorithm remedies this problem.

Figures 2.4 and 2.5 depict the estimated R_0 and open circuit voltage (V_{ocv}) for new and aged battery cells using RLS. The results show that the model parameters change over the entire driving cycle at different SoC level as well as the battery age.

Table 2.1 shows the identified value of model parameters over the entire driving cycle for new and aged battery cells. C_2 and C_3 were almost constant for a range of SoC. The results show that the resistance increases and the capacity decreases as the battery ages as expected. Parameter estimation improves the accuracy of terminal voltage and SoC estimation using the SVSF approach as shown in Figures 2.6 to 2.9. The SVSF parameters used for the simulation are given in Table 2.2 for new

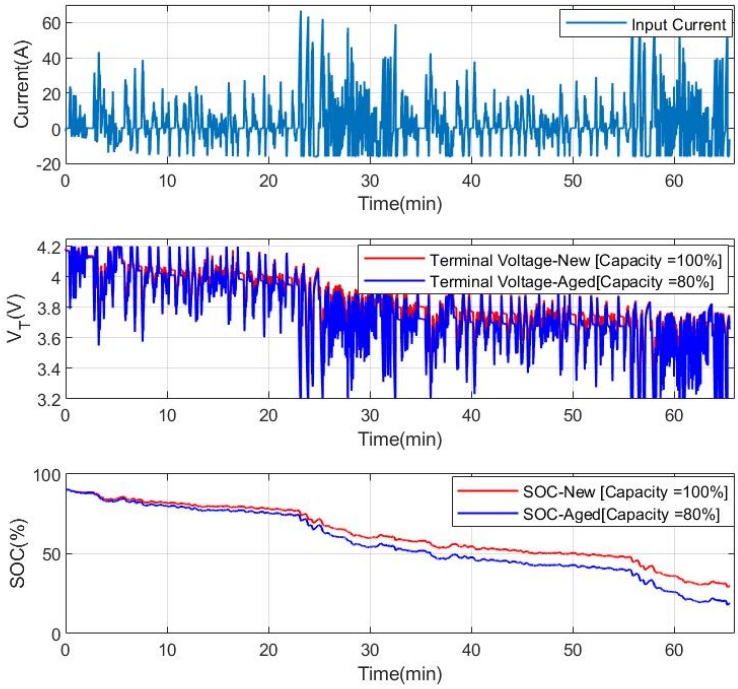

Figure 2.3: Current, Voltage, and SoC for new and aged battery with experienced driving cycle.

and aged battery cells. The Root Mean Square Error (RMSE) between the actual terminal voltage and SoC and the estimated ones are provided in Table 2.3.

2.4 Conclusion and Future Works

In this paper, an online parameter estimation strategy using RLS with a forgetting factor is combined with a state estimation strategy using the Smooth Variable Structure Filter (SVSF) for obtaining the battery SoC and the terminal voltage. The proposed dual estimation approach was then validated using experimental data for new and aged battery cells. A third order equivalent circuit-based battery model

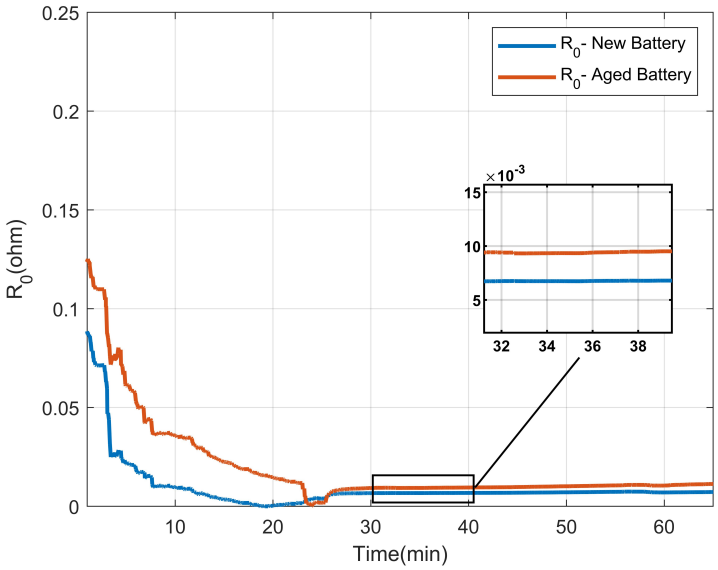

Figure 2.4: Identification result of R_0 by RLS.

(OCV-R-3RC) was considered in this study. The results showed that the identified parameters change with changing SoC as well as SoH. The resistance and capacity of the model change as expected when the battery ages. It was also shown that the online parameter estimation results in more accurate SoC and terminal voltage estimation. Future research involves considering other factors such as temperature and cell-balancing, which can affect the battery parameters, in battery model.

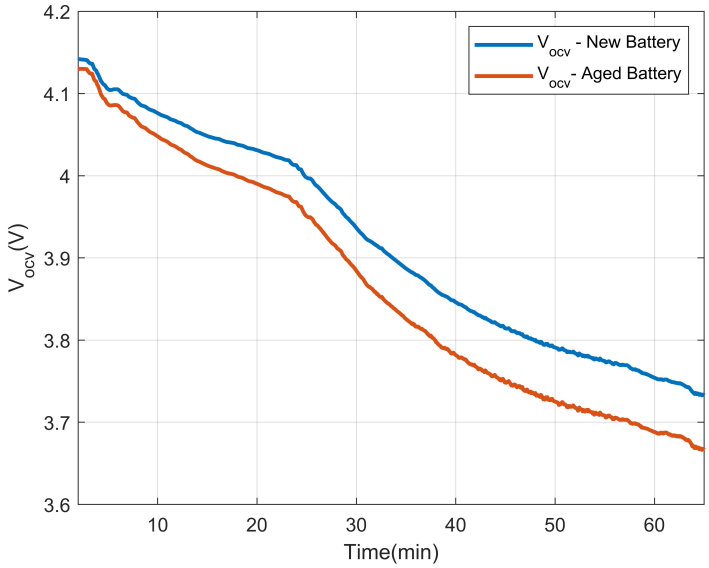

Figure 2.5: Identification result of V_{ocv} by RLS.

Table 2.1: Identification results of 3RC model parameters at different SoC levels.

SOC(%)		20	30	40	50	60	70	80	90
$R_1(m\Omega)$	New cell	0.917	1.14	0.89	0.93	0.41	0.61	1.29	0.724
	Aged cell	1.02	0.85	1.1	0.49	1.57	1.12	1.7	0.975
$R_2(m\Omega)$	New cell	1.02	0.85	0.68	0.49	1.57	1.11	0.68	0.98
	Aged cell	1.2	1.2	0.89	0.93	0.41	1.2	1.29	2.21
$R_3(m\Omega)$	New cell	1.02	0.853	0.69	0.71	0.35	1.2	0.681	0.687
	Aged cell	1.12	6.1	0.69	0.71	0.35	1.2	0.681	1.498
$C_1(F)$	New cell	33168	37344	27534	14417	19682	29433	26311	16231
	Aged cell	33165	37244	27530	14415	19682	29341	26305	16244

Table 2.2: SVSF Parameters for New and Aged battery.

SVSF Parameters	γ	ψ
New cell	0.807	1.44
Aged cell	0.6241	2.7167

Table 2.3: RMSE of estimated states by SVSF.

State	New Cell	Aged Cell
V_T RMSE	.003325	0.0179
SOC(%) RMSE	1.817	3.489

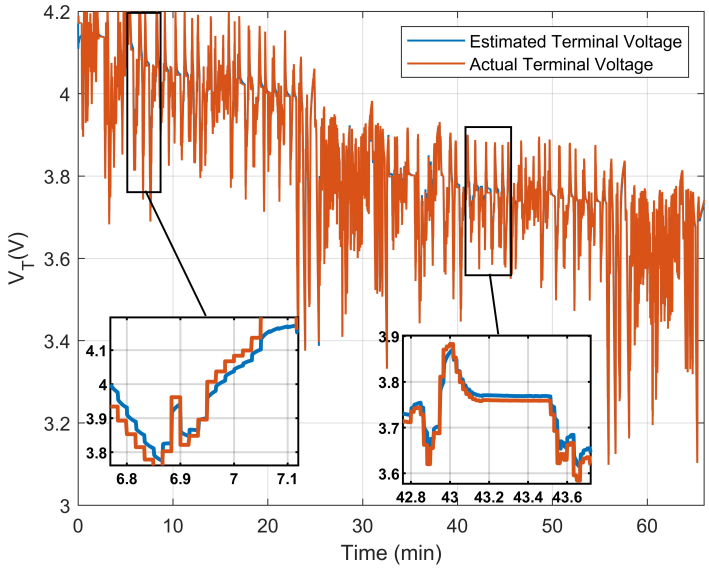

Figure 2.6: Estimated vs. actual terminal voltage by SVSF for new battery [Capacity = 100%].

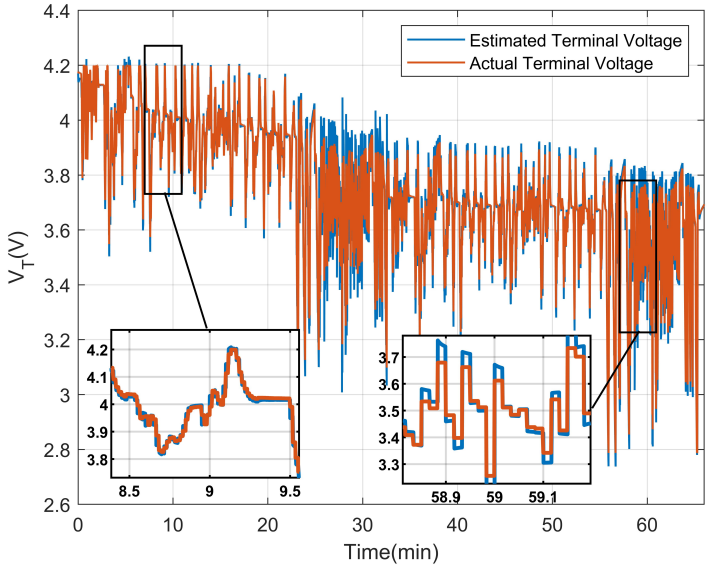

Figure 2.7: Estimated vs. actual terminal voltage by SVSF for aged battery [Capacity = 80%].

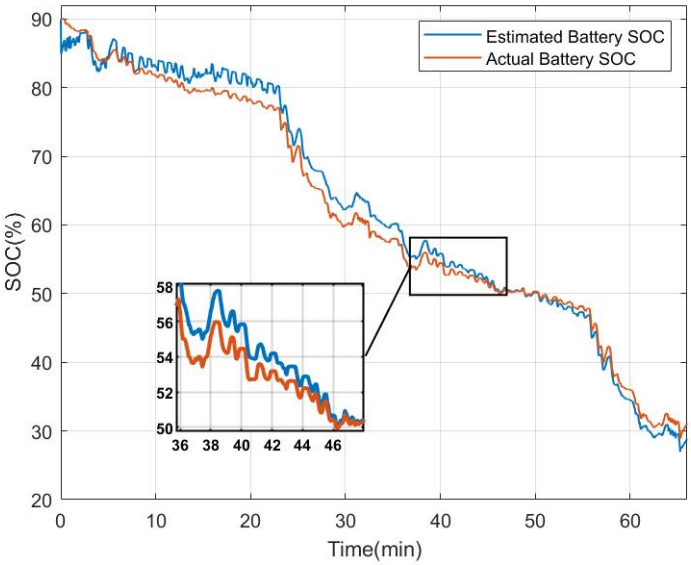

Figure 2.8: Estimated vs. actual SoC by SVSF for new battery [Capacity = 100%].

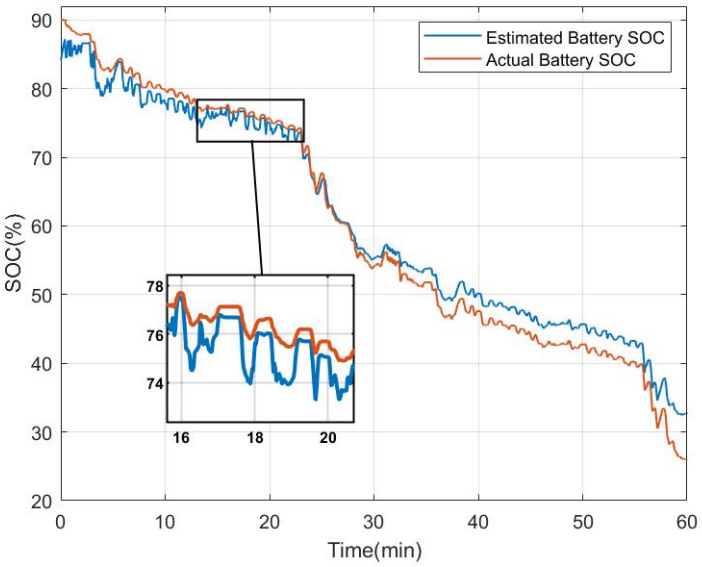

Figure 2.9: Estimated vs. actual SoC by SVSF for aged battery [Capacity = 80%].

Chapter 3: Interacting Multiple Model Strategy for Electric Vehicle Batteries State of Charge/Health/Power Estimation

Sara Rahimifard, Ryan Ahmed, Saeid Habibi

Department of Mechanical Engineering, McMaster University, Hamilton, ON, Canada

This paper is published in 2021 IEEE Access, vol 9, pp. 109875 - 109888, doi: 10.1109/ACCESS.2021.3102607. This paper is republished here with permission.[1]

Abstract: States estimation of Lithium-ion (Li-ion) batteries is an essential element of Battery Management Systems (BMSs) to meet the safety and performance requirements of electric and hybrid vehicles. Accurate estimations of the battery's State of Charge (SoC), State of Health (SoH), and State of Power (SoP) are essential for safe and effective operation of the vehicle. They need to remain accurate despite the changing characteristics of the battery as it ages. This paper proposes an online adaptive strategy for high accuracy estimation of SoC, SoH and SoP to be implemented onboard of a BMS. A third-order Equivalent Circuit Model (ECM) structure

[1]In reference to IEEE copyrighted material which is used with permission in this thesis, the IEEE does not endorse any of McMaster's products or services. Internal or personal use of this material is permitted. If interested in reprinting/republishing IEEE copyrighted material for advertising or promotional purposes or for creating new collective works for resale or redistribution, please go to `http://www.ieee.org/publications_standards/publications/rights/rights_link.html` to learn how to obtain a License from RightsLink.

is considered with its state vector augmented with two more variables for estimation including the internal resistance and SoC bias. An Interacting Multiple Model (IMM) strategy with a Smooth Variable Structure Filter (SVSF) is then employed to determine the SoC, internal resistance, and SoC bias of a battery. The IMM strategy results in the generation of a mode probability that is related to battery aging. This mode probability is then combined with an estimation of the battery's internal resistance to determine the SoH. The estimated internal resistance and the SoC are then used to determine the battery SoP which provides a complete estimation of the battery states of operation and condition. The efficacy of the proposed condition-monitoring strategy is tested and validated using experimental data obtained from accelerated aging tests conducted on Lithium Polymer automotive battery cells.

3.1 Introduction

Electric (EVs) and Hybrid Electric (HEVs) Vehicles are creating a disruptive change in the automotive industry as they present a sustainable alternative to their fossil-fuel based counterparts. The EVs energy storage system consists of a battery pack which is the key to commercial success of such vehicles [12].

Although battery technology is thriving, Lithium-ion (Li-ion) batteries remain the most common in EV and HEV applications due to their high energy and power densities, and long lifetime. Along with the growth of battery technology, the performance of a Battery Management System (BMS) is critically important to ensure safety, and reliability of the battery pack [81]. A comprehensive review of different energy management methods has been presented in [82] for EV and HEV applications. These methods can be used to optimize the performance of a battery. Included

in its functionality, the BMS must also provide an accurate estimation of the State of Charge (SoC), State of Health (SoH), and the State of Power (SoP) of a battery pack [12, 28].

The SoC is an indicator of charge remaining in the battery pack, similar conceptually to the gas gauge in fossil-fuel vehicles. Since there is no sensor available to directly measure the battery SoC, it needs to be estimated from measurements such as terminal voltage, temperature and current. Therefore, an accurate and reliable estimation strategy is critical for maintaining and optimizing battery operations. It also impacts safety as an accurate estimation of SoC in the BMS can prevent the battery from being over-charged or limit the rate of current in terms of charge or discharge to maintain a safe operating temperature [67].

SoC estimation techniques can generally be classified into conventional coulomb counting, direct methods and indirect methods. The direct methods are based on direct measurements such as terminal voltage, impedance or Open Circuit Voltage (OCV) to calculate the battery SoC [23, 31, 83].

Coulomb counting method is the simplest and most common technique used to calculate the battery SoC. This method can be implemented irrespective of battery chemistry and is usually employed as the base technology for SoC estimation onboard of a BMS. However, this approach requires regular calibration due to measurement errors and noise. It also needs a knowledge of the initial SoC [84].

Several enhancements on this method have been proposed in [84, 85, 86, 87]. In [84], a piece wise linear approximation of the functional relation between the OCV and SoC is used to re-calibrate the battery capacity for the SoC calculation. In [85], a least-square based coulomb counting method is provided combined with the

measurement of the open circuit voltage of a battery at rest for finding the initial value of the battery SoC. In [86], Peukert's law is expanded for the discharging process combined with the coulomb counting technique for the charging process to provide a SoC estimation.

Despite the proposed improvements, coulomb counting suffers from being inaccurate due to the uncertainties of measurements and determination of the initial SoC. Furthermore, a regular re-calibration is needed as the battery ages to ensure the accuracy of the SoC with respect to battery capacity [88]. Therefore, closed-loop estimation methods have been of great interest. The so-called indirect strategies are very practical for EV and HEV applications including, but not limited to, fuzzy logic-based estimation, artificial neural networks and filter/observer-based techniques. A robust and stable estimation method along with a reliable battery model must be employed to estimate the battery SoC using filter-based techniques [89]. Fusion-based methods with Machine Learning (ML) can also be used to estimate the states of a battery. However, in most ML applications, large volume of data is needed for initial training. In applications where a model is establish or readily identifiable, it is more convenient to use model-based strategies such as in the case of batteries where the model can provide additional insight into the internal dynamics of the system [20, 90].

Battery models can be categorized into electrochemical and Equivalent Circuit Models (ECMs). An electrochemical model represents the internal reactions and physics of a battery cell. However, due to their high computational complexity, it is quite challenging to use them with estimation algorithms and in real-time. On the other hand, ECMs can be easily parameterized by experimental data using system identification techniques. Although the identified parameters of ECM models do not

reflect the physical reaction within a battery cell, the accuracy of SoC estimation is sufficient for a BMS within bounded operating regions [91, 92]. However, the battery model considered onboard of a BMS, can not represent the inevitable degradation happening inside the battery over time. The BMS should therefore be able to indicate the battery SoH and determine its capacity to store energy. An indicator for SoH is the internal resistance or the capacity of the battery. The aging affects the battery's characteristics and in turn its model. Therefore, the BMS must be able to update the parameters of the model as the battery ages.

Modifications to model parameters can be performed by different techniques such as parameter estimation and model selection [93, 94]. Parameter estimation techniques take available measurements of a battery to estimate model parameters over time as presented in [95, 96, 97]. However, adaptation based on the measurements suffer from the problem of observability and usually entails optimization. Adaptation on its own is therefore not sufficient to guarantee adaptation stability and avoid overparameterization [94]. A model selection and updating strategy would be also required to switch between predefined models usually contained within a library of models with parameters that are accessible through a look-up table. These models can be optimized to capture the changing dynamics of the battery while aging or operating at different regions. This method of model selection not only guarantees stability, but also provides information on the SoH concurrently with SoC. A post-processing method is presented in [93] to estimate parameter values of a reduced-order physics-based model for different states of a battery life.

The performance of a BMS depends as much on the accuracy of states as on the estimation of model parameters. The states of a system can be estimated using

a filter, based on a dynamic model along with sensor measurements. One of the most common estimators is the Kalman Filter (KF); it has been applied to problems including state and parameter estimation, target tracking, signal processing, fault detection and diagnosis. However, this filter can be applied only when the system model is largely and known, the system and measurement noise are white, and the states have initial conditions with known means and variances. For nonlinear systems, the Extended KF (EKF) is one of the most common estimation strategies and has been widely used for management of li-ion batteries [98]. Other methods considered in BMS include the Particle Filter (PF), the Quadrature KF (QKF), and the Unscented KF (UKF) [59, 99].

Robust strategies have been also proposed to decrease the effect of modeling error and uncertainties such as the Variable Structure Filter (VSF) [51] and the Smooth VSF (SVSF) [54]. The SVSF is a method based on sliding mode theory which uses discontinuous gain and a smoothing boundary layer. This method enhances robustness for the SoC estimation. An improved version of SVSF is proposed in [57] using a Variable Boundary Layer (SVSF-VBL) which is more accurate in the presence of varying noise and modeling uncertainties. However, system observability has to be guaranteed in order to use these algorithms [91].

Multiple Model (MM) strategies exploit a finite number of models to provide robustness and adaptability against uncertainties. The MM methods can be considered as being adaptive techniques including renditions as static MM, dynamic MM, Generalized Pseudo-Bayesian (GPB), and the Interacting MM (IMM) [100, 101, 102]. In [103], the combination of IMM with the SVSF was proposed to address fault detection and diagnosis problems. The result reported from IMM-SVSF showed a significant

improvement in estimation accuracy.

This paper includes the following contributions:

1. A modified equivalent circuit model formulation is presented that considers observability in the context of estimating not only the states but also parameters related to the SoH of the battery including the internal resistance, the SoC, and its bias. In the proposed model, the estimated SoC from the conventional coulomb counting method is considered as a measurement for the system. The bias resulting from coulomb counting is then defined as a state to be estimated.

2. An associated estimation strategy is employed which is a combination of IMM with SVSF-VBL approach (IMM-SVSF-VBL). It involves use of multiple models, each for a different state of life of the battery. The proposed approach provides an accurate and robust estimation for the battery states including its SoC and the internal resistance. The battery's SoH is estimated by fusing the results from two approaches: the estimated internal resistance and the model selection probabilities obtained from the IMM-SVSF-VBL strategy.

3. A combined strategy is proposed for estimating the battery SoP by using the estimated internal resistance along with the battery's SoC.

The outline of this paper is as follows: Section 3.2 presents the proposed battery estimation model. Section 3.3 investigates the observability of the new model. The proposed estimation strategy for SoC is presented in Section 3.4 and the co-estimation technique is introduced in Section 3.5. The experimental and validation results are demonstrated in Section 3.6. Section 3.7 contains the conclusions of the work.

3.2 Modeling

ECMs are commonly utilized to model li-ion batteries as shown in Figure 3.1. An ECM model links the OCV of the battery to its SoC. Its multiple Resistance-Capacitance (RC) branches are used to capture the transients and a series resistance defined as internal resistance (R_{in}) relates the terminal voltage to the input. A proper model structure is required to describe the behavior of a battery especially when it ages. As batteries age, higher order models are better suited to capture their dynamic characteristics at the risk of overparametrization. In this article, a third-order model is chosen so as to minimize the possibility of overparametrization as well as providing a trade-off between complexity and accuracy for real-time BMS implementations [104].

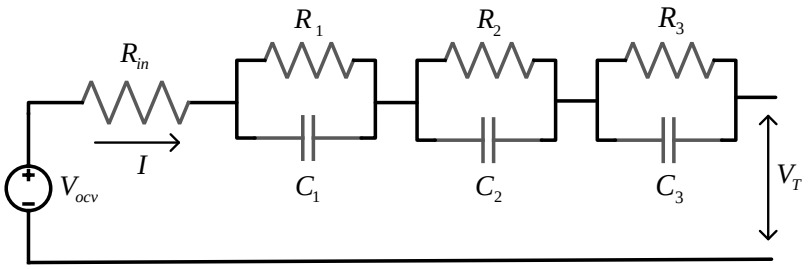

Figure 3.1: Third-order equivalent circuit battery model.

The discrete-time state equations of the battery model in Figure 3.1 are as follows,

$$
\begin{aligned}
V_{1,k+1} &= (1 - \frac{\Delta T}{R_1 C_1}) V_{1,k} + \frac{\Delta T}{C_1} i_k, \\
V_{2,k+1} &= (1 - \frac{\Delta T}{R_2 C_2}) V_{2,k} + \frac{\Delta T}{C_2} i_k, \\
V_{3,k+1} &= (1 - \frac{\Delta T}{R_3 C_3}) V_{3,k} + \frac{\Delta T}{C_3} i_k, \\
SOC_{k+1} &= SOC_k - \frac{\eta \Delta T}{C_n} i_k
\end{aligned} \tag{3.1}
$$

The terminal voltage is the output of the model and is obtained as,

$$V_{T,k} = V_{ocv}(SOC_k) - V_{1,k} - V_{2,k} - V_{3,k} - R_{in} i_k \tag{3.2}$$

In an electrochemical battery, the parameters vary with SoC and temperature. Therefore, model parameters can be considered constant only within a small operating range of SoC, temperature and current level [16]. Switching between models according to the operating region of the battery can be used as a mean for parameter estimation [77, 105]. If the observability condition is satisfied, model switching can be complemented by direct parameter estimation including the internal resistance (R_{in}). Here, the internal resistance is considered as a state described with the following equation,

$$R_{in,k+1} = R_{in,k} + w_{r_k} \tag{3.3}$$

where w_{r_k} is white noise. The internal resistance of a li-ion battery reflects its aging and power capability [106].

Coulomb counting method is a common technique for SoC estimation for a BMS, defined with the following Equation [12],

$$SOC(t) = SOC_0 - \frac{1}{C_n} \int_0^t \eta i(\tau) d\tau \tag{3.4}$$

where SOC_0 is the initial value of the battery SoC. A bias may exist on the calculated SoC with this method, due to the inaccurate SOC_0 and the current sensor. In addition, the nominal capacity of the battery decreases as the battery ages. To

overcome the issue, coulomb counting can be combined with model-based estimation by considering the calculated SoC as being a measurement as an extension of $i(t)$. As such if SoC is a measurement according to Equation 3.4 (as derived from the current), then the proposed strategy is to treat the SoC bias as a state with slow dynamics to be estimated as follows,

$$b_{k+1} = b_k + w_{b_k} \tag{3.5}$$

where w_{b_k} is white noise. Then SoC measure includes this bias such that,

$$SOC_{m,k} = SOC_k + b_k \tag{3.6}$$

The state-space form of the proposed model can be described as,

$$x_{k+1} = f(x_k) + g(x_k)u_k, \tag{3.7}$$

$$y_k = h(x_k, u_k) \tag{3.8}$$

where $x \in X$, $u \in \mathbb{R}$, $y \in \mathbb{R}^m$, $f : X \to \mathbb{R}^n$, $g : X \to \mathbb{R}^n$ and $h : X \to \mathbb{R}^m$ are all differentiable functions.
The state and measurement vectors are $x_k = \begin{bmatrix} V_{1,k} & V_{2,k} & V_{3,k} & SOC_k & R_{in,k} & b_k \end{bmatrix}^{\mathrm{T}}$ and $y_k = \begin{bmatrix} V_{T,k} & SOC_{m,k} \end{bmatrix}^{\mathrm{T}}$, respectively. Note that in this model $f(x_k)$ is linear and $f(x_k) = Ax_k$ and $g(x_k) = B$ are given as,

$$A=\begin{bmatrix} G_3 & 0_3 \\ 0_3 & I_3 \end{bmatrix} \quad B=\Delta T \begin{bmatrix} \frac{1}{C_1} \\ \frac{1}{C_2} \\ \frac{1}{C_3} \\ \frac{-\eta}{C_n} \\ 0 \\ 0 \end{bmatrix} \tag{3.9}$$

where $G_3 \in \mathbb{R}^{3\times 3}$ is defined as,

$$G_3 = \begin{bmatrix} 1-\frac{\Delta T}{R_1 C_1} & 0 & 0 \\ 0 & 1-\frac{\Delta T}{R_2 C_2} & 0 \\ 0 & 0 & 1-\frac{\Delta T}{R_3 C_3} \end{bmatrix} \tag{3.10}$$

The output equations are nonlinear functions as defined by Equations 3.2 and 3.6.

3.3 Nonlinear Observability

An estimation method cannot be employed unless the system observability is guaranteed. This section investigates the observability of the proposed battery model.

3.3.1 Distinguishability and Observability

A full rank observability matrix can guarantee the global observability of a linear time-invariant system defined by a state-space representation. Determining observability of a nonlinear system is more challenging than a linear one. Thus, only local

observability can be analyzed. To illustrate the observability of a nonlinear system a few concepts are required to be introduced.

Definition 3 (see [65]). *For a system represented by Equations 3.7 and 3.8, x_0 and x_1 are declared to be distinguishable states if there exists an input function $u(.)$ such that*

$$y(k, x_0, u) \neq y(k, x_1, u) \tag{3.11}$$

for a finite time. The system is locally observable at $x_0 \in X$ if there exists a neighborhood N of x_0 such that every $x \in N$ excluding x_0 is distinguishable from x_0. Therefore, the system is called locally observable if it is locally observable at each $x \in X$.

A system is globally observable if every pair of states (x_0, x_1) with $x_0 \neq x_1$ is distinguishable. It can be demonstrated that two states are distinguishable for a linear system if $y(k, x_0, u) \neq y(k, x_1, u)$ condition holds for any u. Furthermore, it can be proven that for a linear system, local observability leads to global observability. However, this is not guaranteed for a nonlinear system.

The observability of a nonlinear system can be illustrated using extended Lie-derivative.

Definition 4 (see [66]). *Suppose the output $h(x, u) = \begin{bmatrix} h_1 & h_2 & ... & h_m \end{bmatrix}^T$ is a m dimensional vector function on x and u. The gradient of $h_j, j = 1, ..., m$ denoted by dh_j is a form of,*

$$dh_j = \begin{bmatrix} \frac{\partial h_j}{\partial x_1} & \frac{\partial h_j}{\partial x_2} & ... & \frac{\partial h_j}{\partial x_n} \end{bmatrix} \tag{3.12}$$

Then the extended Lie-derivative of h with respect to f is,

$$\mathcal{L}_f h(x,u) = dh(x,u)f(x) + \sum_{i=0}^{i=\infty} \frac{\partial h(x,u)}{\partial u^i} u^{i+1} \tag{3.13}$$

The Lie-derivatives for higher order than one are obtained as,

$$\mathcal{L}_f^j h(x,u) = d\mathcal{L}_f^{j-1} h(x,u)f(x) + \sum_{i=0}^{i=\infty} \frac{\partial \mathcal{L}_f^{j-1} h(x,u)}{\partial u^i} u^{i+1} \tag{3.14}$$

The following theorem gives the sufficient condition for local observability based on the given definitions. The condition should be guaranteed for a nonlinear system to show observability.

Theorem 2 (see [65]). *For a system described by Equation 3.7 and 3.8 with the assumption of given $x_0 \in X$. Consider the form,*

$$(d\mathcal{L}_{z_s}\mathcal{L}_{z_{s-1}}...\mathcal{L}_{z_1}h_j), s \geqslant 0, z_i \in \{f, g_1, ..., g_p\} \tag{3.15}$$

evaluated at x_0 where $i = 1, ..., s$, $j = 1, ..., m$ and for $s = 0$ the expression is equal to $dh_j(x_0)$. Suppose there are n linearly independent row vectors in this set. Then the system is locally observable around x_0.

The observability condition for a linear system can also be derived from theorem

2. Based on the theorem, $\mathcal{O}_I(x,u)$ for a general nonlinear system is defined as,

$$\mathcal{O}_I(x,u) = \begin{bmatrix} dh(x,u) \\ \mathcal{L}_f h(x,u) \\ \mathcal{L}_g h(x,u) \\ \mathcal{L}_f^2 h(x,u) \\ \mathcal{L}_g^2 h(x,u) \\ . \\ . \\ . \end{bmatrix} \tag{3.16}$$

Therefore, the model described by Equations 3.7 and 3.8 is locally observable if $\mathcal{O}_I(x,u)$ has n linearly independent row vectors.

3.3.2 Observability Analysis of the Battery Model

Based on the notation on Section 3.3.1, $dh(x,u)$ for the proposed battery model in Section 3.2 is,

$$dh = \begin{bmatrix} -1 & -1 & -1 & \frac{\partial V_{ocv}}{\partial SOC} & -u & 0 \\ 0 & 0 & 0 & 1 & 0 & 1 \end{bmatrix} \tag{3.17}$$

The Lie-derivative of $d\mathcal{L}_f h$ with respect to f and g can be found as,

$$\mathcal{L}_f h = -\begin{bmatrix} (1-\frac{\Delta T}{R_1 C_1}) & (1-\frac{\Delta T}{R_2 C_2}) & (1-\frac{\Delta T}{R_3 C_3}) & -\frac{\partial V_{ocv}}{\partial SOC} & u & 0 \\ 0 & 0 & 0 & -1 & 0 & -1 \end{bmatrix} \tag{3.18}$$

$$\mathcal{L}_g h = -\begin{bmatrix} (\frac{1}{C_1}) & (\frac{1}{C_2}) & (\frac{1}{C_3}) & \frac{\eta}{C_n}\frac{\partial V_{ocv}}{\partial SOC} & 0 & 0 \\ 0 & 0 & 0 & \frac{\eta}{C_n} & 0 & 0 \end{bmatrix} \tag{3.19}$$

Based on the observability matrix defined in Equation 3.16, the battery model represented in Section 3.2 is locally observable if there is $n = 5$ independent row vectors. This condition is satisfied if $R_1C_1 \neq R_2C_2 \neq R_3C_3$. In a physical sense, if two RC pairs are equal, they can be combined into one and therefore the voltage across them are not distinctive. Since each RC pairs can be determined uniquely, then if there exists a $k \in \mathbb{Z}$ such that $\frac{\partial V_{ocv}^k}{\partial SOC^k} \neq 0$ the local observability of the battery model can be guaranteed.

3.4 SVSF-based Interacting Multiple Model

The IMM-SVSF-VBL strategy is an adaptive method that relies on a finite number of models instead of a single one. The approach can be utilized for SoC/SoH and SoP estimation since use of multiple models (each for a different age or operating point) achieves better accuracy and robustness in estimation. With battery degradation, the procedure can adjust to any changes in battery dynamics such as capacity fade or changes in internal resistance. The use of ECM with the proposed technique makes the strategy feasible for real-time application in a BMS.

3.4.1 SVSF-VBL

The SVSF approach is a predictor-corrector method based on Sliding Mode Control (SMC) and it was presented in [54]. The stability and robustness of the SVSF method has been demonstrated against uncertainties and noise in relation to the filter model. The SVSF employs a smoothing boundary layer ψ and a discontinuous gain which is similar to the SMC. The SVSF gain forces the states to converge to a neighborhood of the true value. The SVSF is applicable to any observable and differentiable system with the following class of nonlinear equations,

$$\begin{aligned} x_{k+1} &= f(x_k, u_k, w_k), \\ z_k &= h(x_k, u_k, v_k) \end{aligned} \tag{3.20}$$

The SVSF was later improved with several advancements, including the covariance formulation, time-varying smoothing boundary layer (SVSF-VBL) and combinations with different filters such as KF, EKF, UKF, Particle Filter (PF) and more [43, 55, 57, 107]. This paper employs the SVSF-VBL with a time-varying smoothing boundary layer to enhance estimation accuracy. The width of the boundary layer depends on the uncertainty of the filter model, as well as the system and measurement noise. The SVSF-VBL algorithm uses a time-varying boundary layer with saturated limits to guarantee stability and estimation convergence of the method [57]. Figure 3.2 provides an overview of the SVSF-VBL strategy.

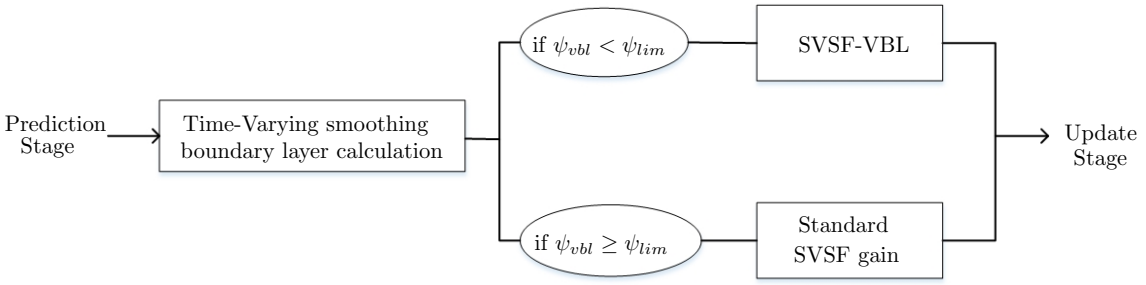

Figure 3.2: Summary of SVSF-VBL procedure [57].

The SVSF-VBL estimation process and equations are as follows, [57]:

- Prediction: The a-priori state estimate is obtained by using an estimated filter model.

$$\hat{x}_{k+1|k} = \hat{A}\hat{x}_{k|k} + \hat{B}u_k, \tag{3.21}$$

$$\hat{z}_{k+1|k} = \hat{H}\hat{x}_{k+1|k} \tag{3.22}$$

$$P_{k+1|k} = \hat{A}P_{k|k}\hat{A}^T + Q_k \tag{3.23}$$

$$e_{z_{k+1|k}} = z_{k+1} - \hat{z}_{k+1|k} \tag{3.24}$$

- Correction: The updated state is acquired using a gain to refine the a-priori estimate into its a-posteriori form.

$$S_{k+1} = \hat{H}P_{k+1|k}\hat{H}^T + R_{k+1} \tag{3.25}$$

$$E_{k+1} = |e_{z_{k+1|k}}| + \gamma|e_{z_{k|k}}| \tag{3.26}$$

$$\psi_{k+1} = (\bar{E}_{k+1}^{-1}\hat{H}P_{k+1|k}\hat{H}^T S_{k+1}^T)^{-1} \tag{3.27}$$

The SVSF gain applied to update the states for the case when $\psi_{k+1} \geqslant \psi_{lim}$ is then evaluated as follows,

$$K_{k+1} = \hat{H}^{-1}\bar{E}_{k+1}sat(e_{z_{k+1|k}}\psi_{k+1}^{-1})\bar{e}_{z_{k+1|k}}^{-1} \tag{3.28}$$

And for the case with $\psi_{k+1} < \psi_{lim}$ the SVSF gain is,

$$K_{k+1} = \hat{H}^{-1}\bar{E}_{k+1}\psi_{k+1}^{-1} \tag{3.29}$$

Finally, the a-posteriori parameters are calculated as,

$$\hat{x}_{k+1|k+1} = \hat{x}_{k+1|k} + K_{k+1}e_{z_{k+1|k}} \tag{3.30}$$

$$P_{k+1|k+1} = (I - K_{k+1}\hat{H})P_{k+1|k}(I - K_{k+1}\hat{H})^T + K_{k+1}R_{k+1}K_{k+1}^T \tag{3.31}$$

$$\hat{z}_{k+1|k+1} = \hat{H}\hat{x}_{k+1|k+1} \tag{3.32}$$

$$e_{z_{k+1|k+1}} = z_{k+1} - \hat{z}_{k+1|k+1} \tag{3.33}$$

Equations 3.21 to 3.33 summarize the SVSF-VBL strategy.

3.4.2 IMM Procedure

The IMM approach employs multiple models to capture the changing dynamics of a system. Since a battery cell ages over time, a new model is needed to describe changes in its dynamics over time. The IMM uses a library of predefined models which in this case are used in SVSF-VBL estimation filters running in parallel. The error covariance matrix quantifies the estimation error for each of these parallel filters and quantifies the applicability of the model. The error covariance matrix is used to

evaluate the mode probabilities, which represents how close the filter model is to the true characteristics of the battery [57, 108]. In this paper, multiple models are used to characterize the aging of the battery. The mode probability indicates the suitable model that captures the aging of the battery and by extension SoH of the battery [23, 57, 108].

The IMM-SVSF-VBL consists of five main steps: 1) calculation of mixing probabilities; 2) mixing stage; 3) mode-matched filtering with the SVSF-VBL; 4) mode probability determination; 5) calculation of the a-posteriori estimate and error covariance matrix. Figure 3.3 shows the strategy employed to estimate the states of a battery using 3 different models at various states of life, namely: new battery (100% capacity), mid-aged battery (90% capacity) and aged battery (80% capacity). The algorithm is demonstrated by the following equation.

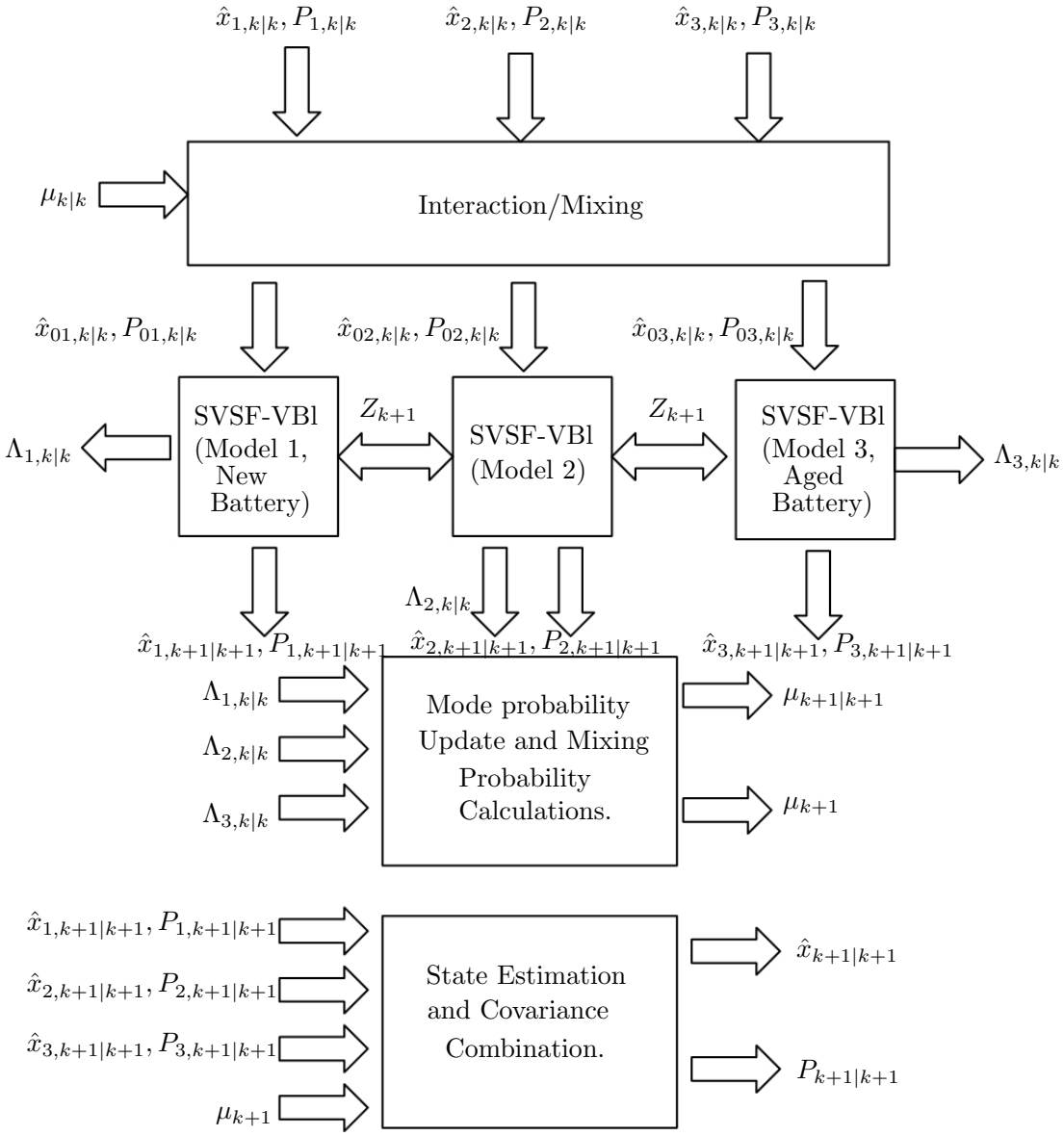

Figure 3.3: IMM-SVSF-VBL strategy for battery states estimation.

- Calculation of mixing probabilities: The mixing probability can be written as,

$$\mu_{i|j}(k-1|k-1)=\frac{1}{\bar{c}_j}p_{ij}\mu_{i|j}(k-1) \quad i,j=1,...,r \tag{3.34}$$

where the probability mass function prediction is,

$$\bar{c}_j=\sum_{i=1}^{r}p_{ij}\mu_i(k-1) \qquad j=1,...,r \tag{3.35}$$

The transition probability matrix is defined as,

$$p_{ij}=P\{M_i(k-1)|M_j(k),Z^k-1\} \tag{3.36}$$

- The Mixing step computes the mixed initial condition for the filters as,

$$\hat{x}^{0j}(k–1|k–1)=\sum_{i=1}^{r}\hat{x}^i(k–1|k–1)\mu_{i|j}(k–1|k–1) \qquad j=1,...,r \tag{3.37}$$

$$P^{0j}(k–1|k–1)=\sum_{i=1}^{r}\mu_{i|j}(k–1|k–1)\{P^i(k–1|k–1)+[\hat{x}^i(k–1|k–1)-\hat{x}^{0j}(k–1|k–1)]$$
$$[\hat{x}^i(k–1|k–1)-\hat{x}^{0j}(k–1|k–1)]^T\} \quad j=1,...,r \tag{3.38}$$

- This step involves mode-matched filtering where one iteration of the SVSF-VBL evaluates in mode j to produce a new state estimate by the provided values of the state and covariance from the mixing step. The likelihood functions of filters

in mode j are then calculated as,

$$\Lambda_j(k)=\mathcal{N}[z(k);\hat{z}^j[k|k-1;\hat{x}^{0j}(k-1|k-1)],S^j[k;\hat{P}^{0j}(k-1|k-1)]] \qquad j=1,...,r \tag{3.39}$$

- Mode probability is updated as follows,

$$\mu_j(k)=\frac{1}{c}\Lambda_j(k)\bar{c}_j \qquad\qquad j=1,...,r \tag{3.40}$$

where the normalizing constant is defined as,

$$c=\sum_{j=1}^{r}\Lambda_j(k)\bar{c}_j \tag{3.41}$$

- The a-posteriori estimated states and covariances from each filter are then combined by their mode probability to compute the outputs of the algorithm,

$$\hat{x}(k|k)=\sum_{j=1}^{r}\hat{x}^j(k|k)\mu_j(k) \tag{3.42}$$

$$P(k|k)=\sum_{j=1}^{r}\mu_j(k)\{P^j(k|k)+[\hat{x}^j(k|k)-\hat{x}(k|k)][\hat{x}^j(k|k)-\hat{x}(k|k)]^T\} \tag{3.43}$$

3.5 Battery States Co-estimation Algorithm

This section presents the co-estimation procedure proposed in this paper to estimate the SoC, SoH and SoP of a battery. The battery SoC is estimated by the IMM-SVSF-VBL presented in Section 3.4 along with its bias and the internal resistance of the battery. The SoH and SoP of the battery are then evaluated by the estimated states

of the system and measurements. Figure 3.4 illustrates the proposed strategy.

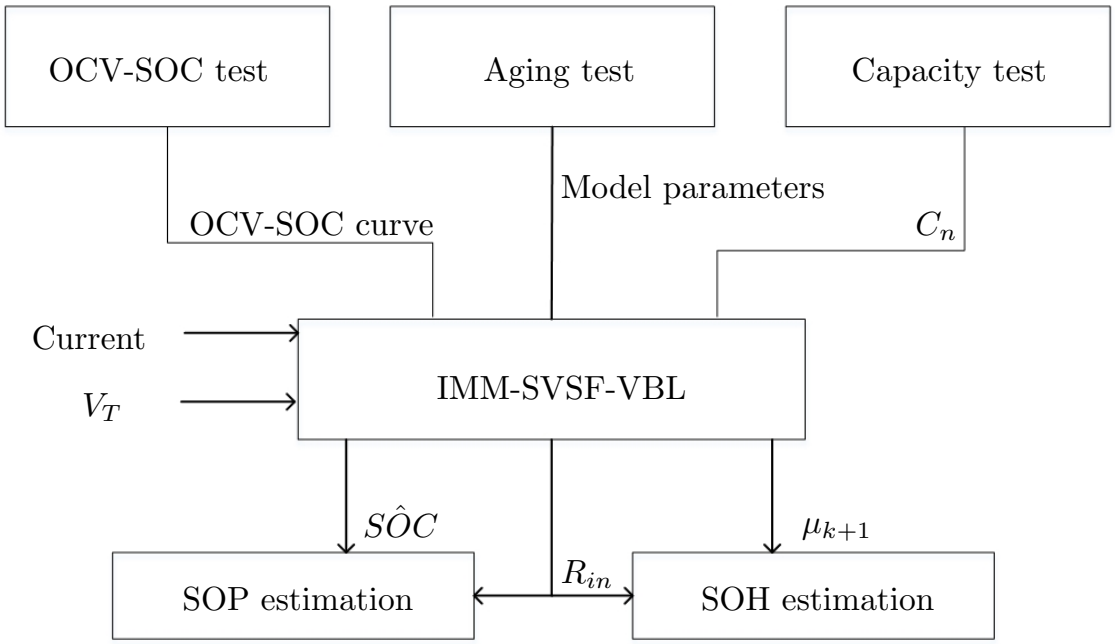

Figure 3.4: Battery states co-estimation.

3.5.1 SoH Estimation

The SoH is a measure of battery aging. It is related to battery capacity that is 100% for a new battery and for automotive application can drop to 80%. The SoH is the ratio of a full charge capacity of a battery to its nominal capacity.

$$SOH_C = \frac{C}{C_n} \times 100\% \tag{3.44}$$

SoH has been linked to different battery parameters including its impedance,

Coulombic Efficiency (CE), internal resistance and self-discharge rate [109]. The SoH is commonly measured through battery capacity and internal resistance which reflect the energy and power potential of a battery, respectively. The proposed method in this paper estimates the internal resistance of a battery in real-time as a measure of SoH. This can be stated as,

$$SOH_R = \frac{R_{EOL} - R_{in}}{R_{EOL} - R_{new}} \times 100\% \tag{3.45}$$

where R_{EOL} is the internal resistance at the end of battery life, R_{new} is the internal resistance for a new battery provided by the manufacture and R_{in} is the estimated internal resistance using the IMM-SVSF-VBL technique.

An accurate estimation of the SoH can help to prevent a sudden degradation of the battery and any potential failures. Additional information can lead to a more precise prediction of the SoH. As it was mentioned in Section 3.4, the mode probability indicates the closeness of the battery dynamics to a specific filter model. Since each model reflects a battery state of life, the mode probability can be employed as another indicator of the SoH. Based on the SoH of the predefined models, a weighting vector is specified to determine the SoH of the battery.

$$SOH_\mu \triangleq \begin{bmatrix} SOH_1 & \dots & SOH_r \end{bmatrix} \begin{bmatrix} \mu_1 \\ . \\ . \\ . \\ \mu_r \end{bmatrix} \times 100\% \tag{3.46}$$

where $0 < SOH_i < 1, i = 1, ..., r$ presents the SoH for mode i and can be defined based

on the models described for the IMM-SVSF-VBL method. In the proposed strategy and further to Equation 3.45 and 3.46, the SOH_R and SOH_μ are combined to provide a measure of the battery SoH onboard of a BMS. An adaptive weighted average is introduced to present a better and smoother outcome for the SoH estimation in the presence of noise or uncertainties.

$$SOH \triangleq \alpha SOH_R + (1-\alpha) SOH_\mu \tag{3.47}$$

The parameter α is found adaptively through the following optimization problem.

$$\begin{aligned} \min_{\alpha} \quad & (\alpha - 0.5)^2 \\ \text{s.t.} \quad & 0 < \alpha < 1 \\ & \mid SOH(k) - SOH(k-1) \mid < \epsilon \end{aligned} \tag{3.48}$$

where $\epsilon \in \mathbb{R}$ is a small positive number. The second constraint of the optimization problem can be followed from Equation 3.47.

3.5.2 SoP Estimation

The SoP is determined as the ratio of peak power to nominal power. The peak power is determined as the maximum power that a battery can persistently provide over a period of time. The SoP describes the power demands of a battery. The maximum available power for a battery is limited because the battery terminal voltage and current are always restricted within a range for battery safety. These limitations are to avoid any over-discharge or over-charge [110]. Different methods have been presented for SoP estimation considering the terminal voltage, SoC and current limitation of

a battery [24, 25, 111]. This paper considers the available current under a specific voltage and in conjunction with limiting factors for current supply usually imposed by the BMS to estimate the SoP. The maximum available charge and discharge current under the terminal voltage limits are computed as follows,

$$I_{max,vol}^{cha} = \frac{V_{max} - V_{ocv}}{R_{in}} \tag{3.49}$$

$$I_{max,vol}^{dch} = \frac{V_{ocv} - V_{min}}{R_{in}} \tag{3.50}$$

where V_{max} and V_{min} denote the voltage limits and V_{ocv} is obtained by the SoC estimation results using a look-up table. The maximum available charge/discharge currents can be evaluated as follows, taking the current limits into consideration,

$$I_{max}^{cha} = min(I_{max,vol}^{cha}, I_{max,cur}^{cha}) \tag{3.51}$$

$$I_{max}^{dch} = min(I_{max,vol}^{dch}, I_{max,cur}^{dch}) \tag{3.52}$$

where $I_{max,cur}^{cha}$ and $I_{max,cur}^{dch}$ are the charge and discharge current thresholds, respectively. Therefore, the maximum available charge/discharge power can be determined as,

$$P_{max}^{cha} = I_{max}^{cha}(V_{ocv} + I_{max}^{cha}R_{in}) \tag{3.53}$$

$$P_{max}^{dch} = I_{max}^{dch}(V_{ocv} - I_{max}^{dch}R_{in}) \tag{3.54}$$

3.6 Experiments

An aging study was conducted over 12 months and used to evaluate the proposed methodology for battery SoC, SoH and SoP estimation. The experimental setup consisted of three-channel Arbin BT2000 cycler, three NMC Lithium Polymer battery cells, three environmental chambers namely Espec and Thermotron, an AVL Lynx data acquisition system, and AVL Lynx user surface software as shown in Figure 3.6. AVL Lynx software was used for data acquisition and setting up of the test procedures. Three battery cells were tested separately in this study in an environmental chamber [16]. Three categories of tests were conducted, namely: characterization, aging, and reference tests. The characterization tests include static capacity, Hybrid Pulse Power Characterization (HPPC), and efficiency tests. Aging tests, including cycle life and calendar life, are utilized to predict battery performance. Cycle life aging tests perform accelerated aging in a short period of time.

A mid-sized EV model as derived in [16] and as shown in Figure 3.5 is used to generate the current profile from the velocity profile of a combined driving cycle. The profile is a mixture of three common driving cycles including an Urban Dynamometer Driving Schedule (UDDS); a light duty drive cycle for high speed and high load (US06); and, a Highway Fuel Economy Test (HWFET) drive cycle. These simulate different driving habits as presented in [16]. The UDDS cycle can present the driving habits of an average driver in the city. The US06 provides a high acceleration associated with an aggressive driving habit, and the HWFET presents highway driving conditions. The pack current profile is then scaled down to obtain the cell-level current profile. The aging data was collected for battery cells over time at elevated

temperatures ranging from 35° to 40° scanning the entire range of SoC from 90% to 20% [12, 16].

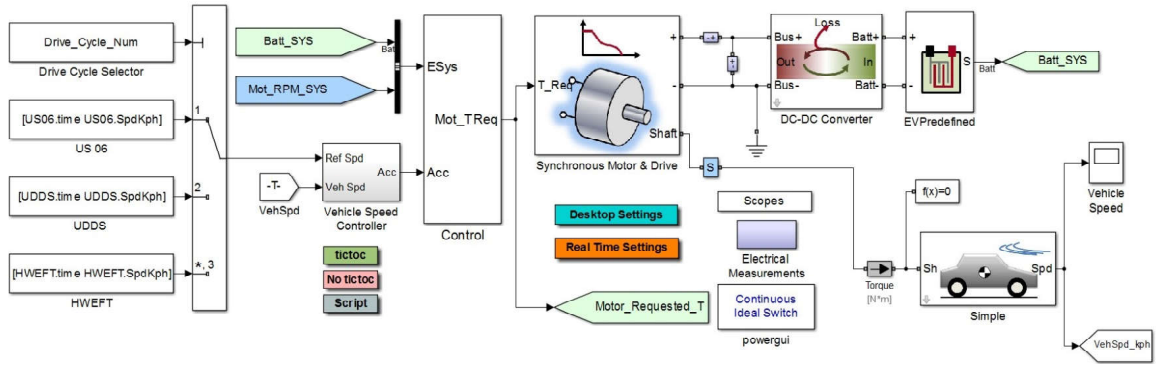

Figure 3.5: All-Electric mid-size sedan simulation model [16].

Figure 3.6: Experimental setup including cyclers, environmental chambers, and Data Acquisition systems [16].

Reference Performance Tests (RPTs), track changes in battery characteristics, is considered in this study for various states of life. Associated characterization tests conducted in series to cycling included static capacity test, OCV-SoC test, pulse

charge/discharge test, and driving cycle tests [16, 28, 29]. Figure 3.7 depicts the OCV-SoC curve of the battery obtained for different SoH. The figure illustrates that the OCV curve is correlated with SoH.

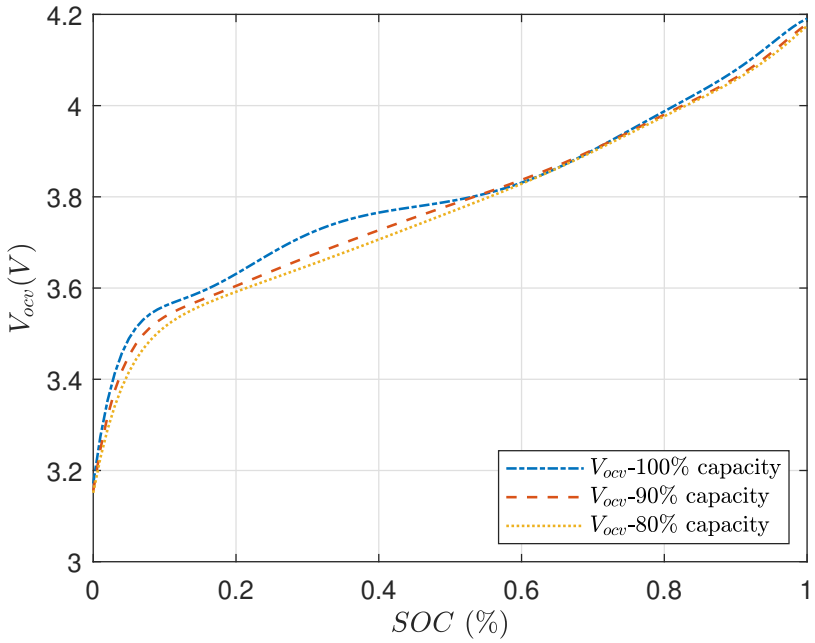

Figure 3.7: Open circuit voltage for new (100% capacity) and aged (90% and 80% capacity) battery from OCV-SoC test.

The driving profile considered in this paper is shown in Figure3.8. The driving profile is applied at different states of life including 100%, 90%, and 80% to explore the degradation behavior of the battery. Figure 3.9 demonstrates the measured terminal voltage and SoC at different SoH. It is evident from Figure 3.9a that the terminal voltage is dropping as the battery ages and therefore the battery depletes faster (as shown in Figure 3.9b). The measured SoC is evaluated from the cycler using the coulomb counting method.

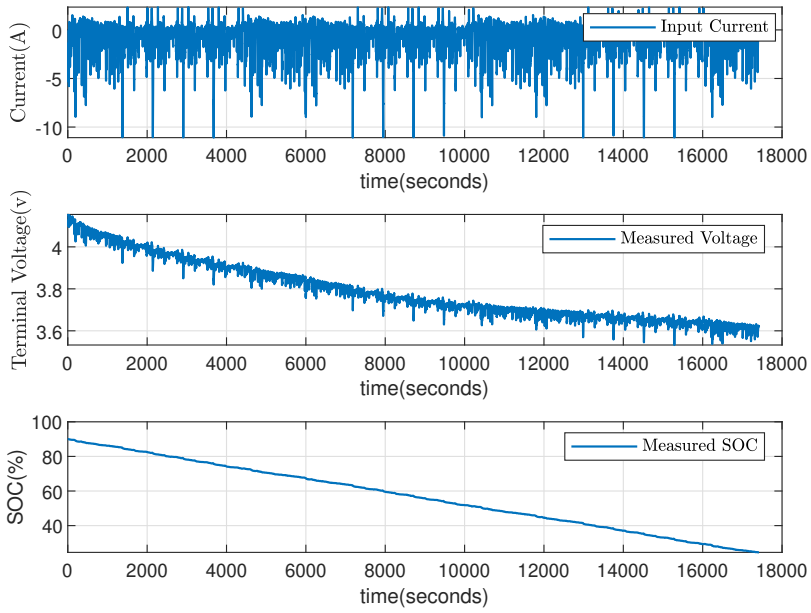

Figure 3.8: Current, voltage, and SoC of the driving schedule.

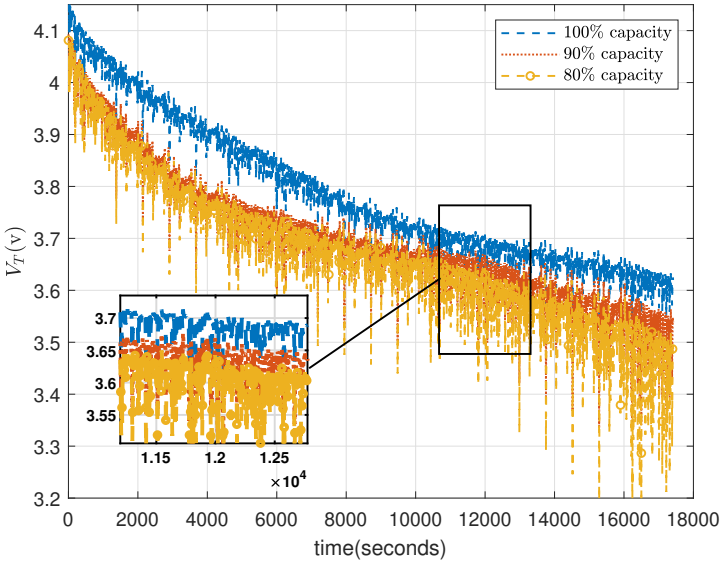

(a)

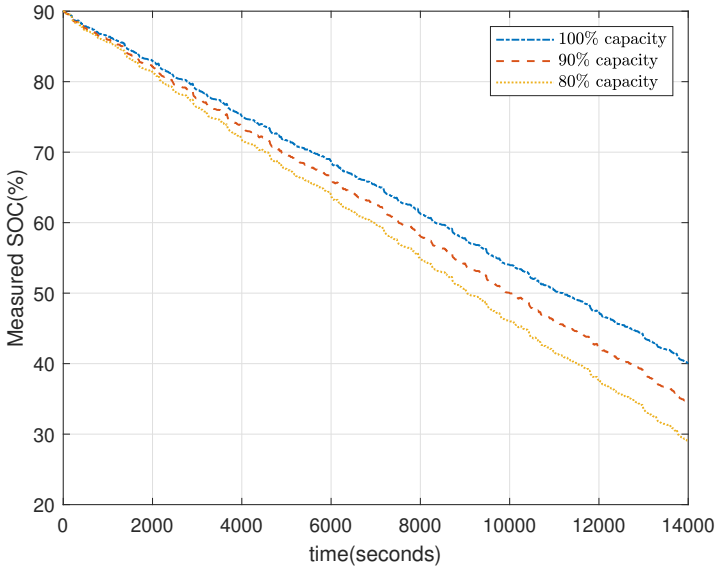

(b)

Figure 3.9: a) Terminal voltage and b) SoC for new (100% capacity) and aged (90% and 80% capacity) battery using the driving Schedule.

An important element of the estimation is the determination of the filter model.

For better performance, battery model parameters are required to change with SoC as well as SoH. A Least-Square (LS) optimization methodology is used with the collected data to identify the parameters of the battery in a range of SoC at different SoH. Table 3.1 shows the bounds of time constants ($\tau_i = R_i C_i, i = 1, 2, 3$) and resistances of the equivalent circuit model described in Section 3.2.

Table 3.1: Model Parameters bound of a third-order ECM. Example given for 60% SoC and 90% SOH.

Parameters	$R_1(\Omega)$	$R_2(\Omega)$	$R_3(\Omega)$	$\tau_1(s)$	$\tau_2(s)$	$\tau_3(s)$
Upper Bound	0.025	0.0079	0.089	1	27	355
Lower Bound	0.00117	0.000038	0.0012	0.1	8	74
Example	0.00565	0.00377	0.00908	0.162	13.34	250

In this paper, three models corresponding to 100%, 90% and 80% capacity of SoH are used and the associated bound of parameters in Table 3.1 define the three models of the IMM-SVSF-VBL approach as explained in Section 3.4. The IMM-SVSF-VBL strategy estimates the states of a battery including the internal resistance, the SoC and the SoC bias. The tuned parameters for the SVSF-VBL filters are as follows: the initial noise covariance matrix and the initial system error covariance matrix are selected as $R = diag[5, 0.095]$ and $Q = diag[10^{-8}, 10^{-8}, 10^{-8}, 10^{-10}, 10^{-10}, 10^{-10}]$, respectively. The initial value of the state error covariance matrix is set to $P = I_6$. The SVSF-VBL convergence and the initial boundary layer are chosen as $\gamma = 0.38$ and $\psi = 3.2I_2$, respectively. A Genetic Algorithm (GA) is used to tune the noise covariance matrices of the Kalman. The same noise covariance matrices are used for the SVSF-VBL filters for providing a direct comparison between the performance of the two filters. For the IMM settings, the mode transition matrix and the initial mode probability are required to be initialized. The initial pertinent filter model is

unknown at the start of the estimation process and, therefore the mode probabilities are initially selected to be equal for each mode. The time-invariant mode transition probabilities provide a mechanism for adjusting the speed at which the IMM can switch between different modes. The selected values present a moderate speed to allow a smooth mode transition and switching behavior for the IMM.

$$p = \begin{bmatrix} 0.998 & 0.001 & 0.001 \\ 0.001 & 0.998 & 0.001 \\ 0.001 & 0.001 & 0.998 \end{bmatrix}, \quad \mu = \begin{bmatrix} 1/3 \\ 1/3 \\ 1/3 \end{bmatrix} \tag{3.55}$$

Figure 3.10 shows the terminal voltage error and the percentage of SoC estimation error for the proposed strategy using the experimental data at different SoH. Two different initial conditions are considered for the battery SoC as $SOC_0 = 75\%, 85\%$ to verify the proposed methodology. It can be seen from Figure 3.10b that the proposed strategy can keep the percentage of SoC error to less than 1% with the terminal voltage error of less than 0.03 with various initial conditions over an entire range of SoC.

A comparison of the proposed procedure and the IMM-EKF method is then conducted. A simple third-order ECM structure has been considered for the IMM-EKF method. The proposed IMM-SVSF-VBL strategy uses the same initial parameters as the IMM-EKF except for the additional parameters specific to the SVSF-VBL method, namely γ and ψ. The Root Mean Square Error (RMSE) of the results are presented in Figure 3.11. The results indicate that the proposed algorithm using IMM-SVSF-VBL provides a more reliable performance. Figure 3.12 also shows the mode probability of the proposed strategy in contrast with the IMM-EKF. It is

demonstrated that the proposed strategy is superior in identifying the correct model compared to the IMM-EKF method.

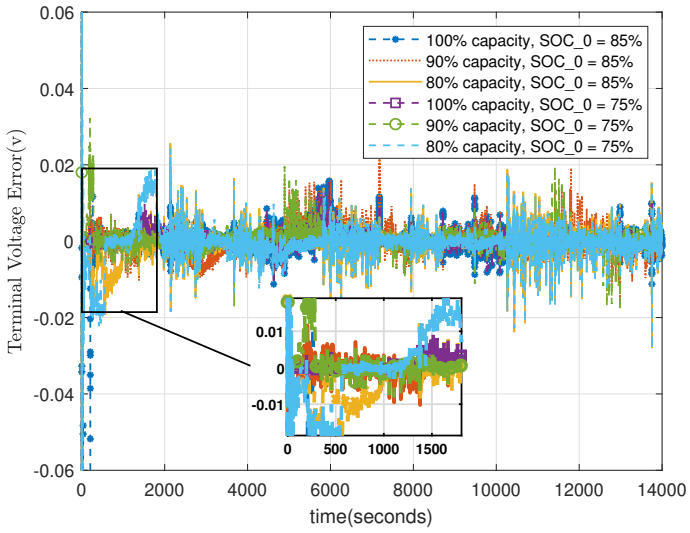

(a)

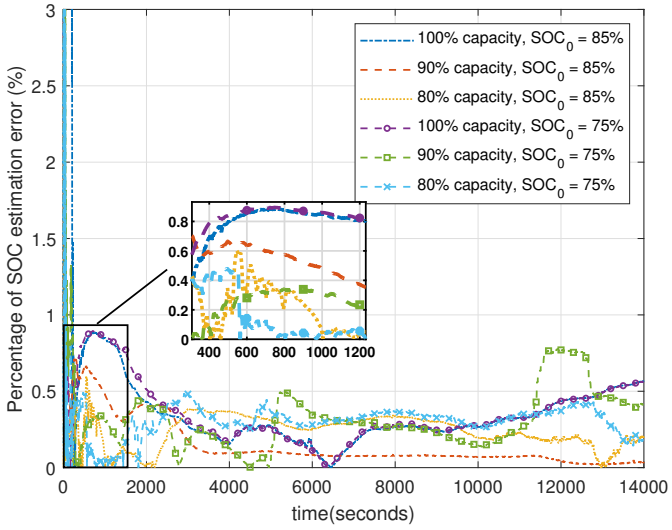

(b)

Figure 3.10: a) Estimated terminal voltage and b) percentage of SoC estimation error for new (100% capacity) and aged (90% and 80% capacity) battery using the driving Schedule.

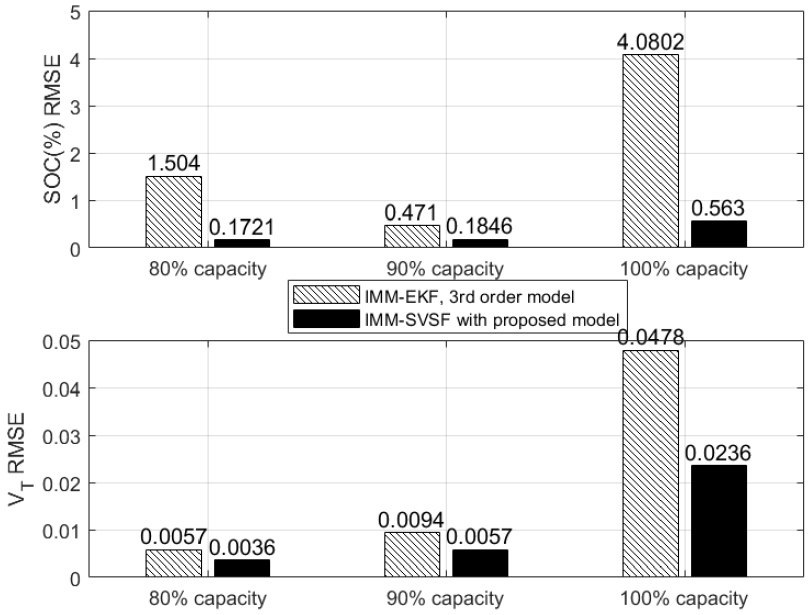

Figure 3.11: Root mean square errors with the proposed IMM-SVSF-VBL algorithm and the IMM-EKF for different SoH.

The estimated internal resistance is displayed in Figure 3.13 which is used to estimate the SoH of the battery along with the mode probability of the IMM-SVSF-VBL demonstrated in Figure 3.12. Figure 3.13 illustrates that the internal resistance increases as the battery ages. Reference points are provided in Figure 3.13, based on the characterization tests for various SoH, to verify the estimated values of the internal resistance. The internal resistance is not always a constant value which affects the estimation of the SoH. The mode probability is also considered to enhance the performance of the SoH estimation as it can identify the operating mode of the battery using Equation 3.46 where $\begin{bmatrix} SOH_1 & SOH_2 & SOH_3 \end{bmatrix} = \begin{bmatrix} 1 & 0.9 & 0.8 \end{bmatrix}$. The estimated SoH obtained by the proposed method in Section. 3.5.1 is shown in Figure 3.14. Figure 3.15 shows the estimated SoC bias which is in turn used to refine the measure of

SoC obtained by coulomb counting according to Equation 3.4. A larger SoC bias will increase the SoC estimation error which is compensated by the estimated SoC bias. The existing bias could affect the real-time estimation of the states. However, the proposed strategy is able to provide an accurate estimation of the states of the battery by refining the measured value of SoC.

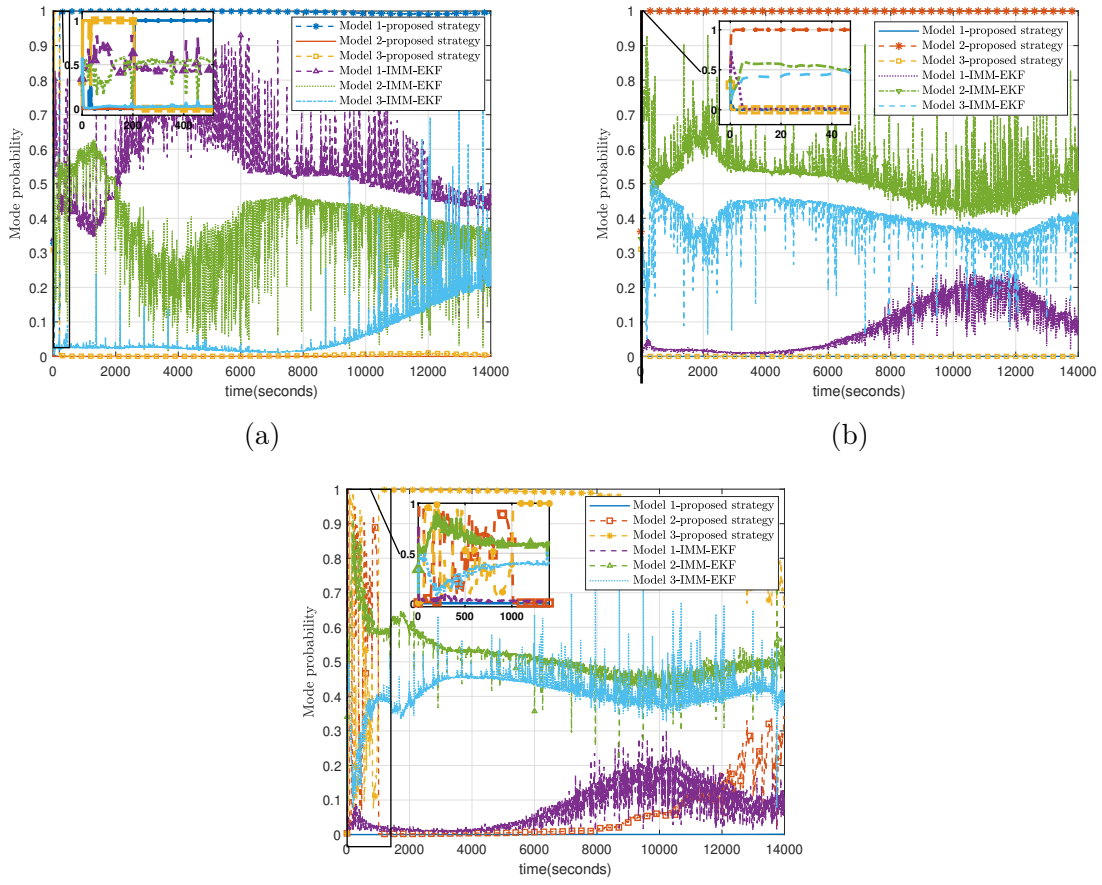

Figure 3.12: Mode probability of the proposed IMM-SVSF-VBL and IMM-EKF algorithms for new (a) 100% capacity) and aged (b) 90% and c) 80% capacity) battery using the driving schedule.

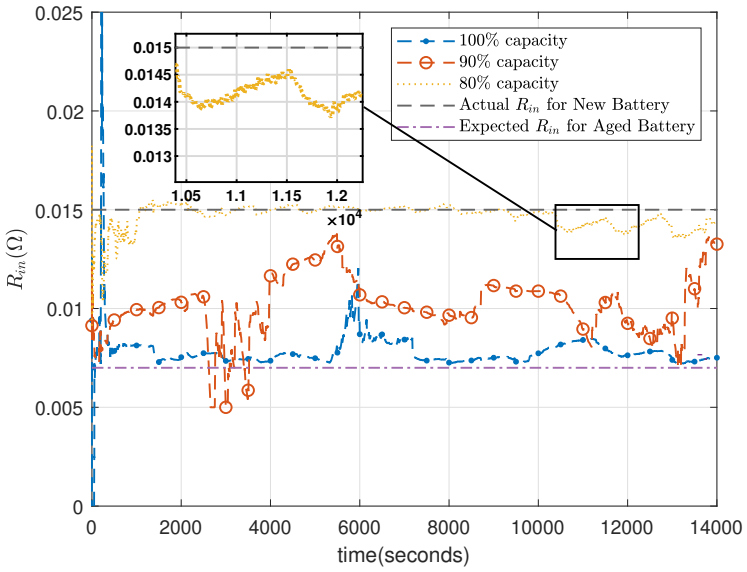

Figure 3.13: Estimated internal resistance by the IMM-SVSF-VBL strategy for new (100% capacity) and aged (90% and 80% capacity) battery using the driving Schedule.

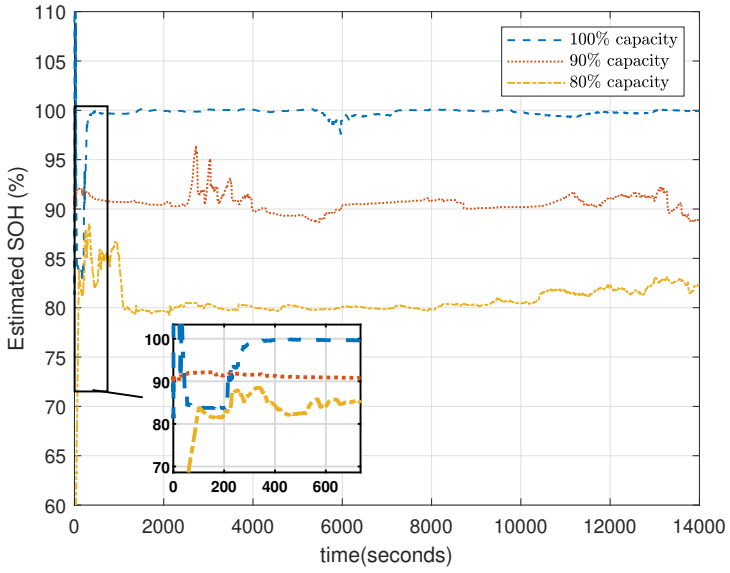

Figure 3.14: Estimated SoH by the proposed algorithm using the driving Schedule.

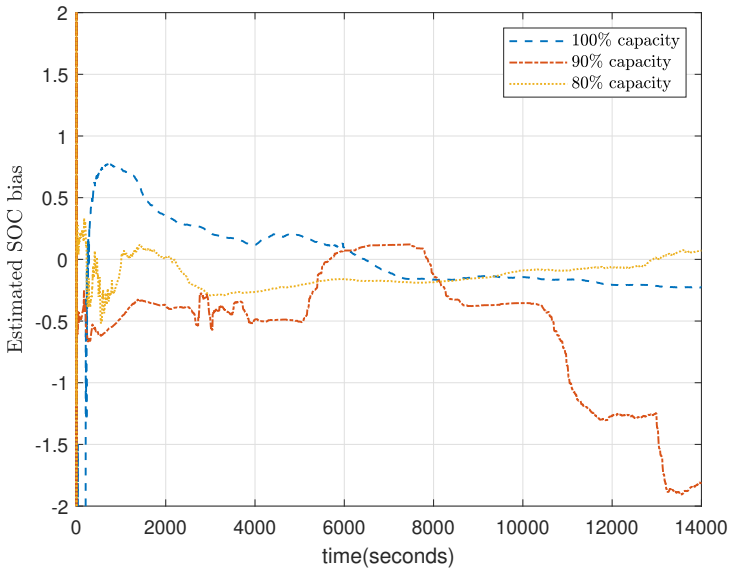

Figure 3.15: Estimated SoC bias for new (100% capacity) and aged (90% and 80% capacity) battery using the driving schedule.

Since the internal resistance and the SoC of the battery are estimated accurately, the SoP can be calculated as described in Section 3.5.2. Figure 3.16 shows the maximum power for charge and discharge at different SoH of the battery.

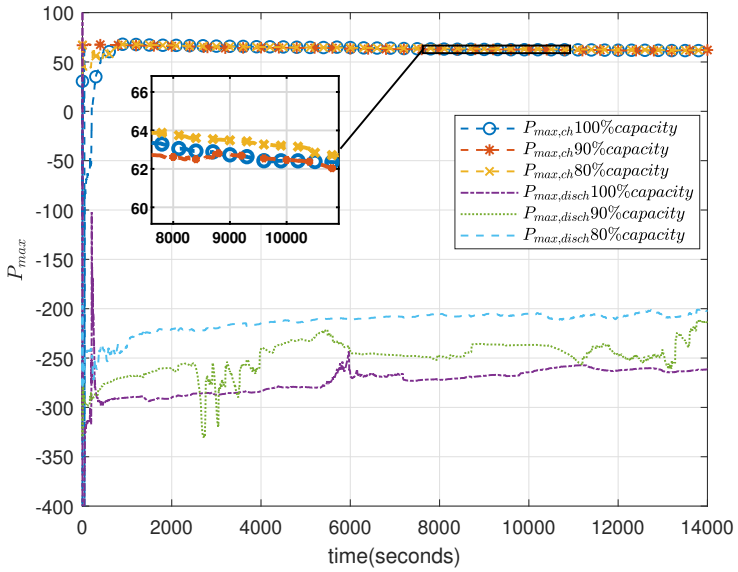

Figure 3.16: Maximum output charge and discharge power for new (100% capacity) and aged (90% and 80% capacity) using the driving schedule.

A subset of driving profile is also considered to assess the efficacy of the proposed strategy to recognize the battery SoC, and SoH for unknown cases as shown in Figure 3.17. Figure 3.18 indicates the mode probability when the battery SoH is in between the level associated with the filter models.

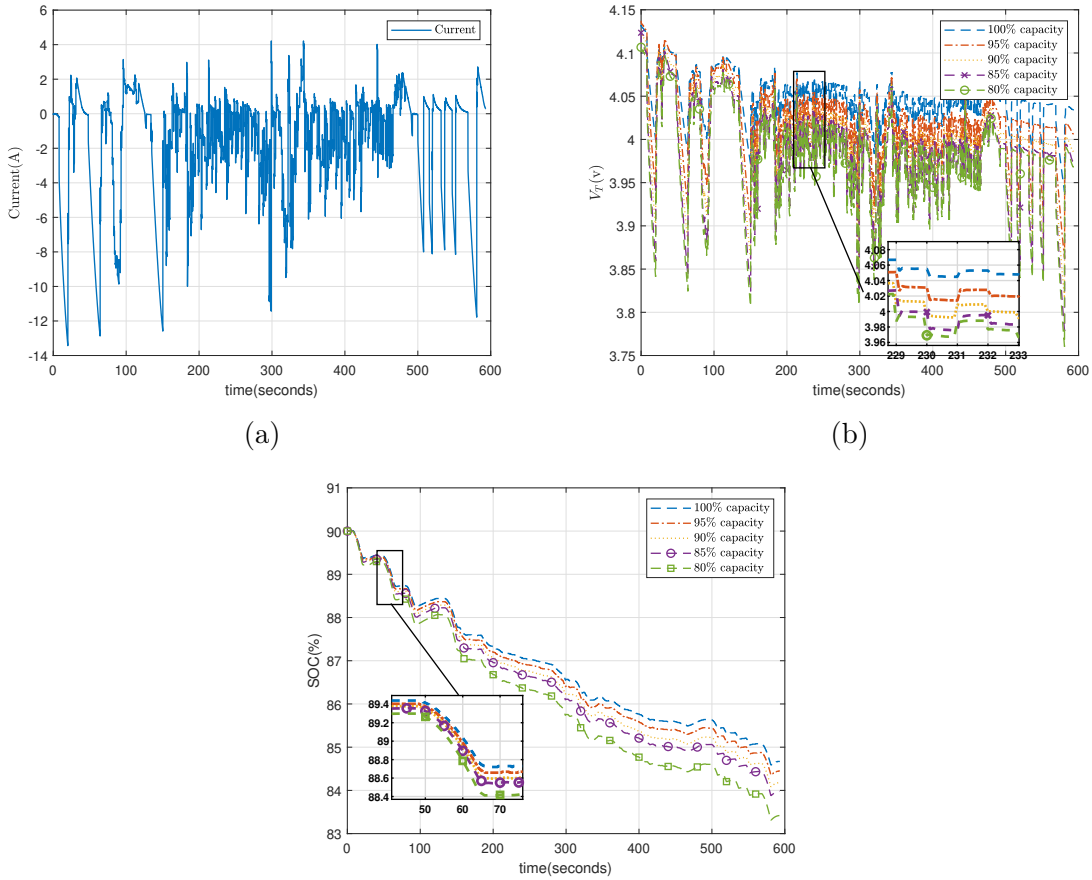

Figure 3.17: a) Current, b) terminal voltage, and c) SoC of the validation schedule for new (100% capacity) and aged (95%, 90%, 95% and 80% capacity) battery.

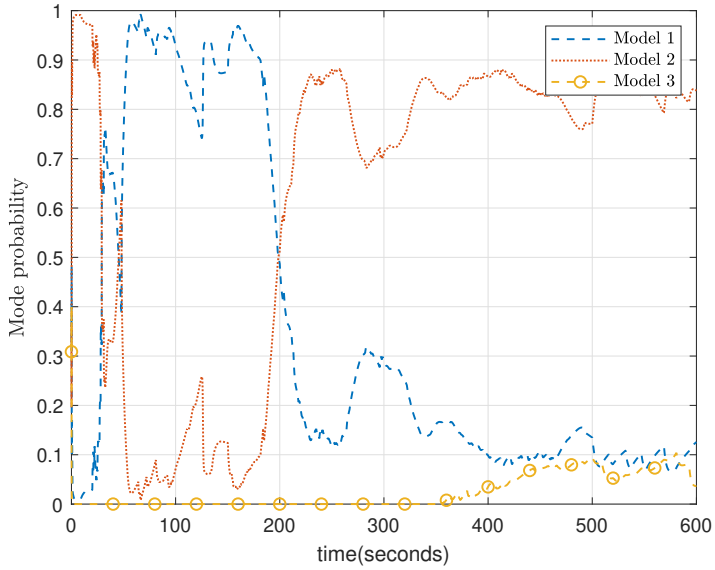

(a)

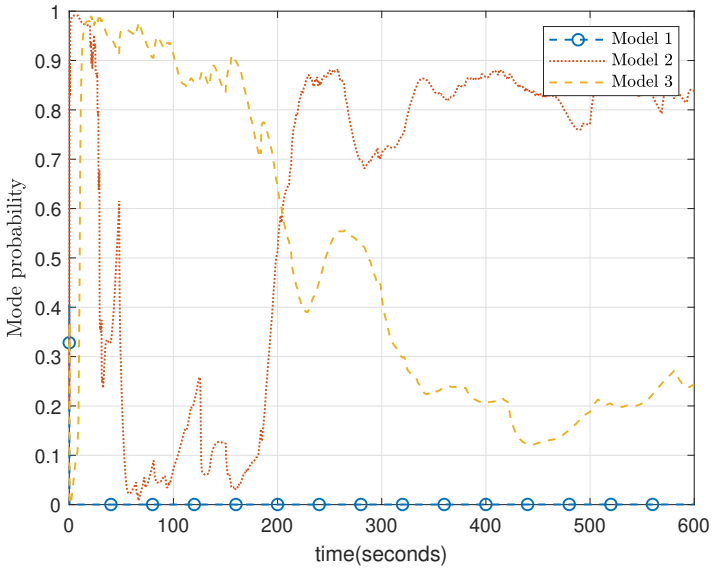

(b)

Figure 3.18: IMM-SVSF-VBL mode probability for a) 95% and b) 85% capacity using the validation data.

Figure 3.18a provides the mode probability for the battery with actual SoH of

approximately 95%. Figure 3.18b displays the mode probability where the actual SoH is about 85%. Figure 3.19 confirms the changes in the estimated internal resistance as the battery ages. The estimated SoH using the mode probability and the internal resistance is demonstrated in Figure 3.20 for the test profile presented in Figure 3.17.

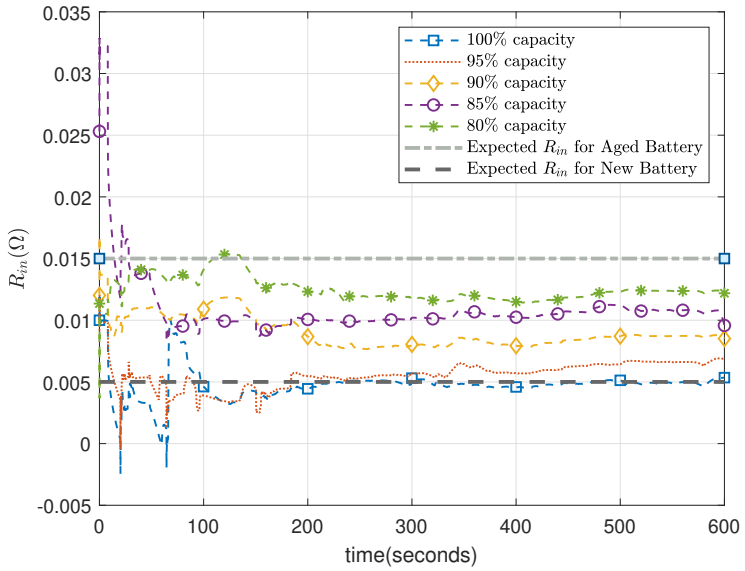

Figure 3.19: Estimated internal resistance for new (100% capacity) and aged (95%, 90%, 85% and 80% capacity) battery using the validation data.

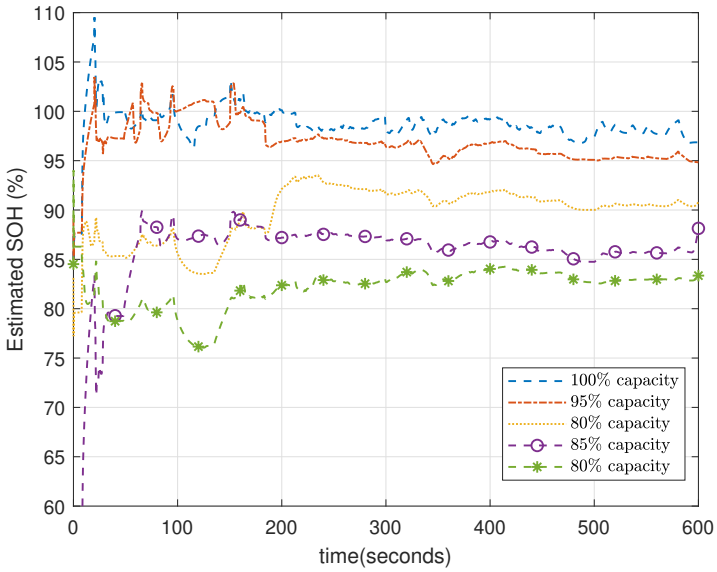

Figure 3.20: Estimated SoH using the validation data.

The efficacy of the proposed strategy has been presented for a single battery cell. However, this algorithm can be expanded to a pack level as voltage and current measurements are readily available in Battery Management Systems and given that with the proposed method, no additional measurements are needed. The estimated SoC bias is used here to refine a measure of the SoC obtained by coulomb counting. Moreover, the battery's SoH has a slow dynamic and is not required to be estimated continuously if there are constraints associated with the availability of computational resources.

3.7 Conclusion

This paper proposed an interacting multiple model framework to estimate the SoC, SoH, and SoP of a battery. A modified third-order ECM model is proposed to enable

the combined estimation of the internal resistance, the SoC, and the SoC bias. The observability of the proposed model is investigated and guaranteed. The observability ensures that states of the system can be uniquely extracted from measurements. Since the characteristics of a battery changes over time, an Interacting Multiple Model (IMM) strategy with the Smooth Variable Structure Filter with Variable Boundary Layer (SVSF-VBL) is used to track and adjust to the aging of the battery. The estimated SoC bias is used to update the measure of SoC obtained by coulomb counting which leads to a more accurate SoC estimation. Moreover, the estimated internal resistance and the mode probability of the IMM-SVSF-VBL are utilized to present an accurate estimation of the battery SoH. The estimated states of the battery are then used for obtaining the battery SoP. The proposed combined method for SoC/SoH/SoP estimation is validated with experimental data.

Nomenclature

V_T	Cell terminal voltage.
V_j	Voltage across RC branch, $j = 1, 2, 3$.
V_{ocv}	Open Circuit Voltage (nonlinear function of SoC).
SOC	State of Charge.
SOH	State of Health.
SOP	State of Power.
C_n	Cell nominal capacity.
R_{in}	Cell internal resistance.
R_j	Resistance of RC branch, $j = 1, 2, 3$.
C_j	Capacitor of RC branch, $j = 1, 2, 3$.
η	Cell Coulombic Efficiency.
ΔT	Sampling period.
k	Time step.

i	Current flowing across the cell.
b	SoC bias.
x	State vector or values.
u	Input to the system.
y	Measurement vector or values.
f	Nonlinear system function.
g	Input gain function.
h	Nonlinear measurement function.
X	An open subset of $\mathbb{R}^n$.
A	State matrix.
B	Input matrix.
I_j	Identity matrix ($I_j \in \mathbb{R}^{j \times j}$).
0_j	Zero matrix ($0_j \in \mathbb{R}^{j \times j}$).
$k+1 \mid k$	A-priori time step (i.e., before applied gain).
$k+1 \mid k+1$	A-posteriori time step (i.e., after update).
Q	System noise covariance matrix.
R	Measurement noise covariance matrix.
Diag(a) or $\bar{a}$	diagonal matrix of some vector a.
γ	SVSF "convergence" or memory parameter.
ψ	SVSF smoothing boundary layer width.
K	SVSF gain matrix.
P	State error covariance matrix.
$\hat{}$	Estimated vector or values.
S	Innovation covariance matrix.
$\mid a \mid$	Absolute value of some parameter a.
T	Transpose of some vector or matrix.
e	Measurement (output) error vector.
E	Combination of measurement error vectors.
$sat(a)$	Defines a saturation of the term a.
H	Jacobian matrix of h.
m	Number of measurements.
n	Number of states.
w	System noise vector.
v	Measurement noise vector.
dh	Gradient of h.

$\mathcal{L}_f h(.)$	Lie-derivative of h with respect to f.
$\mathcal{O}_I(.)$	Observability matrix.
$I^{cha}_{max,vol}$	Maximum cell charge current limited by terminal voltage.
$I^{dch}_{max,vol}$	Maximum cell discharge current limited by terminal voltage.
I^{cha}_{max}	Maximum cell charge current.
I^{dch}_{max}	Maximum cell discharge current.
P^{cha}_{max}	Maximum cell available charge power.
P^{dch}_{max}	Maximum cell available discharge current.
Λ	Likelihood function.
c	Normalizing constant.
r	Number of models in IMM.
$\mu_{i\|j}$	Mixing probabilities of i and j.
μ_j	Mode probability of j.
p	Transition probability matrix.
$\bar{c}$	Probability mass function prediction.
α	Adaptive weighted average of the SoH estimation.
τ_j	Time constant of RC branch, $j = 1, 2, 3$.

Chapter 4: Adaptive Smooth Variable Structure Filter Strategy for State Estimation of Electric Vehicle Batteries

Sara Rahimifard[1], Saeid Habibi[1], Gillian Goward[2], Jimi Tjong[1]

[1] Department of Mechanical Engineering, McMaster University;

[2] Department of Chemistry and Chemical Biology, McMaster University, Hamilton, ON L8S 4L8, Canada

This paper is published in Energies 2021, 14(24), 8560, doi: 10.3390/ en14248560.

Abstract: Battery Management Systems (BMSs) are used to manage the utilization of batteries and their operation in Electric (EVs) and Hybrid Electric (HEVs) Vehicles. It is imperative for reliable and safe operation of batteries to be able to accurately estimate the State of Charge (SoC), State of Health (SoH) and State of Power (SoP). The SoC and SoH estimation must remain robust and accurate despite aging and in presence of noise, uncertainties and sensor biases. This paper introduces a robust adaptive filter referred to as the Adaptive Smooth Variable Structure Filter with a time-Varying Boundary Layer (ASVSF-VBL) for the estimation of the SoC and SoH in electrified vehicles. The internal model of the filter is a third-order Equivalent Circuit Model (ECM) and its state vector is augmented to enable estimation of the internal resistance and current bias. It is shown that system and measurement noise covariance adaptation for the SVSF-VBL approach improves the performance

in state estimation of a battery. The estimated internal resistance is then utilized to improve determination of the battery's SoH. The effectiveness of the proposed method is validated using experimental data from tests on Lithium Polymer automotive batteries. The results indicate that the SoC estimation error can remain within less than 2% over the full operating range of SoC along with an accurate estimation of SoH.

4.1 Introduction

Lithium-ion (Li-ion) Batteries are extensively used for energy storage in Electric (EVs) and Hybrid Electric (HEVs) Vehicles due to their high energy and high power densities. The performance of EVs and HEVs are largely affected by their Battery Management Systems (BMSs) that need to ensure a safe, stable and reliable operation for the battery pack. State of Charge (SoC), State of Health (SoH), and State of Power (SoP) are key operational parameters of the battery that need to be estimated and managed. These elements together provide a comprehensive view of the battery and the pack's capabilities [28, 112, 113].

The battery SoC represents remaining charge in a battery which is similar to the gas-gauge in fossil-fuel vehicles. The SoC is a short-term indicator of the battery ability, however, it cannot provide valuable information about the health of the battery. The battery SoH is an indicator of the remaining battery capacity and life. The battery SoC and SoH need to be estimated as there are no sensors for their direct measurement. Accurate estimation of SoC and SoH are required to ensure an equal distribution of load among cells in the pack and to determine where a cell is in its life cycle. A wide range of strategies have been presented for both SoC and SoH estimation. The SoC estimation methods are categorized into direct and indirect methods

[29, 84].

Measurements of the terminal voltage, current and impedance are commonly employed in direct methods to calculate the battery SoC. Methods based on the open circuit voltage, terminal voltage, internal resistance and coulomb counting are commonly used. However, these methods require regular calibration due to error propagation related to changes in the internal characteristics of the battery due to aging, inaccuracies in the assumed initial conditions, and measurement biases [114]. Temperature and mechanical measurements of a cell have also been taken into consideration to improve the battery management and therefore states estimation [115]. However, indirect methods have been proven to be highly beneficial especially in uncertain conditions. Indirect methods include fuzzy logic-based estimation, artificial neural networks, and filter/observer-based techniques. Model-based strategies provide an insight into the internal dynamics of a battery and therefore could be more practical to use onboard of a BMS [23, 67, 83].

The battery SoH estimation has to take into account the battery capacity fade and impedance changes. SoH estimation methods are generally categorized into experimental or model-based techniques. Experimental-based techniques rely on characterization of batteries using cycling data. These methods involve measurement of internal resistance, impedance measurement, coulomb counting and regression analysis. Model-based strategies use filters and observers in conjunction with battery models to provide a real-time indicator for SoH estimation [22, 116].

Battery models used in BMSs have included electrochemical and Equivalent Circuit Models (ECMs). Electrochemical models are structured to represent the physical

reactions inside a battery and therefore are suitable for degradation analysis. However, they have not been proven to be more accurate in SoC and SoH estimation and due to their complexity, are not commonly used onboard of a BMS. ECMs, on the other hand, provide a simple model which can be easily parameterized using experimental data, and provide sufficient accuracy for real-time parameter and state estimation. Additionally, in their modified forms provide thermal modeling or a measure of SoH [117]. For better accuracy, the parameters of ECMs require to be adjusted according to the battery's SoH, temperature, and current (or C-rate). Different strategies have been reported for model adjustment including look-up tables as well as parameter estimation and multiple model strategies. Online parameter estimation is commonly considered to improve the performance by adapting the model for different conditions [118]. Multiple model strategies can also increase the adaptation of a battery by considering a range of scenarios [119, 120]. Once a model is chosen to determine the dynamics of the battery, a robust filter is needed to estimate the states of the battery [89, 93, 121].

The Extended Kalman Filter (EKF) is the most commonly used filter for parameter estimation. Other methods include the Unscented KF (UKF), Quadrature KF (QKF), Sigma Point KF (SPKF), Cubature KF (CKF) and Particle Filter (PF) [43, 100, 122]. These strategies have been applied to li-ion batteries for state and parameter estimation [71, 98, 112, 123]. Robust filtering strategies such as the Robust Kalman Filters, H_∞ Filtering and the Smooth Variable Structure Filter (SVSF) have also been employed to deal with uncertainties [43, 51, 54]. In [55], SVSF with a Variable Boundary Layer (SVSF-VBL) is introduced to improve the performance of SVSF in presence of noise and uncertainties. More advancements on SVSF strategy

have also been presented to boost the efficiency of the SVSF including the second-order SVSF, square-root SVSF, its combination with different filters such as KF, EKF, UKF, CKF, PF and more [108, 124, 125]. Although these methods enhance the accuracy of state estimation, they do not consider adaptability. Additionally, these algorithms can only be employed if the system is observable [91].

In the above filters, knowledge of the system's model is an essential requirement for reliable state and parameter estimation. Characterization of noise statistics is needed as well as the dynamic model and affect the filter's stability and performance. When this information is not correct, the performance of the designed filter may worsen significantly and could lead to divergence. Model-based filters such as the EKF assume that the system model is largely known together with the input functions and the noise statistics. However, this may not be the case in all applications and may need to be remedied through adaptive filters [68, 126].

Two types of adaptation are considered in this paper, including filter tuning and Multiple Model (MM) methods. MM methods consider switching between a finite number of models to provide adaptability against changes and uncertainties. Different forms of multiple model methods have been proposed for state and parameter estimation of batteries [94, 119, 120]. Filter tuning methods, on the other hands, are used to adjust filter and model parameters as the system changes. Filter tuning methods can be categorized into noise adaptation, parameter tuning and joint filtering of parameters and states. Dual and joint estimation methods have been proposed in recent research for estimating both parameters and states of a battery simultaneously [62, 74].

Noise statistics need to be captured for model-based filters. However, most filters

usually assume that the noise is white, Gaussian and zero mean. If this assumption is not satisfied, the filter performance degrades. This has generated a great deal of interest in noise adjustments in a variety of applications. A wide range of studies have been performed concerning the properties, advantages, and disadvantages of different methods. In [64] different approaches for noise adaptations have been proposed for a KF. In [127], the maximum likelihood method is used in an Adaptive KF (AKF) for an INS/GPS integration algorithm. A comparison of different strategies for noise covariance adaptation is presented in [63]. In [128], noise covariance adaptation is employed to a KF. Zhang proposed an adaptive KF for joint polarization tracking [126]. In [129], a comparison between different adaptive strategies for EKF is presented. In [130], sufficient conditions for noise covariance identification of a KF have been introduced.

Noise covariance estimation techniques can be broadly divided into two groups including feedback methods and feedback-free methods [63]. Simultaneous estimation of the states as well as the noise covariance matrices is performed in feedback methods. These methods include the covariance matching and the Bayesian methods. For feedback-free methods, on the other hand, estimated noise covariances are not required for state estimation. Examples are the correlation and the maximum-likelihood methods [63, 64].

In battery states estimation, the current supplied by the battery and the terminal voltage are measured. Measurement uncertainties include sensor noise, drift, and bias. The disturbances in current and voltage sensors affect the performance of a BMS, so they need to be taken into account. Adaptive methods boost the performance of the estimation methods in presence of noise, sensor drift and bias. However, sensor drift

and bias should still be identified, as well as noise, for calibration purposes and to ensure a reliable and safe operation [89]. Different strategies are employed for sensor calibration which often require operation of specific instruments irregularly. Online estimation of sensor bias is a widely used technique in real-time applications. In [91], the observability of a battery model is investigated in the presence of sensor bias. The effect of sensor bias and drift estimation on SoC estimation is considered in [89].

This work considers adaptation for both sensor bias as well as modeling uncertainties. An adaptive SVSF-VBL based strategy is proposed to reduce state estimation errors of a battery. The contributions of this paper are as follows:

- An equivalent circuit model formulation augmented with internal resistance and sensor bias is used as the model. The estimated internal resistance is employed as an indicator of SoH while the estimated bias is to improve estimation accuracy.

- The Adaptive Smooth Variable Structure Filter with Variable Boundary Layer (ASVSF-VBL) strategy is introduced for state estimation (SoC and SoH) in presence of changing statics of noise and uncertainties. The proposed strategy provides noise adaptation which improves estimation robustness and accuracy.

- The performance of the ASVSF-VBL is then compared to conventional SVSF-VBL and EKF using experimental data.

Section 4.2 of this paper presents the model of the battery. The proposed ASVSF-VBL estimation strategy is introduced in Section 4.3. In Section 4.4, the proposed method is tested and validated using experimental data and its performance is comparatively analyzed. Section 4.5 concludes the paper.

4.2 Modeling

Equivalent Circuit Model (ECM) provides a simple and effective approach for battery characterization. Although, higher order models can be used to improve the battery model's performance, a trade-off between complexity and accuracy should be considered to avoid over-parametrization that could affect estimation of the internal resistance. This study employs a third-order ECM to provide enough accuracy for a battery model especially when the battery ages while retaining the influence of aging on the internal resistance. Figure 4.1 shows a circuit diagram of a third-order ECM. The model contains different elements including a series resistance defined as internal resistance (R_{in}) and the Open Circuit Voltage (OCV) of the battery which relates to its SoC. The battery model also has multiple Resistance-Capacitance (RC) branches that describe the transients of the battery including the diffusion, the Solid Electrolyte Interface (SEI) dynamics and the charge transfer kinetics. The structure of the model should reflects the dynamic complexity of the battery as it ages [104].

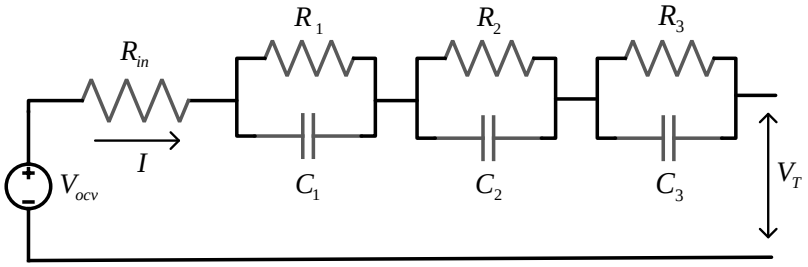

Figure 4.1: Third-order equivalent circuit battery model.

The battery model in Figure 4.1 is formulated with discrete-time state equations

as follows,

$$
\begin{aligned}
V_{1,k+1} &= (1 - \frac{\Delta T}{R_1 C_1})V_{1,k} + \frac{\Delta T}{C_1} i_k, \\
V_{2,k+1} &= (1 - \frac{\Delta T}{R_2 C_2})V_{2,k} + \frac{\Delta T}{C_2} i_k, \\
V_{3,k+1} &= (1 - \frac{\Delta T}{R_3 C_3})V_{3,k} + \frac{\Delta T}{C_3} i_k, \\
SOC_{k+1} &= SOC_k - \frac{\eta \Delta T}{C_n} i_k
\end{aligned} \tag{4.1}
$$

where $V_j, j = 1, 2, 3$ are voltage across the RC branches, $C_j, j = 1, 2, 3$ are capacitor and $R_j, j = 1, 2, 3$ are resistance of the RC branches, i is the actual current flowing across the cell, C_n is nominal capacity of the battery, η is the cell Coulombic Efficiency (CE), ΔT is the sampling period, and k is a time sample.

The output of the model is terminal voltage of the battery and is described as,

$$V_{T,k} = V_{ocv}(SOC_k) - V_{1,k} - V_{2,k} - V_{3,k} - R_{in} i_k \tag{4.2}$$

where V_T is the cell terminal voltage, V_{ocv} is the open circuit voltage (nonlinear function of SoC), and R_{in} is the cell internal resistance.

The parameters of the model change with SoC and temperature. Therefore, parameters are constant within a small range of SoC, temperature and current level [16]. Updates of the model parameters or possibly its structure are needed for determining the battery SoH. The model can be modified using two approaches including model switching or parameter updating or estimation [105, 119]. Parameter estimation can be employed if observability condition is satisfied. Here, the internal resistance is

considered as a state that indicates the battery SoH and power capability [106].

$$R_{in,k+1} = R_{in,k} + w_{r_k} \tag{4.3}$$

where w_{r_k} is white noise.

A bias may exist in the measured current of the battery due to sensor error [89, 91]. Here, the current sensor bias is considered as an augmented state to the battery model to be estimated. This modification could optimize the estimation performance. The sensor bias is defined as follows,

$$I_{b,k+1} = I_{b,k} + w_{b_k} \tag{4.4}$$

where i_b is the bias from the current sensor and w_{b_k} is white noise. The measured current flowing across the cell (i_m) includes this bias and is defined as follows,

$$I_{m,k} = I_k + I_{b,k} \tag{4.5}$$

The modification is then applied to the model. Therefore, the state-space form of the proposed model is described as,

$$x_{k+1} = f(x_k) + g(x_k)u_k, \tag{4.6}$$

$$y_k = h(x_k, u_k) \tag{4.7}$$

where $x \in X$ is the state vector, $u \in \mathbb{R}$ is the input to the system, $y \in \mathbb{R}^m$ is the measurement vector, $f : X \to \mathbb{R}^n$ is the nonlinear system function, $g : X \to \mathbb{R}^n$ is the input gain and $h : X \to \mathbb{R}^m$ is the nonlinear measurement function where

they are all differentiable functions. The state and measurement vectors are $x_k = \begin{bmatrix} V_{1,k} & V_{2,k} & V_{3,k} & SOC_k & I_{b,k} & R_{in,k} \end{bmatrix}^{\mathrm{T}}$ and $y_k = V_{T,k}$, respectively. Note that in this model $f(x_k)$ is linear and $f(x_k) = Ax_k$ and $g(x_k) = B$ are given as,

$$A = \begin{bmatrix} 1-\frac{\Delta T}{R_1 C_1} & 0 & 0 & 0 & -\frac{\Delta T}{C_1} & 0 \\ 0 & 1-\frac{\Delta T}{R_2 C_2} & 0 & 0 & -\frac{\Delta T}{C_2} & 0 \\ 0 & 0 & 1-\frac{\Delta T}{R_3 C_3} & 0 & -\frac{\Delta T}{C_3} & 0 \\ 0 & 0 & 0 & 1 & \frac{\eta \Delta T}{C_n} & 0 \\ 0 & 0 & 0 & 0 & 1 & 0 \\ 0 & 0 & 0 & 0 & 0 & 1 \end{bmatrix}, \quad B = \Delta T \begin{bmatrix} \frac{1}{C_1} \\ \frac{1}{C_2} \\ \frac{1}{C_3} \\ \frac{-\eta}{C_n} \\ 0 \\ 0 \end{bmatrix} \tag{4.8}$$

The output equation is a nonlinear function that can be specified as follows,

$$V_{T,k} = V_{ocv}(SOC_k) - V_{1,k} - V_{2,k} - V_{3,k} + R_{in} i_{b,k} - R_{in} i_{m,k} \tag{4.9}$$

The observability of this battery model can be guaranteed if $R_1 C_1 \neq R_2 C_2 \neq R_3 C_3$ and there exists a $k \in \mathbb{Z}$ such that $\frac{\partial V_{ocv}^k}{\partial SOC^k} \neq 0$ [119]. Therefore, estimation strategies can be used here for state and parameter estimation.

4.3 Adaptive Smooth Variable Structure Filter with Variable Boundary Layer

The Adaptive Smooth Variable Structure Filter with Variable Boundary Layer (ASVSF-VBL) strategy is a method that adapt to the changes in the noise statistics. The

approach improves the performance of the original SVSF-VBL and provides better accuracy and robustness in presence of noise and uncertainties. It is particularly applicable to battery SoC estimation as current bias is estimated and this increases the speed of noise statistic estimation. This section provides details on the proposed approach for state estimation.

4.3.1 Smooth Variable Structure Filter with Variable Boundary Layer

The Variable Structure filter (VSF) approach was first presented in [51]. A revised version of it named SVSF was then introduced in [54] that is a predictor-corrector strategy based on the sliding mode concept. The method is applicable to linear and nonlinear systems with the assumption that the system under consideration is observable. The method provides stability and robustness to modeling uncertainties and noise with a given upper bound for the level of noise and unmodeled dynamics. Assuming a typical model is represented as follows,

$$x_{k+1} = f(x_k, u_k, w_k), \tag{4.10}$$

$$z_k = h(x_k, u_k, \upsilon_k) \tag{4.11}$$

where υ_k is the measurement noise and w_k is the system noise and they are uncorrelated white noise with the following mean and covariance,

$$E[w_k] = 0, \quad E[w_k w_k^T] = Q_k \tag{4.12}$$

$$E[\upsilon_k] = 0, \quad E[\upsilon_k \upsilon_k^T] = R_k \tag{4.13}$$

The discontinuous corrective action of the SVSF method leads to chattering as shown in Figure 4.2. This chattering can be removed by using a smoothing boundary layer. The smoothing boundary layer will be inefficient if the disturbance exceeds the assumed upper bound [54]. A time-varying smoothing boundary layer eliminates chattering and excessive switching as presented in [57]. More advancement to the SVSF have also been proposed, including but not limited to covariance formulation, second-order SVSF, and combination of SVSF with other filters such as KF, EKF, UKF, PF, Square-Root SVSF and Two-pass SVSF [43, 55, 103, 124]. The SVSF-VBL estimation is formulated as follows,

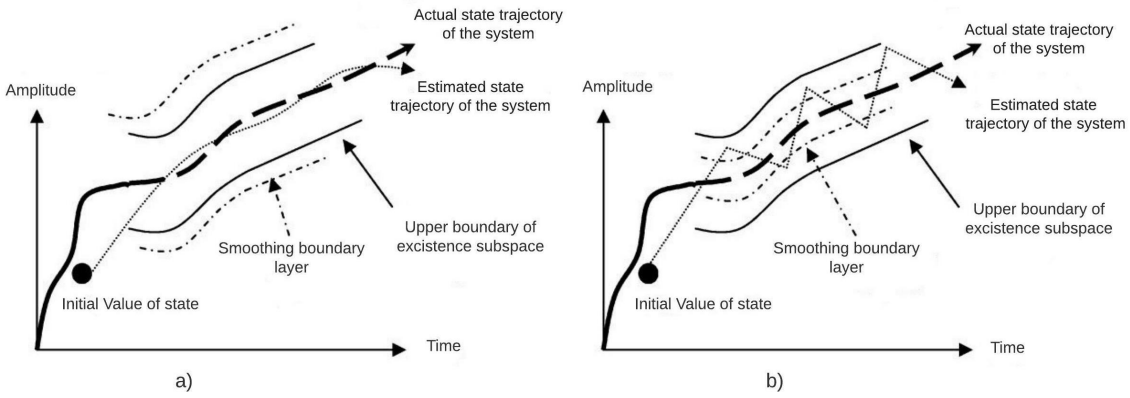

Figure 4.2: Effect of smoothing boundary layer (**a**) $\psi > \beta$, (**b**) $\psi < \beta$ (β is the upper boundary of existence subspace).

- Prediction: An estimated filter model is used to obtain the a-priori state estimates.

$$\hat{x}_{k+1|k} = \hat{A}\hat{x}_{k|k} + \hat{B}u_k, \tag{4.14}$$

$$\hat{z}_{k+1|k} = \hat{H}\hat{x}_{k+1|k} \tag{4.15}$$

$$e_{k+1|k} = z_{k+1} - \hat{z}_{k+1|k} \tag{4.16}$$

$$P_{k+1|k} = \hat{A}P_{k|k}\hat{A}^T + Q_k \tag{4.17}$$

where P is the state vector covariance matrix, H is the jacobian matrix of H, and $e_{k+1|k}$ is called the filter innovation measurement sequence.

- Correction: The correction gain is obtained and, the estimated states are then updated from their a-priori into their a-posteriori by using this gain.

$$S_{k+1} = \hat{H}P_{k+1|k}\hat{H}^T + R_{k+1} \tag{4.18}$$

$$E_{k+1} = |e_{k+1|k}| + \gamma|e_{k|k}| \tag{4.19}$$

$$\psi_{k+1} = (\bar{E}_{k+1}^{-1}\hat{H}P_{k+1|k}\hat{H}^T S_{k+1}^T)^{-1} \tag{4.20}$$

where S is the innovation covariance matrix, E is the combination of measurement error vector, γ is the SVSF convergence parameter and ψ_{k+1} is the SVSF smoothing boundary layer width.

The SVSF is a predictor-corrector method and its gain is employed to update the a-priori estimated states. The gain $\psi_{k+1} < \psi_{lim}$ is as follows,

$$K_{k+1} = \hat{H}^{-1}\bar{E}_{k+1}\psi_{k+1}^{-1} \tag{4.21}$$

where ψ_{lim} is upper limit for the boundary layer. For the case when $\psi_{k+1} \geqslant \psi_{lim}$ the SVSF gain is:

$$K_{k+1} = \hat{H}^{-1}\bar{E}_{k+1}sat(e_{k+1|k}\psi_{k+1}^{-1})\bar{e}_{k+1|k}^{-1} \tag{4.22}$$

Finally, the a posteriori parameters are calculated as:

$$\hat{x}_{k+1|k+1} = \hat{x}_{k+1|k} + K_{k+1}e_{k+1|k} \tag{4.23}$$

$$P_{k+1|k+1} = (I - K_{k+1}\hat{H})P_{k+1|k}(I - K_{k+1}\hat{H})^{T} + K_{k+1}R_{k+1}K_{k+1}^{T} \tag{4.24}$$

$$\hat{z}_{k+1|k+1} = \hat{H}\hat{x}_{k+1|k+1} \tag{4.25}$$

$$e_{k+1|k+1} = z_{k+1} - \hat{z}_{k+1|k+1} \tag{4.26}$$

where $e_{k+1|k+1}$ is called the filter measurement residual sequence. Equations (4.14) to (4.26) summarize the SVSF-VBL strategy.

4.3.2 Noise Adaptation for Smooth Variable Structure Filter

This paper proposes a novel form of SVSF-VBL that incorporates adaptation to noise statistics. Although the stability and estimation convergence of the SVSF-VBL method is proven with the time-varying boundary layer, its performance is significantly enhanced with adaptation to noise statistics variation and by including bias estimation in measurements. Figure 4.3 offers a brief overview of the ASVSF-VBL strategy that is explained on this section.

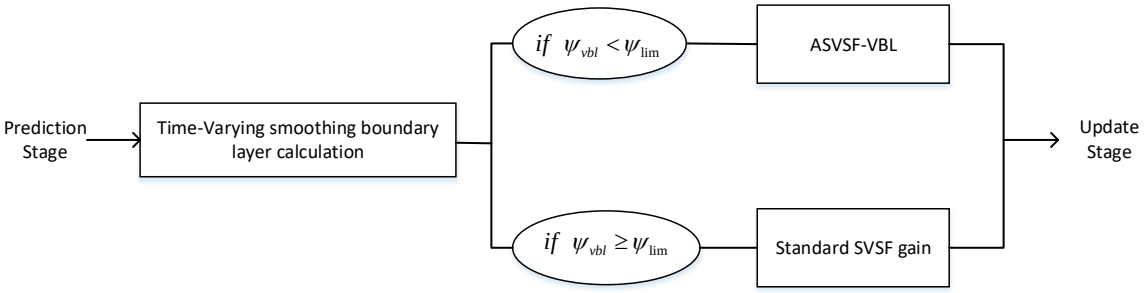

Figure 4.3: Overview of ASVSF-VBL strategy.

Different strategies have been proposed for noise adaptation including covariance matching, Bayesian, Maximum likelihood and correlation method. These methods have been tested in different applications to improve estimation performance. In the ASVSF-VBL, the system and measurement noise covariance matrices (Q and R) are adapted in time using the covariance matching method. The covariance matching technique employs the innovation and the residual defined in Equations (4.16) and (4.26) to adapt the estimated value of the system and measurement noise covariance matrices. Maximization of likelihood functions is used here to derive innovation-based adaptation for the measurement noise covariance matrix (R) using the SVSF-VBL method. The likelihood maximization estimation provides a unique and consistent value for measurement noise covariance matrix (R) estimation. The system noise covariance matrix (Q) is then estimated using the difference between a-posteriori and a-priori states. The optimization is performed in real-time for each time instant [128, 129, 130, 131]. The assumptions for the ASVSF-VBL are as follows,

- The states are independent of the adaptive parameters.
- The system and measurement matrices are time variant within a piece-wise limit and independent of adaptive parameters.

- The innovation sequence is white and ergodic within the estimation window.

For Gaussian distribution, the probability density function of the measurements conditioned on an adaptive parameter at a specific epoch of $k+1$ is defined as,

$$P(z|\alpha)_{k+1} = \frac{1}{\sqrt{(2\pi)^m |C_{\epsilon_{k+1}}|}} e^{-\frac{1}{2}\epsilon_{k+1}^T C_{\epsilon_{k+1}}^{-1} \epsilon_{k+1}} \tag{4.27}$$

where $\epsilon_{k+1} = z_{k+1} - z_{k+1|k}$ is the innovation sequence, $C_{v_{k+1}}$ is the innovation sequence covariance matrix, m is the number of measurements, and α is the adaptive parameter. The $z_{k+1|k}$ is obtained from Equation (4.15). The logarithmic form of the above equation is

$$\ln\left(P(z|\alpha)_{k+1}\right) = -\frac{1}{2}\{m\ln(2\pi) + \ln\left(|C_{\epsilon_{k+1}}|\right) + \ln\left(\epsilon_{k+1}^T C_{\epsilon_{k+1}}^{-1} \epsilon_{k+1}\right)\} \tag{4.28}$$

For a fixed-length memory filter, the innovation matrix will only be considered inside a window of size N. Therefore, the ML optimization problem is defined as follows,

$$\min_{\alpha} \quad \sum_{i=i_0}^{k+1} \ln|C_{\epsilon_i}| + \sum_{i=i_0}^{k+1} (\epsilon_i^T C_{\epsilon_i}^{-1} \epsilon_i) \tag{4.29}$$

where $i_0 = k - N + 2$ is the first epoch inside the estimation. The above formula defines the best estimate as it has the maximum likelihood based on the adaptive parameters. This optimization problem can be simplified using matrix differential

calculus as,

$$\sum_{i=i_0}^{k+1} \Big[tr\Big\{ C_{\epsilon_i}^{-1} \frac{\partial C_{\epsilon_i}}{\partial \alpha_{k+1}} \Big\} - \epsilon_i^T C_{\epsilon_i}^{-1} \frac{\partial C_{\epsilon_i}}{\partial \alpha_{k+1}} C_{\epsilon_i}^{-1} \epsilon_i \Big] = 0 \tag{4.30}$$

The partial derivative of Equation (4.18) with respect to α is,

$$\frac{\partial C_{\epsilon_k}}{\partial \alpha_{k+1}} = \frac{\partial R_{k+1}}{\partial \alpha_{k+1}} + H \frac{\partial P_{k+1|k}}{\partial \alpha_{k+1}} H^T \tag{4.31}$$

And taking partial derivative from Equation (4.17) with respect to α gives,

$$\frac{\partial P_{k+1|k}}{\partial \alpha_{k+1}} = A \frac{\partial P_{k|k}}{\partial \alpha_{k+1}} A^T + \frac{\partial Q_k}{\partial \alpha_{k+1}} \tag{4.32}$$

Assuming that the process inside the estimation window is in steady state, Equation (4.32) can be written as,

$$\frac{\partial P_{k+1|k}}{\partial \alpha_{k+1}} = \frac{\partial Q_k}{\partial \alpha_{k+1}} \tag{4.33}$$

By substituting Equation (4.33) into (4.31) and applying it into (4.30) the maximum likelihood equation for the adaptive SVSF-VBL is as follows,

$$\sum_{i=i_0}^{k+1} tr\Big\{ \big[C_{\epsilon_i}^{-1} - C_{\epsilon_i}^{-1} \epsilon_i \epsilon_i^T C_{\epsilon_i}^{-1} \big] \big[\frac{\partial R_i}{\partial \alpha_{k+1}} + H \frac{\partial Q_{i-1}}{\partial \alpha_{k+1}} H^T \big] \Big\} = 0 \tag{4.34}$$

Both system and measurement noise covariance matrices (Q and R) can be adapted based on α from the computed equation. To achieve an expression for R, $\alpha_{ii} = R_{ii}$ is

considered where the adaptive parameters are the variance of the updated measurement. Therefore, Equation (4.34) is modified as follows,

$$\sum_{i=i_0}^{k+1} tr\{C_{\epsilon_i}^{-1}[C_{\epsilon_i} - \epsilon_i \epsilon_i^T] C_{\epsilon_i}^{-1}\} = 0 \tag{4.35}$$

This equation is solved by defining the innovation sequence as,

$$C_{\epsilon_{k+1}} = \frac{1}{N} \sum_{i=i_0}^{k+1} \epsilon_i \epsilon_i^T \tag{4.36}$$

Replacing Equation (4.36) into (4.18),

$$R_{k+1} = C_{\epsilon_{k+1}} - \hat{H} P_{k+1|k} \hat{H}^T \tag{4.37}$$

Since the measurement noise covariance should be positive definite, a more stable expression is required. For the case with $\psi_{k+1} < \psi_{lim}$, it can be shown that the adaptation rule for R is,

$$R_{k+1} = \hat{C}_{\varepsilon_{k+1}} + \hat{H} P_{k+1|k+1} \hat{H}^T \tag{4.38}$$

where the residual sequence is $\varepsilon = z_{k+1} - z_{k+1|k+1}$ and residual covariance matrix $\hat{C}_{\varepsilon_{k+1}}$ can be calculated as,

$$\hat{C}_{\varepsilon_{k+1}} = \frac{1}{N} \sum_{i=i_0}^{k+1} \varepsilon_i \varepsilon_i^T \tag{4.39}$$

A forgetting factor is then employed to provide a smoother estimation of R,

$$R_{k+1} = \lambda_R R_k + (1 - \lambda_R)(\hat{C}_{\varepsilon_{k+1}} + \hat{H} P_{k+1|k+1} \hat{H}^T) \tag{4.40}$$

where $0 \leq \lambda_R \leq 1$.

The process noise covariance (Q) can be achieved using the SVSF-VBL formulation. Considering the system Equation (4.10) as,

$$w_k = x_{k+1} - f(x_k, uk) \tag{4.41}$$

From Equations (4.41) and (4.14), the estimated system noise can be obtained as,

$$\hat{w}_k = x_{k+1|k+1} - f(x_{k|k}, uk) = x_{k+1|k+1} - x_{k+1|k} = K e_{k+1|k} \tag{4.42}$$

Covariance of $\hat{w}_k$ can be written as,

$$E[\hat{w}_k \hat{w}_k^T] = E[K e_{k+1|k} [K e_{k+1|k}]^T] = K C_{\epsilon_{k+1}} K^T \tag{4.43}$$

$$Q_k = K C_{\epsilon_{k+1}} K^T \tag{4.44}$$

A forgetting factor is also considered for Q to update it gradually [128],

$$Q_{k+1} = \lambda_Q Q_k + (1 - \lambda_Q)(K \hat{C}_{\epsilon_{k+1}} K^T) \tag{4.45}$$

where $0 \leq \lambda_R \leq 1$.

Figure 4.4 illustrates an overview of the proposed ASVSF-VBL method specified for state estimation of electric vehicle batteries. The SVSF filter guarantees stability

using a Lyapunov function. Based on Lyapunov theory, if a Lyapunov function (V) is locally positive definite and the time derivative of it is locally negative semi-definite, the filter is stable [54]. The following Lyapunov function is considered based on the a-posteriori estimation error (residual error),

$$V = e_{k+1|k+1}^T e_{k+1|k+1} > 0 \tag{4.46}$$

Therefore, the estimation process is stable if the following condition is satisfied,

$$\Delta V \leqslant 0 \tag{4.47}$$

where ΔV is defined as follows,

$$\Delta V = e_{k+1|k+1}^T e_{k+1|k+1} - e_{k+1|k}^T e_{k+1|k} \tag{4.48}$$

Therefore, the following condition which is equal to Equation (4.46) satisfies the stability condition of the estimation process [54].

$$|e_{k|k}|_{Abs} > |e_{k+1|k+1}|_{Abs} \tag{4.49}$$

Theorem 2 ([54])**.** *On the stability of the SVSF strategy, if the system is stable, consecutive bijective (or completely observable and completely controllable in the case of linear systems), then the SVSF corrective gain K_{k+1} that would satisfy the stability*

condition of (4.49) is subject to the following conditions,

$$|e_{k+1|k}|_{Abs} \leqslant |K_{k+1}|_{Abs} < |e_{k+1|k}|_{Abs} + |e_{k|k}|_{Abs} \tag{4.50}$$

The corrective gain K_{k+1} of the SVSF as Equation (4.22) satisfies this condition [54]. The SVSF gain is not affected by the adaptive scheme outside the boundary layer and hence BIBO stability of the ASVSF-VBL remains unaffected.

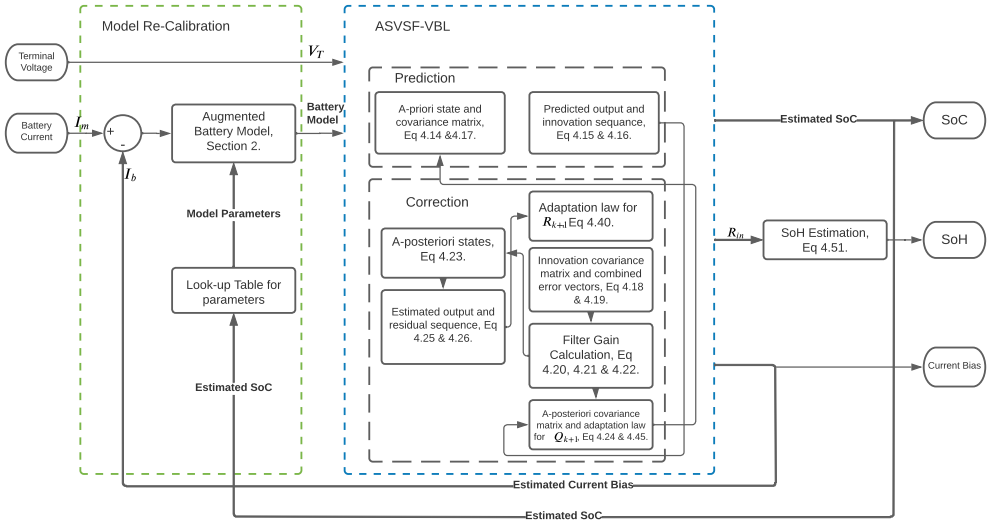

Figure 4.4: An overview of the proposed strategy for battery state estimation.

4.4 Experimental Results

The ASVSF-VBL was validated and comparatively studied further to experiments conducted on NMC Lithium Polymer battery cells. Battery cells specifications are presented in Table 4.1. The experiments were conducted by using an experimental setup consisting of an Arbin BT2000 cycler, environmental chambers , an AVL Lynx data acquisition system, and AVL Lynx software [16]. The characterization tests included static capacity, internal resistance, OCV-SOC and efficiency tests; these were conducted to obtain a baseline for the battery cell performance. In addition, cycling tests were done to investigate the impact of aging on the battery's performance and dynamics.

Table 4.1: Battery cells specifications.

Manufacture	Batterist
Type	NMC Li-ion Polymer
Nominal Capacity (mAh)	5400
Nominal Voltage (V)	3.7
Minimum Voltage (V)	2.8
Maximum Voltage (V)	4.2

Different driving cycles including an Urban Dynamometer Driving Schedule (UDDS); a light duty drive cycle for high speed and high load (US06); and, a Highway Fuel Economy Test (HWFET) drive cycle were used in this study. Figure 4.5 presents the standard driving cycles considered in this article. These drive cycles simulate common driving patterns. The driving patterns of an average driver in the city are illustrated

in Figure 4.5 and were assumed to be the UDDS cycle. High acceleration driving conditions with aggressive driving patterns are performed by US06 drive cycle. The HWFET drive cycle represents highway driving. A mixture of these velocity profiles was used to generate a current profile for the battery cell as presented in Figure 4.6. The experimental data was collected for battery cells over time at elevated temperatures ranging from 35° to 40° to accelerate aging for a full range of SoCs from 90% to 20% [12, 16].

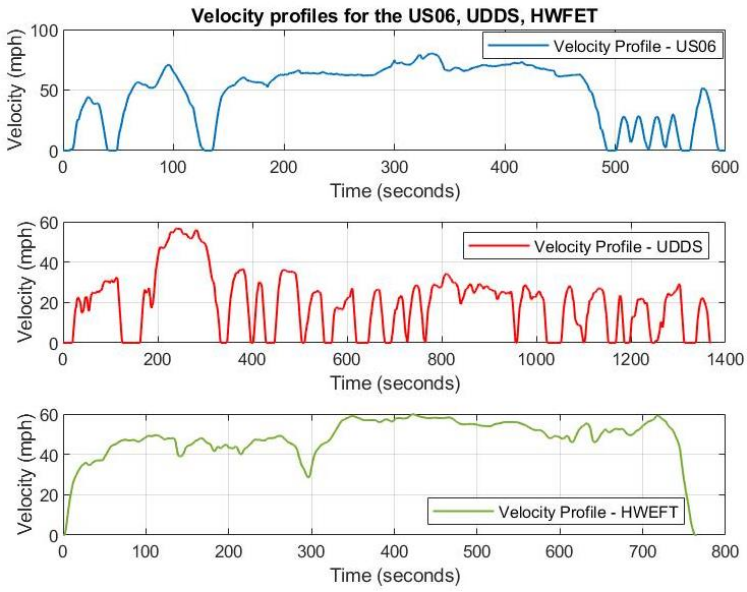

Figure 4.5: Velocity profiles for the UDDS, US06, and HWFET driving cycles (Data set from [18]).

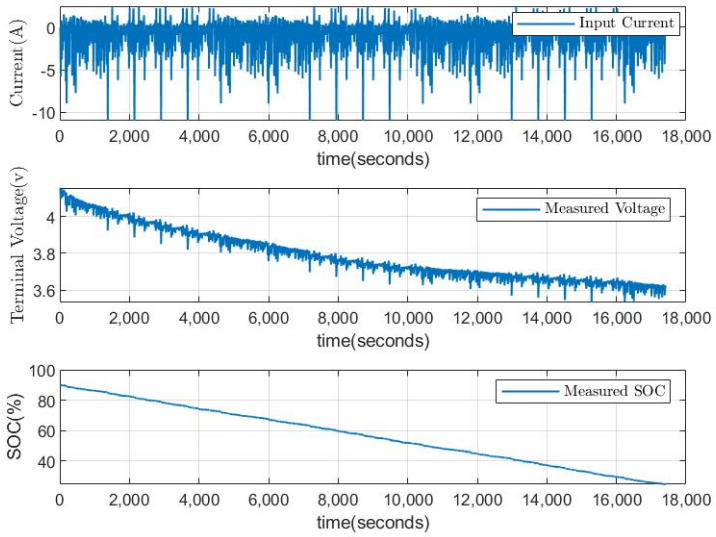

Figure 4.6: Voltage , current, and SoC for a cell using a mixed drive cycle.

The battery model should be determined as an essential part of estimation. Battery model parameters are first identified for different levels of SoC (Figure 4.6) as well as SoH [16]. Table 4.2 provides the parametric bound of the equivalent circuit model presented in Section 4.2. The internal resistance of the battery is considered as a parameter to be estimated in real time. The internal resistance is one of the key factors for determining the battery's SoH and reflects the power capability of a battery. The battery's SoH is estimated using an indicator as follows,

$$SOH_R = \frac{R_{EOL} - R_{in}}{R_{EOL} - R_{new}} \times 100\% \tag{4.51}$$

where R_{EOL} is the internal resistance of a fully aged battery, R_{new} is the internal

resistance of a fresh battery where it can be estimated based on experimental characterization or obtained from manufacturer's specifications. The R_{in} is the estimated internal resistance provided by the ASVSF-VBL strategy. The end of life for a battery in electric applications is usually where the nominal capacity is about 80% compared to its value when the battery is new. Equation 4.51 indicates a value in range of $0 \leqslant SoH_R \leqslant 1$ which means that the battery reached its end of life and should be replaced. The presented value should be redefined in the range of $0.8 \leqslant SoH_R \leqslant 1$ which means that $C_{n,old} = 0.8C_{n,new}$ [116, 132].

The ASVSF-VBL strategy as illustrated in Figure 4.4 is then employed to estimates the states of a battery including the internal resistance, the SoC and the current bias. Figure 4.7 demonstrates the validation data used to investigate the performance of the proposed method. Data was collected during experiments for a smaller range of SoC based on a US06 drive cycle for validation. Through the validation cycle, the battery cell's voltage is measured and recorded as fast as 10 Hz. These measurements are then employed to evaluate the proposed strategy. A comparison of the ASVSF-VBL versus the SVSF-VBL and the EKF methods is provided to investigate the performance of the proposed strategy under different conditions. All filters use the same models with the same initial parameters for providing a direct comparison between the performance of the three filters. Optimal and non-optimal initial parameters are considered to show the effect of Q and R on the filters as listed in Table 4.3. In a non-ideal scenario a current bias of $I_b = 1A$ has been added to the current measurement. In addition, extra noise has been added to measurements to simulate changing statistics of noise under controlled conditions.

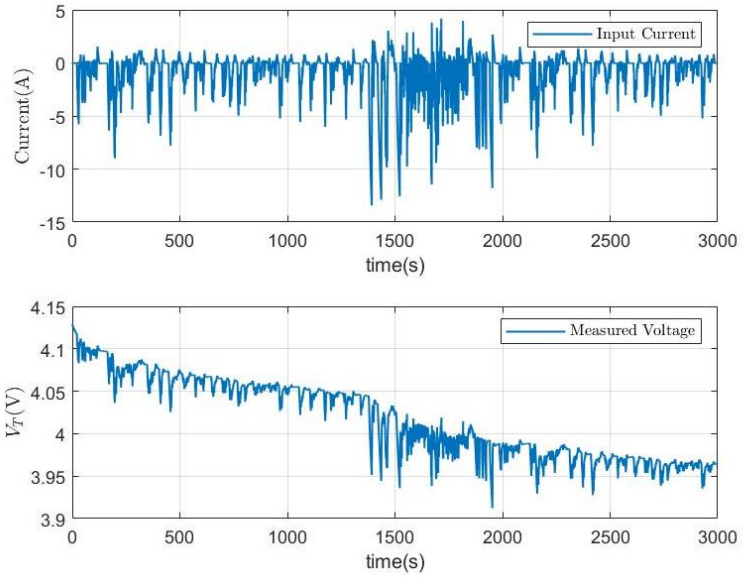

Figure 4.7: Current and voltage of the validation data.

Table 4.2: Model Parameters bound of a third-order ECM. Example given for 80% SoC and 100% SOH.

Parameters	$R_1(\Omega)$	$R_2(\Omega)$	$R_3(\Omega)$	τ_1(s)	τ_2(s)	τ_3(s)
Upper Bound	0.025	0.0079	0.089	1	27	355
Lower Bound	0.00117	0.000038	0.0012	0.1	8	74
Example	0.0018	0.0028	0.0082	0.5543	11.929	111.57

Table 4.3: Initial parameters used for the filters.

Parameters	**R**	**Q**	**P**	I_{b0}	ψ	γ
Optimal Value	5	$0.1I_6$	I_6	0	6	0.23
Non-Optimal Value	50	I_6	I_6	1	6	0.23

Table 4.4 provides the Root Mean Square Error (RMSE) of the results for two

different scenarios. Firstly, an ideal scenario is considered where there are no added measurement bias and noise. Secondly, the filters have been tested in the presence of added noise and bias to the measurements. The results indicate that the proposed method using ASVSF-VBL provides a more accurate performance especially in the presence of added noise and bias disturbances. To illustrate the sensitivity of other methods to unknown noise statistics, Q and R are incorrectly specified as in Table 4.3. Figure 4.8a,b show the estimated SoC for both scenarios. The actual SoCs in these figures are evaluated using coulomb counting method from the cycler's data. This is because the initial value of SoC and nominal capacity of a battery are both known during a laboratory experiment. It can be seen from Figure 4.8b that after 1500 s the EKF error increases when the drive cycle C-rate is high as illustrated in Figure 4.7. Figure 4.9a,b display the percentage of SoC estimation error for both scenarios. It can be observed that the proposed strategy can keep the percentage of SoC error to less than 2%. It is also shown in Figures 4.10 and 4.11 that the proposed strategy is superior in identifying the current bias and internal resistance compared to the EKF and SVSF-VBL methods.

Table 4.4: Root mean square errors of ASVSF-VBL in comparison with SVSF-VBL and EKF for different scenarios..

Different Scenarios		**Ideal Scenario**		**In Presence of Noise and Current Bias**	
Initial Conditions		**Optimal Initial Noise Covariance**	**Non-Optimal Initial Noise Covariance**	**Optimal Initial Noise Covariance**	**Non-Optimal Initial Noise Covariance**
$RMSE_{SOC}$	EKF	0.5033	1.9735	1.2640	2.5416
	SVSF-VBL	0.3776	0.3776	0.5207	0.6462
	ASVSF-VBL	0.4304	0.4304	0.5386	0.5386
$RMSE_{V_T}$	EKF	0.000499	0.000695	0.0005477	0.000441
	SVSF-VBL	0.000276	0.000276	0.000241	0.000241
	ASVSF-VBL	0.00014	0.00014	0.00032	0.00032

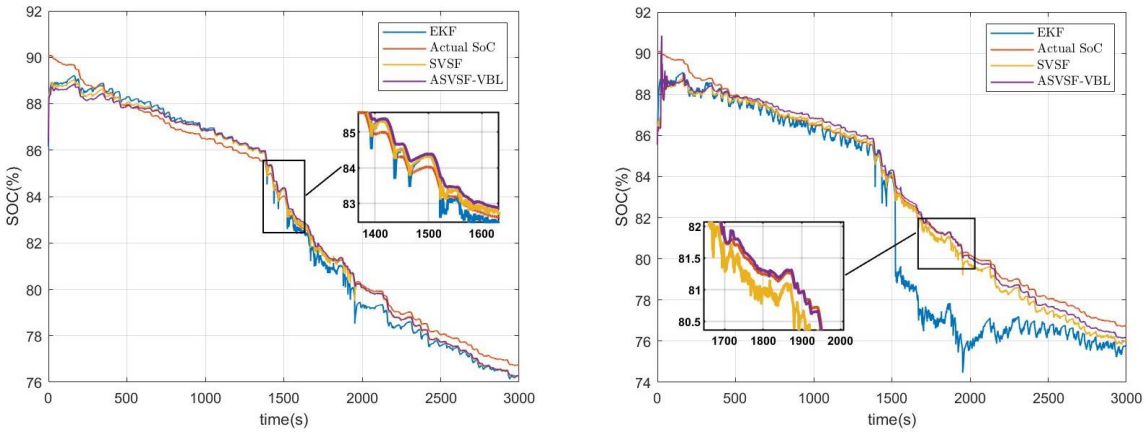

Figure 4.8: (**a**) Estimated SoC for an ideal scenario, (**b**) Estimated SoC in presence of noise and current bias.

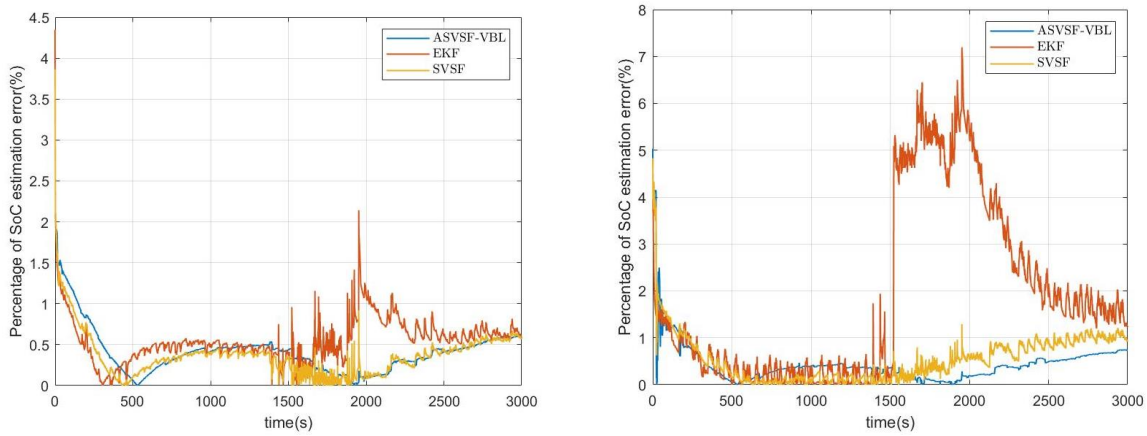

Figure 4.9: (**a**) Percentage of estimated SoC error for an ideal scenario, (**b**) Percentage of estimated SoC error in presence of noise and current bias.

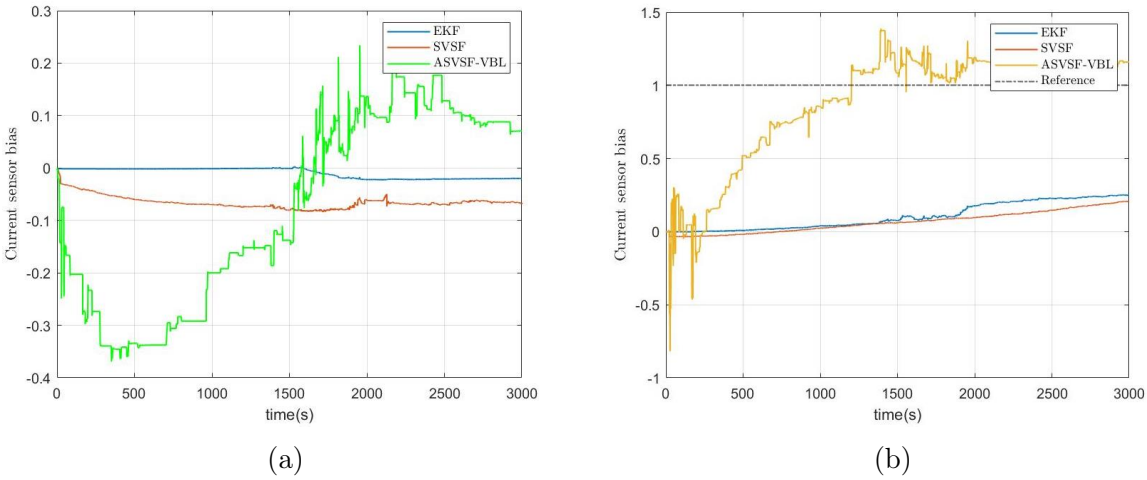

Figure 4.10: (**a**) Estimated current bias for an ideal scenario, (**b**) Estimated current bias in presence of noise and current bias.

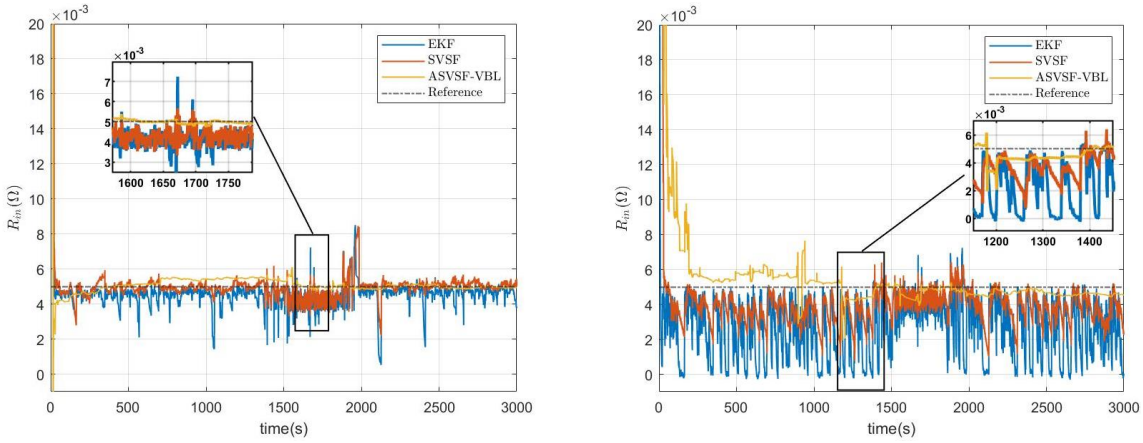

Figure 4.11: (**a**) Estimated internal resistance for an ideal scenario, (**b**) Estimated internal resistance in presence of noise and current bias.

4.5 Conclusions

An adaptive strategy referred to as the Adaptive Smooth Variable Structure Filter with Variable Boundary Layer (ASVSF-VBL) is proposed to estimate the SoC and SoH of a battery. The ASVSF-VBL is model-based and, in this study, a third-order Equivalent Circuit Model (ECM) was used as the filter model. In addition to the SoC and SoH, the state vector was augmented to estimate the bias in current measurement and the battery's internal resistance. The ASVSF-VBL adjusts the unknown system and measurement noise covariance matrices to provide a better performance under conditions involving noise with changing statistics. The adaptation scheme does not affect the stability of the estimation process. The estimated internal resistance of the ASVSF-VBL is used as an indicator of the battery SoH in addition to SoC. The proposed strategy was comparatively validated using experimental data and demonstrated a considerable improvement in performance. The proposed

ASVSF-VBL reduced the estimated error of voltage to about 0.14 mV compared to the SVSF-VBL and EKF. The presented strategy showed the lowest SoC estimation error that remains within 2% with an RMSE of approximately 0.4.

List of Notations

The following notations have been used within the body of this article.

V_T	Cell terminal voltage.
V_j	Voltage across RC branch, $j = 1, 2, 3$.
V_{ocv}	Open circuit voltage (nonlinear function of SoC).
SOC	State of Charge.
SOH	State of Health.
SOP	State of Power.
C_n	Cell nominal capacity.
R_{in}	Cell internal resistance.
R_j	Resistance of RC branch, $j = 1, 2, 3$.
C_j	Capacitor of RC branch, $j = 1, 2, 3$.
η	Cell Coulombic Efficiency.
ΔT	Sampling period.
k	Time sample.
i	Actual current flowing across the cell.
i_m	Measured current flowing across the cell.
i_b	Bias from the current sensor.
x	State vector or values.
u	Input to the system.
y	Measurement vector or values.
f	Nonlinear system function.
g	Input gain function.
h	Nonlinear measurement function.
X	An open subset of $\mathbb{R}^n$.
A	State matrix.
B	Input matrix.
w	System noise vector.

υ	Measurement noise vector.
$k+1 \mid k$	A-priori time step (i.e., before applied gain).
$k+1 \mid k+1$	A-posteriori time step (i.e., after update).
Q	System noise covariance matrix.
R	Measurement noise covariance matrix.
Diag(a) or $\bar{a}$	diagonal matrix of some vector a.
γ	SVSF "convergence" or memory parameter.
ψ	SVSF smoothing boundary layer width.
K	SVSF gain matrix.
P	State error covariance matrix.
$\hat{}$	Estimated vector or values.
S	Innovation covariance matrix.
$\mid a \mid$	Absolute value of some vector a.
T	Transpose of some vector or matrix.
e	Measurement (output) error vector.
E	Combination of measurement error vectors.
$sat(a)$	Defines a saturation of the term a.
H	Jacobian matrix of h.
m	Number of measurements.
n	Number of states.
$ln(a)$	Defines a natural logarithm of a.
$P(z \mid a)$	Probability density function of z conditioned to a.
α	Adaptive parameter.
$tr(A)$	Trace of matrix A.
λ_R	Forgetting factor of estimated measurement noise covariance.
λ_Q	Forgetting factor of estimated system noise covariance.
ϵ	Innovation Sequence.
ε	Residual Sequence.
I_j	Identity matrix ($I_j \in \mathbb{R}^{j \times j}$).
0_j	Zero matrix ($0_j \in \mathbb{R}^{j \times j}$).
V	Lyapunov function.

Chapter 5: Robust Estimation Strategy for Parallel-Connected Battery Cells

Sara Rahimifard[1], Marvin Messing[1], Saeid Habibi[1], Gillian Goward[2], Jimi Tjong[1]

[1] Department of Mechanical Engineering, McMaster University;

[2] Department of Chemistry and Chemical Biology, McMaster University, Hamilton, ON L8S 4L8, Canada

Abstract: State of Charge (SoC) and State of Health (SoH) estimation play a significant role in Battery Management Systems (BMSs) of Electric Vehicles (EVs) as the battery's safe and reliable operation heavily relies on them. Cell-to-cell variations in a battery pack can affect the performance of the BMS, resulting in the battery degradation and safety concerns. Although inconsistencies between parallel-connected cells are unpredictable, it is important to consider the influence of these changes in the BMS. A robust and adaptive estimation technique is required to provide a higher accuracy for SoC and SoH estimation when cell differences exist. This paper investigates the impact of the occurrence and existence of a faulty cell amongst a set of parallel-connected battery cells in a module. An estimation algorithm is proposed using a Smooth Variable Structure Filter with a Variable Boundary Layer (SVSF-VBL) to determine the SoC, SoC bias, and terminal voltage bias. In addition, online parametrization is considered to find the parameters of the pack and provide an indicator for SoH. In order to show the effectiveness of the proposed estimation algorithm, experimental data is collected from a parallel-connected battery cells configuration. The results show that the proposed methodology provides a highly

accurate estimation of the battery SoC and SoH for parallel-connected cells in the presence of faulty cells.

5.1 Introduction

The climate crisis is continuing to be a major problem and Greenhouse Gas (GHG) emissions are reaching new high records each year. Therefore, the transition to a cleaner and green economy needs to be a priority. Consequently, vehicle manufacturers are planning to introduce millions of Electric (EVs) and Hybrid Electric (HEVs) Vehicles in the near future. Lithium-ion (Li-ion) batteries are currently the preferred choice to produce the EVs and HEVs battery packs. Hundreds of Li-ion battery cells need to be connected in parallel and series to meet the required power and energy of an EV or HEV [133, 134].

To maximize a battery pack's performance and life expectancy, a robust strategy should be developed to adaptively estimate the states of operation of a battery pack considering the complexity of the connections. The key states for providing accurate indicators to the driver include State of Health (SoH), State of Charge (SoC), and State of Power (SoP). Where the SoC is an indicator of the remaining charge in a battery pack and SoH determines its capacity and remaining life. The SoP is also defined as the maximum available power that can be obtained subject to operational limits on battery voltage, current and SoC [135].

An ideal battery pack would provide an equal performance from each individual cell. There are, however, inconsistencies between cells stemming from battery manufacturing and packaging. In conditions where cells are produced under the same

conditions, even cells of the same chemistry display small variations [136]. In addition, while the battery pack is in operation, battery cells could differ in their SoC and SoH over time. These factors could have an impact on the performance of the battery pack and lead to uneven and faster aging of the cells [137]. For series connected cells, balancing must be used to equalize cell inconsistencies. The current of individual battery cells connected in series remains the same, but this configuration could lead to different SoC and voltage for each cells. Generally, balancing strategies for series-connected cells could be divided into two groups, including passive balancing and active balancing [138]. It is possible to increase the overall power and capacity of a battery pack by using these strategies, as well as preventing individual cells from getting overly charged or discharged [133, 139].

Passive balancing methods employ shunting resistors to remove the extra charge from a cell with a higher voltage until its charge matches those cells with lower voltages in the pack. These methods can only be used during battery charging [140]. On the other hand, active balancing methods use capacitors or inductors to balance the energy transferred among the cells. These methods transfer energy from cells with higher SoC to cells with lower SoCs until all the cells are balanced [135, 141].

Despite the variety of balancing methods offered for series-connected cells, it is quite challenging to diagnose cell inconsistencies in parallel-connected battery cells configurations. In [142], the characteristics of parallel-connected battery cells have been investigated. The study shows how cell inconsistencies could lead to accelerated degradation of a pack. A simplified battery pack model is also presented for a battery pack in [143]. The paper combines the Equivalent Circuit Model (ECM) of individual cells into a single equivalent model. However, the parameters of each ECM are

required to provide the pack model. Although, variations between parallel-connected cells can be investigated experimentally, it is impractical and costly to measure the current of individual cells connected in parallel. Therefore, parallel-connected cells are commonly modelled as a single cell where all the cells consume the same amount of current. The robustness of the energy management strategy is crucial to detecting cell differences with respect to the existing sensors [142]. The literature presents different energy management strategies that can be implemented to improve the performance of a battery pack [119, 135].

An important feature of the Battery Management System (BMS) is providing an accurate estimation of the battery pack SoC and SoH. These states can be estimated using existing measurements such as terminal voltage, current and temperature. The SoC of a battery can be estimated using different strategies which can be categorized into different groups including measurement-based methods, model-based methods, and data-driven methods. In a BMS, a combination of different estimators are usually considered to provide a better performance. Measurement-based methods are commonly used in industry as the base technology to estimate the SoC. These methods use measurements such as terminal voltage, impedance, or Open Circuit Voltage (OCV) to calculate the SoC. Coulomb counting is a most commonly used method where the SoC is estimated by integrating current. However, regular calibration is required over time due to inaccurate initial value of SoC, measurement bias and changing capacity [23, 31, 83].

Compared to measurement-based methods, model-based approaches provide a better insight into the battery's internal dynamics, therefore they are more practical to be implemented onboard of a BMS. For these methods, a proper model should be

provided for the battery that can represent the cell characteristics under different operating conditions. Battery models commonly used in BMSs are categorized into two groups including electrochemical and ECM. Electrochemical models are quite complicated to use with estimation algorithms onboard of a BMS. Although, ECMs do not model electrochemical effects within a battery, they can provide an accurate temporal model within the bounded operating range of a battery for real-time applications [91, 92].

In addition to a battery model, an estimation strategy is required to be implemented. These methods include but are not limited to the Extended Kalman Filter (EKF), Particle Filter (PF), Least Square Filter (LSF), Unscented KF (UKF) or the more robust strategies such as the Adaptive EKF (AEKF), H_∞ Filtering and Smooth Variable Structure Filter (SVSF) [71, 98, 112].

Different algorithms can be employed for adaptability to different operating conditions and battery degradation. Common approaches include adaptive filter and Multiple Model (MM) strategies where the battery model parameters can be updated as they change [74, 94]. Noise tuning and parameter tuning can be considered as adaptive filter adjustment. Noise tuning method such as AEKF and Adaptive SVSF could provide a more robust estimate in presence of changing measurement noises [144]. Parameter tuning strategies include joint and dual estimation methods where they take available measurements of a battery to estimate model parameters in real-time [62, 75]. These methods provide an updated battery model over time which leads to a more accurate estimate. MM methods, on the other hand, employ a finite number of pre-defined models to work with different operating conditions of a battery such as temperature, current rate, and SoH [93, 119, 120].

Although, different methods are presented in literature that can provide robustness and accuracy for state estimation of a battery cell, it is quite challenging to get the same result in a pack. Cell-to-cell variations should be considered for battery pack states estimation. Additionally, the method should not place an excessive amount of computational burden on the BMS. Battery pack state estimation strategies, therefore, can be categorized into two groups. The first group considers the entire battery pack to be one single large cell to estimate the state of the battery pack as a function of its voltage and current, where the pack ECM model parameters are typically determined offline [137, 145]. These approaches can be implemented easily, but cell inconsistencies can not be considered and therefore accurate estimation can not be provided [146].

Battery pack states can also be estimated by considering the states of individual cells. These methods can also be simplified by selecting a reference cell or a mean cell. The reference cell is usually the weakest cell in a pack, where the cell has maximum voltage during charging or minimum voltage during discharging [134, 147, 148]. The individual state estimation can also be estimated by comparing to a mean cell defined by all voltages [149, 150, 151]. These strategies along with an estimator such as EKF, AEKF, Sigma Point KF (SPKF) and UKF are typically considered onboard of a BMS [135]. It is imperative to use a more robust approach not only to improve the state estimation, but also to detect cell inconsistencies to enhance battery pack safety.

SVSF-VBL and EKF methods are compared in this paper in terms of accuracy and robustness to cell inconsistencies for state estimation of a parallel-connected battery module. A new formulation for the ECM is presented with this method where the states are augmented with two more variables including the SoC bias and

voltage sensor bias to provide a better performance. A Recursive Least Square (RLS) method is also considered to adaptively estimate the parameters of the ECM for a parallel-connected module over time.

This paper includes the following contributions:

1. SoC bias and terminal voltage bias are considered as states of the ECM to provide a more accurate result for SoC in presence of a faulty cell in a parallel-connected battery module.

2. Online parametrization is employed to update the model of a battery module over time.

3. The Smooth Variable Structure Filter with Variable Boundary Layer (SVSF-VBL) and Extended Kalman Filter (EKF) strategies are compared in terms of their accuracy of SoC estimation in presence of cell inconsistencies.

4. The proposed methods are validated using experimental data.

The outline of this paper is as follows: Section 5.2 presents the battery pack model. The proposed estimation technique for SoC and SoH is introduced in Section 5.3. Section 5.4 demonstrates the experimental procedure and validation results. The conclusions are presented in Section 5.5.

5.2 System Modeling

This section describes the modified ECM to be used for state estimation of parallel-connected battery cells. ECMs are typically used to model a single Li-ion battery

cell. The transient response of a battery can be captured by multiple Resistance-Capacitance (RC) branches in an ECM. A first order model is considered in this paper to provide a balance between complexity and accuracy with online parametrization. Figure 5.1 shows the ECM considered for a single battery cell. The series internal resistance (R_{in}) is used to relate the battery's terminal voltage to its current. The terminal voltage of a battery can be obtained from discrete-time state equations as follows, [104, 152].

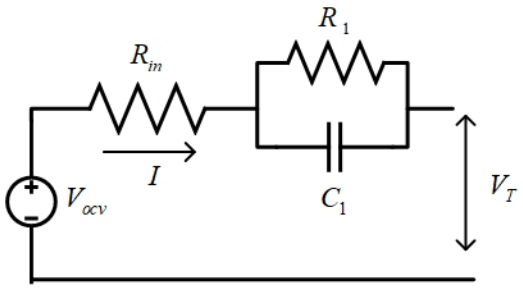

Figure 5.1: First-order equivalent circuit battery model.

$$V_{1,k+1} = (1 - \frac{\Delta T}{\tau_1})V_{1,k} + \frac{R_1 \Delta T}{\tau_1} i_k \tag{5.1}$$

$$SOC_{k+1} = SOC_k - \frac{\eta \Delta T}{C_n} i_k \tag{5.2}$$

$$V_{T,k} = V_{ocv}(SOC_k) - V_{1,k} - R_{in} i_k \tag{5.3}$$

where V_T is the Cell terminal voltage, V_1 is the voltage across the RC branch, V_{ocv} is the OCV (nonlinear function of SoC), C_n is the cell nominal capacity, R_{in} is the cell internal resistance, R_1 is the resistance of RC branch, τ_1 is the time constant of

RC branch, η is the cell Coulombic Efficiency (CE), ΔT is the sampling period, i is the current flowing across the cell, and k is the time step.

In a BMS, coulomb counting is commonly used as one of the SoC estimation methods through the following Equation [29],

$$SOC(t) = SOC_0 - \frac{1}{C_n}\int_0^t \eta i(\tau)d\tau \tag{5.4}$$

where SOC_0 is the battery SoC's initial value. This method may lead to a bias in the SoC calculation due to an inaccurate SOC_0, bias in current sensor, and changes in the nominal capacity over time. In [119], the coulomb counting method is combined with model-based estimation as an extra measure to overcome this issue. Therefore, the so-called SoC bias can be considered as a state with slow dynamics to be estimated as follows,

$$SOC_{b,k+1} = SOC_{b,k} + w_{b_k} \tag{5.5}$$

where SOC_b is the SoC bias and w_{b_k} is white noise. The measured SoC includes this bias such that,

$$SOC_{m,k} = SOC_k + SOC_{b,k} \tag{5.6}$$

where SOC_m is the measured SoC from coulomb counting method and SOC is the actual SoC. Since there are not enough sensors in parallel-connected cells, the voltage drop due to cell inconsistencies can not be detected easily. Therefore, a bias

may exist in the measured voltage of the battery. Here, the voltage sensor bias is considered as a state augmented with the ECM model to be estimated. This could improve the estimation performance and can be used to detect voltage drop in a pack. The voltage sensor bias is defined as follows,

$$V_{b,k+1} = V_{b,k} + w_{v_k} \tag{5.7}$$

where V_b is the bias from the voltage sensor and w_{v_k} is white noise. The measured terminal voltage across the cell includes this bias and is defined as follows,

$$V_{m,k} = V_{T,k} + V_{b,k} \tag{5.8}$$

where V_m is the measured terminal voltage, and V_T is the actual terminal voltage of a battery cell.

The state-space form of the modified model can be described as,

$$x_{k+1} = f(x_k) + g(x_k)u_k, \tag{5.9}$$

$$y_k = h(x_k, u_k) \tag{5.10}$$

where $x \in X$ is state vector, $u \in \mathbb{R}$ is input to the system, $y \in \mathbb{R}^m$ is measurement vector. Here, $f : X \to \mathbb{R}^n$ is nonlinear system function, $g : X \to \mathbb{R}^n$ is input gain function and $h : X \to \mathbb{R}^m$ is nonlinear measurement function where all are differentiable functions. The state and measurement vectors are $x_k = \begin{bmatrix} V_{1,k} & SOC_k & SOC_{b,k} & V_bk \end{bmatrix}^{\mathrm{T}}$ and $y_k = \begin{bmatrix} V_{m,k} & SOC_{m,k} \end{bmatrix}^{\mathrm{T}}$, respectively. Note that in this model $f(x_k)$ is linear and $f(x_k) = Ax_k$ and $g(x_k) = B$ are given as,

$$A=\begin{bmatrix} 1-\frac{\Delta T}{\tau_1} & 0_{1\times 3} \\ 0_{3\times 1} & I_3 \end{bmatrix}, \quad B=\Delta T \begin{bmatrix} \frac{R_1}{\tau_1} \\ \frac{-\eta}{C_n} \\ 0 \\ 0 \end{bmatrix} \tag{5.11}$$

Here, A is the state matrix and B is the input matrix, I_j is an identity matrix ($I_j \in \mathbb{R}^{j\times j}$), and $0_{i\times j}$ is a Zero matrix ($0_{i\times j} \in \mathbb{R}^{i\times j}$). The output equations can be defined by substituting Equation 5.3 into 5.8 along with Equation 5.6.

Parallel-connected battery cells can be regarded as a single cell with a higher capacity. The battery module can be described with an ECM as presented in Figure 5.2 where the parameters of the module's model are different than a single cell. However, the battery module's model can be described using the same equations presented for a single cell. The following equations should be considered for the battery model of the parallel-connected module.

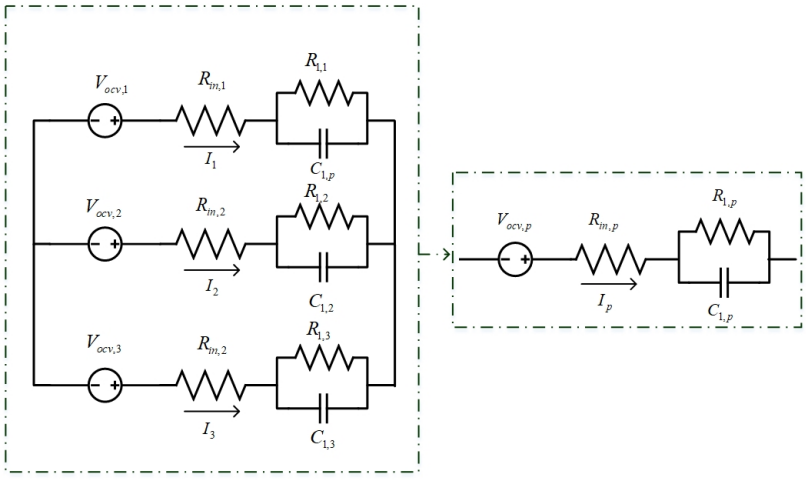

Figure 5.2: ECM for parallel-connected battery cells.

$$i_p = \sum_{j=1}^{N_p} i_j \tag{5.12}$$

$$C_{n,p} = N_p C_n = \sum_{j=1}^{N_p} C_{n,j} \tag{5.13}$$

where i_j is the current flowing through the jth battery cell, i_p presents the current flowing through the battery module (input to the model for the module), N_p is the number of cells connected in parallel, $C_{n,j}$ is the nominal capacity of the jth battery cell, and $C_{n,p}$ is the nominal capacity of the module.

5.3 The Proposed Estimation Approach

This section proposes a robust strategy for state estimation of a parallel-connected battery module. The RLS strategy used for online parameter identification of the module is defined in this section. EKF and SVSF-VBL for state estimation are later expressed in details.

5.3.1 Dual Estimation Strategy

This section describes the dual estimation strategy considered for parallel-connected battery cells. Figure 5.3 provides the key points of the proposed strategy. First, the terminal voltage and current of the parallel-connected module are measured. Given the number of parallel connected cells, the battery module can be considered as a single cell. If there is no variation amongst the cells, the current flow through each cell can be defined as follows,

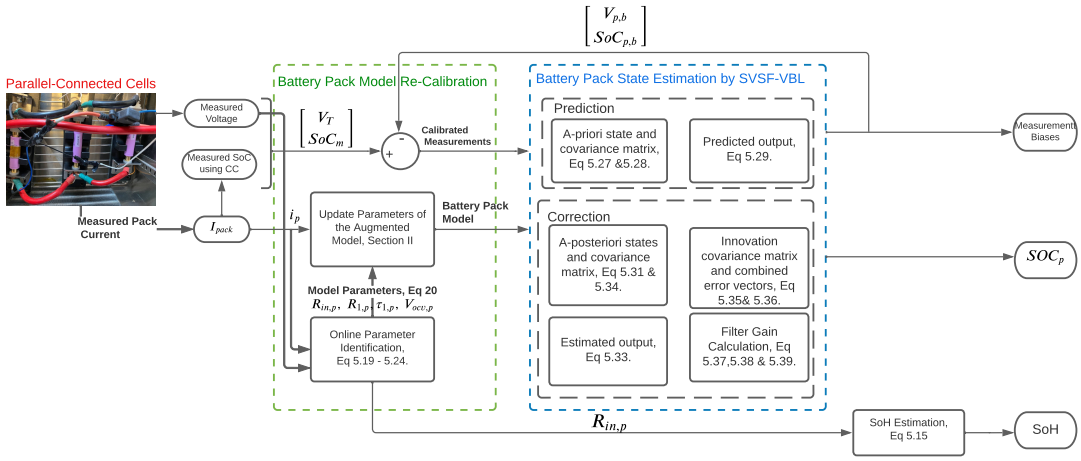

Figure 5.3: Estimation Strategy for Parallel-Connected Cells.

$$i_{cell} = \frac{i_p}{N_p} \tag{5.14}$$

However, in real-time applications, some cell variations cannot be avoided, and cell-to-cell inconsistencies can become worse over time. Therefore, the current consumed by each cell is not the same and Equation 5.14 cannot be applied. Therefore, an estimation algorithm based on the pack current (i_p) is more reliable.

An online parameter identification method (Section 5.3.2) is used to re-define the internal resistance (R_{in}), the time constant and OCV of the parallel-connected battery module. Although standard tests are defined for estimating parameters of a single cell, parameters of a battery module are more difficult to identify. Therefore, online parametrization is considered to provide a more accurate model for the battery module over time. The obtained parameters are then employed along with the SVSF-VBL to estimate the states of the battery including its SoC and measurement biases.

The estimated SoC bias and voltage sensor bias are then utilized to re-calibrate the measurements to provide an optimized model identification along with a more accurate estimate of the states. The estimated internal resistance (R_{in}) from the RLS strategy is considered as an indicator for SoH of the battery pack to be calculated as follows,

$$SOH = \frac{R_{EOL,p} - R_{in}}{R_{EOL,p} - R_{new,p}} \times 100\% \tag{5.15}$$

where $R_{EOL,p}$ is the internal resistance at the end of life of the battery module, and $R_{new,p}$ is the internal resistance of the battery pack with new batteries. The $R_{new,p}$ of a parallel-connected battery module can approximately be calculated as follows,

$$R_{new,p} = \frac{R_{new,cell}}{N_p} \tag{5.16}$$

where $R_{new,cell}$ is the internal resistance of a new battery cell that is usually provided by its manufacturer. $R_{EOL,p}$ can similarly be obtained, knowing the internal resistance of a battery cell in its end of life. The methods used in this algorithm are described in the remainder of this section.

5.3.2 Online Parameters Estimation

This section provides a description of a real-time parameter estimation method, instrumental to more accurate state estimation for parallel-connected battery cells.

Battery model parameters can be affected by different factors including SoC, temperature, and SoH. It is critical to update the parameters of a battery model to provide an accurate estimation of its states. In addition, model parameters of a parallel-connected battery module cannot be identified offline and it is costly to determine the parameters of every single cell. Online parameter estimation is effective for parallel-connected cells to determine the effect of the weakest cell in the module's model [36, 105]. Recursive Least Square (RLS) with a forgetting factor is considered here to capture the changes in parameters of the battery module to diagnose slow variations in the ECM. This strategy is used to refine parameters including the internal resistance ($R_{in,p}$), the resistor ($R_{1,p}$) and time constant ($\tau_{1,p}$) of the RC branch, and the open circuit voltage ($V_{ocv,p}$) of the ECM for the battery module.

$$V_{T,p_k} = V_{ocv,p} - (1 - \frac{\Delta T}{\tau_{p,1}})V_{1,k} - R_{in,p}i_{p,k} \tag{5.17}$$

where V_{T,p_k} is the actual terminal voltage of the battery module. Using Laplace transformation, the following equation can be obtained that relates the load current (i_k) to the known voltage.

$$V_{T,p}(s) = V_{ocv,p} - (R_{in,p} + \frac{R_{1,p}}{\tau_{1,p}s + 1})I_p(s) \tag{5.18}$$

Using the inverse laplace transform of Equation 5.18, a linear regression model can be constructed based on the ECM as follows [79, 80],

$$V_k = \theta^T \Phi_k \tag{5.19}$$

where $\Phi_k = [i_{p,k-1} \quad i_{p,k} \quad V_{k-1} \quad 1]^T$ is the regressor of known signals and $\theta = [\theta_1 \quad ... \quad \theta_4]^T$ is the parametric vector defined as,

$$\begin{aligned}
\theta_1 &= R_{1,p}(1 - e^{-\frac{T_s}{\tau_{1,p}}}) - R_{in,p}e^{-\frac{T_s}{\tau_{1,p}}} \\
\theta_2 &= R_{in,p} \\
\theta_3 &= e^{-\frac{T_s}{\tau_{1,p}}} \\
\theta_4 &= (1 - \theta_3)V_{ocv,p}
\end{aligned} \tag{5.20}$$

The loss function of the RLS method can be defined as follows [36],

$$V(\hat{\theta}, k) = \frac{1}{2}\sum_{i=1}^{k} \lambda^{k-i}(y_i - \hat{\theta}_k^T \Phi_i) \tag{5.21}$$

Here, λ is called the forgetting factor and $0 < \lambda < 1$. This loss functions is used to obtain, the parametric vector (θ) as follows,

$$\hat{\theta}_k = \hat{\theta}_{k-1} + L_k(y_k - \hat{\theta}_{k-1}^T \Phi_k) \tag{5.22}$$

$L(k)$ and $P(k)$ are the gain and covariance matrix, that are updated as follows,

$$L_k = P_{k-1}\Phi_k(\lambda + \Phi_k^T P_{k-1}\Phi_k)^{-1} \tag{5.23}$$

$$P_k = (I - L_k\Phi_k^T)P_{k-1}\frac{1}{\lambda} \tag{5.24}$$

The online parameter identification is used to update parameters of the model for the battery module as shown in Figure 5.3.

5.3.3 Extended Kalman Filter

This section summarizes the EKF formulation. The EKF is a common strategy for battery state estimation as it can easily be applied in a BMS. It is used here to provide a fair comparison. Further to the following nonlinear model of a system,

$$\begin{aligned} x_{k+1} &= f(x_k, u_k, w_k), \\ y_k &= h(x_k, u_k, v_k) \end{aligned} \tag{5.25}$$

w and v are the system and measurement noise vectors that are white with covariance matrices Q_k and R_k, respectively. Linearization is required for the presented ECM in Section 5.2 to employ the EKF. The matrix form of the system equation is presented in Equation 5.11 and the jacobian matrix derived from the nonlinear measurement function ($h(x_k, u_k)$) is as follows,

$$H = \begin{bmatrix} -1 & \frac{\partial V_{ocv,p}}{\partial SOC_p} & 0 & 1 \\ 0 & 1 & 1 & 0 \end{bmatrix} \tag{5.26}$$

The EKF uses the following steps in an iterative fashion:

- Prediction: The a-priori state estimate are first obtained from Equation 5.27. The error covariance is then calculated as in Equation 5.28. Substituting Equation 5.27 into the system measurement equation provides the predicated output.

$$\hat{x}_{k+1|k} = A\hat{x}_{k|k} + Bu_k \tag{5.27}$$

$$P_{k+1|k} = AP_{k|k}A^T + Q_k \tag{5.28}$$

$$\hat{y}_{k+1|k} = \hat{H}\hat{x}_{k+1|k} \tag{5.29}$$

- Correction: The EKF gain as presented in Equation 5.30 is used to refine the a-priori state estimate and error covariance into its a-posteriori form as presented in Equations 5.31 and 5.33.

$$K_k = P_{k+1|k}H_k^T[\hat{H}_k P_{k+1|k}\hat{H}_k^T + R_k]^{-1} \tag{5.30}$$

$$\hat{x}_{k+1|k+1} = \hat{x}_{k+1|k} + K_k[z_k - \hat{z}_{k+1|k}] \tag{5.31}$$

$$P_{k+1|k} = [I - K_k\hat{H}_k]P_{k+1|k} \tag{5.32}$$

$$\hat{y}_{k+1|k+1} = \hat{H}\hat{x}_{k+1|k+1} \tag{5.33}$$

Equations 5.27 through 5.33 summarize the EKF algorithm [100].

5.3.4 Smooth Variable Structure Filter

The SVSF is a state and parameter estimation approach that was first introduced in 2007. The strategy works based on the sliding-mode concept in a predictor-corrector framework where a discontinuous gain and a smoothing boundary layer is employed. The smoothing boundary layer reduces chattering caused by using a discontinuous corrective action. In the SVSF, the discontinuous corrective action forces the estimated states to converge to a neighbourhood of the actual value. It has been shown that the SVSF method is stable and robust against uncertainties and noise [153]. The strategy can be applied to any observable and differentiable system with a nonlinear equation as presented in Equation 5.25.

The SVSF has been enhanced with modifications such as its optimal formulation with a time-varying smooth boundary layer (SVSF-VBL), and its combinations with other filters such as PF, KF, EKF, and UKF [55, 103, 108]. It is also shown that SVSF based strategies could provide a better performance for EV applications [70]. Similar to EKF, the SVSF contains two main steps called prediction and correction as presented in Section 5.3.3. The differences between these two strategies are the SVSF gain applied in the correction step and the a-posteriori covariance error where it can be defined as follows,

$$P_{k+1|k+1} = (I - K_{k+1}\hat{H})P_{k+1|k}(I - K_{k+1}\hat{H})^{T} + K_{k+1}R_{k+1}K_{k+1}^{T} \tag{5.34}$$

The SVSF smoothing boundary layer width (ψ_{k+1}) can be obtained from Equation

5.37,

$$S_{k+1} = \hat{H} P_{k+1|k} \hat{H}^T + R_{k+1} \tag{5.35}$$

$$E_{k+1} = |e_{k+1|k}| + \gamma |e_{k|k}| \tag{5.36}$$

$$\psi_{k+1} = (\bar{E}_{k+1}^{-1} \hat{H} P_{k+1|k} \hat{H}^T S_{k+1}^T)^{-1} \tag{5.37}$$

where S is the innovation covariance matrix, E is the combination of the a-priori and a-posteriori measurement error vector, γ is the SVSF convergence parameter, $e_{k+1|k} = z_{k+1} - \hat{z}_{k+1|k}$ is the a-priori measurement error, and $e_{k|k} = z_k - \hat{z}_{k|k}$ is the a-posteriori measurement error from previous correction iteration.

The SVSF-VBL gain for $\psi_{k+1} < \psi_{lim}$ is calculated as follows,

$$K_{k+1} = \hat{H}^{-1} \bar{E}_{k+1} \psi_{k+1}^{-1} \tag{5.38}$$

where ψ_{lim} is upper limit for the boundary layer. The SVSF-VBL gain when $\psi_{k+1} \geqslant \psi_{lim}$ is obtained as,

$$K_{k+1} = \hat{H}^{-1} \bar{E}_{k+1} sat(e_{k+1|k} \psi_{k+1}^{-1}) \bar{e}_{k+1|k}^{-1} \tag{5.39}$$

The SVSF-VBl is used for state estimation of the battery module. The prediction and correction steps are shown in Figure 5.3.

5.4 Experimental Validation

This section describes the experiments and experimental setup used in this study to validate the proposed strategy. The results are then presented and discussed in this section.

5.4.1 Testbed

Laboratory tests are conducted on a parallel-connected battery module to evaluate the performance of the proposed approach. The experimental setup consisted of a *D&V* Electronics Ltd battery cycler (BCT-150), an environmental chamber namely Associated Environmental Systems, and Four Samsung INR18650-35E Li-ion battery cells. Batteries purchased on the same date are used to minimize the cell-to-cell variations. Tables 5.1 and 5.2 provide a summary of the specifications of the test equipment and battery cells, respectively. Figure 5.4 depicts the equipment used. Three cells were connected in parallel into a module and housed in a thermal chamber to provide a controlled environmental condition. The terminal voltage and current flowing through the module are measured. A thermocouple is attached to the cells for the measurement and monitoring of the surface temperature of the cells during the test. The tests have been performed at room temperature ($25°C$).

Table 5.1: A summary of specifications for BCT-150 Battery Cell Testing.

	Cycler	EIS	Coulombic
Voltage Range	1-6 V	1-6 V	1-6 V
Maximum Current	100 A	5 A	2 A
Current Range	5 A / 25 A / 100 A	5 A	2 A / 5 A
Band Width	-	0-50 kHz	-

Table 5.2: Battery Cells Specifications.

Manufacture	Samsung
Type	Lithium-ion
Model Name	INR18650-35E
Nominal Capacity (mAh)	3400
Nominal Voltage (V)	3.6
Minimum Voltage (V)	2.65
Maximum Voltage (V)	4.2

Figure 5.4: Experimental Setup.

To introduce a faulty cell among the parallel-connected battery cells, an aging study was conducted for one of the Li-ion cells. Standard charge and discharge cycles were used in the aging procedure. During cycling, a constant current (CC) charge was applied until the cell reached its maximum voltage ($4.2V$), followed by a constant voltage (CV) charge at $4.2V$ with a current cut-off of $0.02C = 0.068A$ as recommended by the manufacturer. Then a CC discharge was applied until the minimum voltage ($2.65V$) was reached. The discharge current was set to the maximum discharge current

($2.35C = 8A$) recommended by manufacturer. The cell was cycled to reach 90% capacity of a new cell to establish a clear difference in age.

Reference Performance Tests (RPTs) were conducted for the new and aged (90% capacity) battery cells to capture their characteristics including capacity, internal resistance, and OCV. Pulse charge/discharge tests were considered in this study for offline parameter identification. Offline parameter identification was used as a baseline for comparison.

Velocity profiles of different drive cycles were used to generate current profiles, which were then applied to the battery module. The Urban Dynamometer Driving Schedule (UDDS), shown in Figure 5.5a, was applied to provide baseline results for the estimation method. A mixture of different drive cycles, consisting of the driving schedule called the UDDS, US06, and HWFET, was then implemented on the battery module as shown in Figure 5.5b to obtain the voltage profiles from the battery pack for a range of SoCs. The mixed drive cycle was used to validate the proposed strategy.

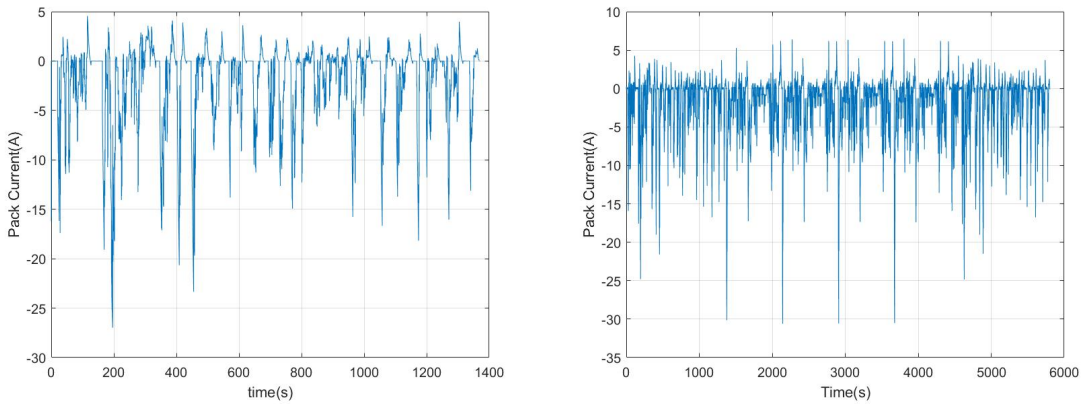

(a) (b)

Figure 5.5: Current profile applied to the battery pack for the a) UDDS, b) mixed drive cycle.

Two testing scenarios were conducted. First, three new cells were considered for the parallel-connected battery module to represent the healthy condition. The aged battery cell was then connected in parallel to two new battery cells to test the proposed method under a defective condition where one cell is different from others. Figure 5.6 displays the measured voltage of the battery module for the healthy and faulty conditions using the mixed drive cycle as shown in Figure 5.5b. A small voltage drop is shown when there is variation among cells in a parallel-connected battery module. It is important to update the estimation strategy to be able to capture any changes in the battery cells and provide better performance in state estimation of the module.

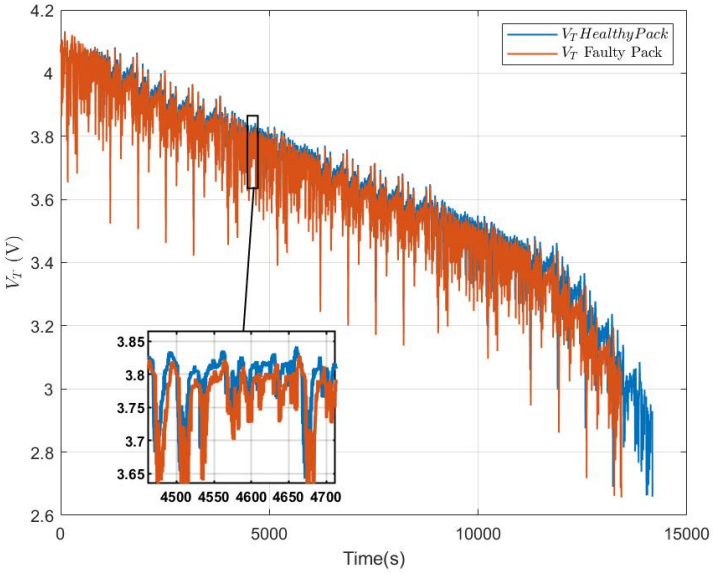

Figure 5.6: Measured terminal voltage of the parallel-connected pack using validation data.

5.4.2 Filter Initialization

The parameters of the filters must be tuned properly to provide a fair comparison. The tuned parameters for the EKF and SVSF-VBL are as follows: the measurement noise and process noise covariance matrices of the SVSF-VBL and EKF with a simple first-order ECM were selected as $R = 5$ and $Q = 10^{-8}I_2$, respectively where I_2 is an 2-by-2 identity matrix. A small value of Q implies some trust in the model. The measurement noise covariance (R) represents the degree of uncertainty. The initial value of the state error covariance matrix is set to $P = 10^{-2}I_2$. The same initial parameters were used for the EKF and SVSF-VBL filters to provide a direct comparison. The SVSF-VBL requires two additional parameters including its convergence parameter and upper limit of its boundary layer to be specified. These were chosen as $\gamma = 0.54$ and $\psi = 0.05$, respectively. The battery model used in the proposed algorithm includes two measurements as well as two additional states referring to the SoC bias and sensor voltage bias. Therefore, the measurement and process noise covariance were set to $R = diag[5, 5]$ and $Q = 10^{-8}I_4$, respectively as the size of the matrices were different. The state error covariance matrix was set to $P = 10^{-2}I_4$. For the RLS filter, the covariance matrix is set to $P = 10^2$ and the forgetting factor is set to $\lambda = 0.95$. The initial battery SoC is considered as $SOC_0 = 75\%$ to verify the performance of the proposed strategy. Table 5.3 provides a summary of the initial parameters.

5.4.3 Results

The EKF and SVSF are first applied to the measured data from the UDDS cycle current profile as depicted in Figure 5.5a. This profile was used to tune the parameters

Table 5.3: Filters Initialization Parameters.

Parameters	Symbol	Value
RLS forgetting Factor	λ	0.95
RLS Covariance Matrix	P	10^2
SVSF Convergence Parameter	γ	0.54
SVSF Upper Limit of the Boundary Layer	ψ	0.05

of the SVSF-VBL and EKF. The performance of these filters is later compared to the proposed strategy for a fair comparison. To evaluate the EKF and SVSF, the ECM should be parameterized. A first-order model is considered for the EKF and SVSF to provide a decent comparison to the proposed method. The conducted pulse discharge test is used along with an automated battery model parameter identification to provide offline parameters of the first-order ECM [16]. Lookup tables are provided for the parameters for a full range of SoCs. Table 5.4a presents a summary of the parameters of the first-order ECM. Equation 5.14 is used to obtain the approximate current flowing across a single cell. The SoC of a single battery cell is estimated by the SVSF and EKF filters using the current of a single cell. The estimated SoC is then considered as the SoC of the parallel-connected battery module.

Figure 5.7a displays the estimated terminal voltage using EKF and SVSF-VBL for a healthy condition where all the cells have the same SoH. Figure 5.7b displays the estimated terminal voltage using EKF and SVSF-VBL for a faulty condition where cell-to-cell variation exists. The EKF and SVSF-VBL are both using the same ECM model of a new battery cell. Therefore, the amount of current consumed by each parallel-connected cell is the same as shown in Equation 5.14. EKF and SVSF-VBL are expected to perform similarly in the healthy condition as shown in Figure 5.7a. However, if there is a faulty cell amongst the parallel-connected cells, the ECM is no

longer able to describe the exact behavior of the battery and therefore may not be suitable for an accurate state estimation. The parameters of the ECM (presented in Table 5.4a) should be updated when a battery ages. Further, Equation 5.14 is no longer applicable as the aged cell has a higher resistance but with the same terminal voltage, and has less current in comparison to the new cells connected to it in parallel. Since the capacity of the module decreases due to the existence of an aged cell, the terminal voltage of the module is expected to drop. This inconsistency provides uncertainty and bias in state estimation which should be taken into consideration. Slight differences can be seen between the EKF and SVSF-VBL in the estimated terminal voltages demonstrated in Figure 5.7b. This is because the performance of the EKF is compromised by the uncertainty caused by the faulty condition. In contrast, the robustness of the SVSF-VBL to the model uncertainty and drift improves the estimation in comparison to the EKF. Therefore, the SVSF-VBL was able to identify the voltage decrease, resulting in increased estimation accuracy. The terminal voltage errors of the EKF versus the SVSF-VBL for healthy and faulty conditions are shown in Figure 5.8. It is shown that a more robust filter is significantly more effective in detecting any voltage decrease in parallel-connected battery cells due to cell-to-cell variability.

To implement the proposed strategy, the parallel-connected battery module is considered as one cell and its parameters are estimated using the RLS filter described in Section 5.3.2. The parameters of a battery model change with SoH and SoC. Online parameter detection is effective in state estimation. Figure 5.9 shows the online predicted parameters for healthy and faulty conditions as they change with the battery module's SoC and SoH. The parameters are influenced by the malfunctioning

Table 5.4: Model Parameters bound of a) the first-order and b) the second-order ECMs for a single battery cell. Example given for 50% SoC.

(a)

Parameters	R_{in}	$R_1(\Omega)$	$\tau_1(s)$
Upper Bound	0.0766	0.0594	176.97
Lower Bound	0.0595	0.0115	29.281
Example 1st Order	0.0631	0.024461	59.011

(b)

Parameters	R_{in}	$R_1(\Omega)$	$R_2(\Omega)$	$\tau_1(s)$	$\tau_2(s)$
Upper Bound	0.0979	0.0099	0.0078	89.3900	106.7200
Lower Bound	0.0657	0.00047630	0.00049631	20.4130	48.0590
Example	0.0780	0.0027	0.00049631	63.5050	96.8920

cell in the module, which leads to module degradation. The presence of an aged cell alters the module's capacity and resistance. As a result, the parameters of the ECM model provided for the module must be updated. The internal resistance of an aged cell increases and therefore, the internal resistance of the battery module should increase as well, as shown in Figure 5.9b. The terminal voltage and the OCV of an aged cell is lowers in compared to a new cell. Similarly, the OCV of the battery module should decrease in the presence of an aged cell as presented in Figure 5.9a. Figure 5.9c and 5.9d show the parameters of the RC branch for the healthy and faulty conditions. Resistance and time constant are altered with SoC and SoH, similar to other parameters.

To validate the proposed strategy, the SVSF-VBL with online parametrization using the augmented form of ECM is implemented to investigate the effect of real-time parameter identification in state estimation of the parallel-connected battery module. The validation data displayed in Figure 5.5b and its measured terminal voltage for the healthy and faulty conditions presented in Figure 5.6 are considered to

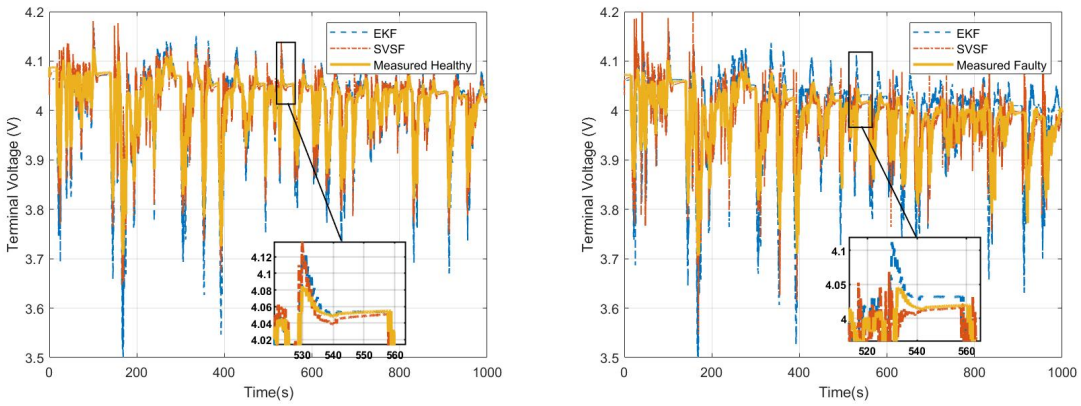

(a) (b)

Figure 5.7: Estimated terminal voltage using EKF and SVSF for a) healthy and b) faulty parallel-connected cells.

evaluate the performance of different filters. To provide a better performance while using offline parameter identification, a second-order model is also considered for the EKF and SVSF to be compared to the first-order one and the proposed algorithm. The parameters of the second-order model are presented in Table 5.4b. Figure 5.10a exhibits the estimated terminal voltage for the healthy condition where all three cells are new. As there is no uncertainty or bias in the battery module, it is demonstrated that all filters provide the same performance. Figure 5.10b displays the estimated terminal voltage for the faulty condition where an aged cell is placed in the battery module. The SVSF-VBL based filters are able to capture the voltage drop and a better estimate for the terminal voltage is obtained. Figure 5.11a shows the estimated SoC for a healthy condition. To take a closer loop into the SoC estimation, a smaller range is displayed. Despite the fact that EKF and SVSF-VBL with offline parameter identification were able to estimate the terminal voltage accurately, the SVSF-VBL method with a second-order ECM improved the estimated SoC. The parameters of

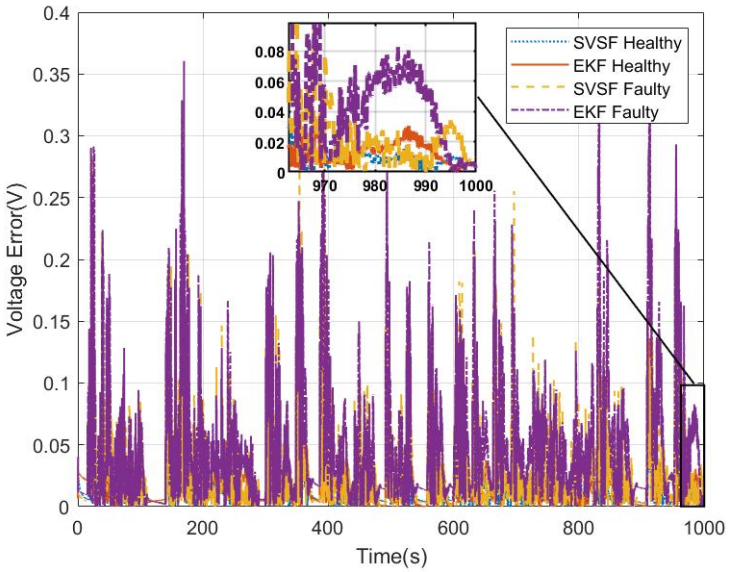

Figure 5.8: Terminal voltage error using EKF and SVSF-VBL for healthy and faulty condition.

ECMs for EKF and SVSF-VBL are identified using specific test. However, the parameters of a model could change when a battery cell placed in a pack. Online parameter estimation enhances state estimation by identifying the parameters of the ECM in real-time. Although, SoC estimation is improved by using online parametrization, the estimated SoC using the proposed method changed significantly as it also considers measurement biases and the biases change significantly as shown in Figure 5.12. This could affect the results of the faulty condition even more. Figure 5.11b presents the estimated SoC for a faulty condition. The figure displays that the proposed method provides a higher accuracy for the SoC estimation even when there is cell-to-cell variation. The estimation errors increase for the faulty condition using EKF and SVSF-VBL even with online parametrization. Although, the SVSF-VBL with the modified model employs a first-order ECM, the accuracy of the SoC estimation is

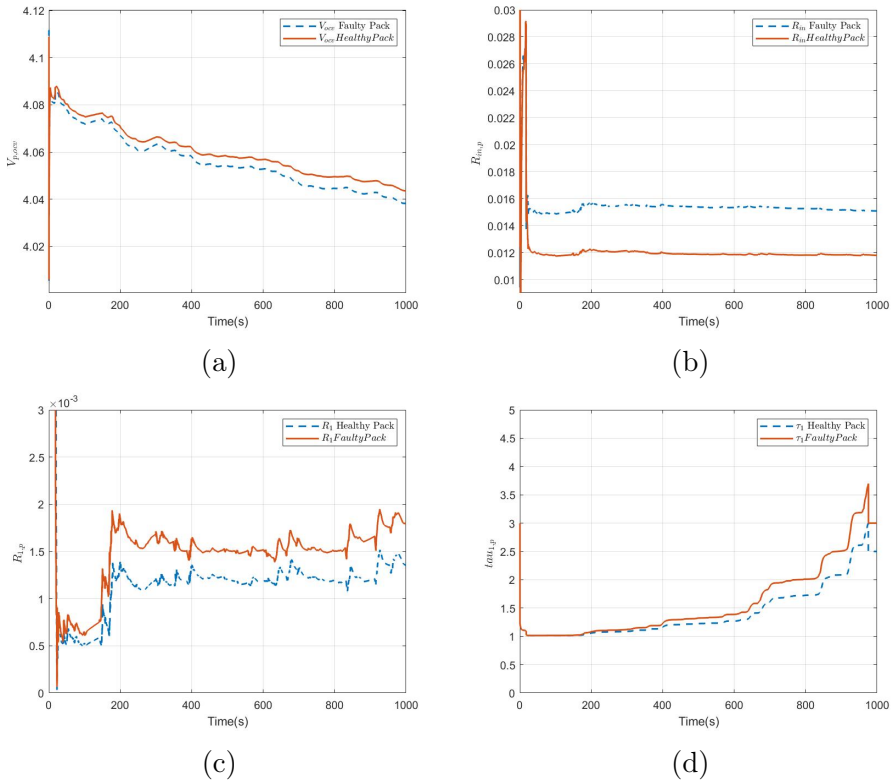

Figure 5.9: Estimated Parameters of the parallel-connected pack, a)$V_{ocv,p}$, b) $R_{in,p}$, c) $R_{1,p}$, d) $C_1 1, p$.

greatly enhanced and the convergence time to the actual value of SoC is also reduced. The estimated voltage sensor bias and the SoC bias using the introduced algorithm are shown in Figure 5.12. Measurement biases are increased for the faulty condition. These estimated values improve the performance of the filter extensively. Estimated measurement biases provided adaptability against uncertainties and changes in the battery module. With the help of the proposed method, loss of SoC accuracy in a BMS can be avoided over time. Table 5.5 summarizes the performance of each filter using the Root Mean Square Error (RMSE) for the healthy and faulty cases. The proposed estimation has the best performance compared to other filters especially

when there is cell variability. The method can easily be implemented on a BMS as no additional measurements are required.

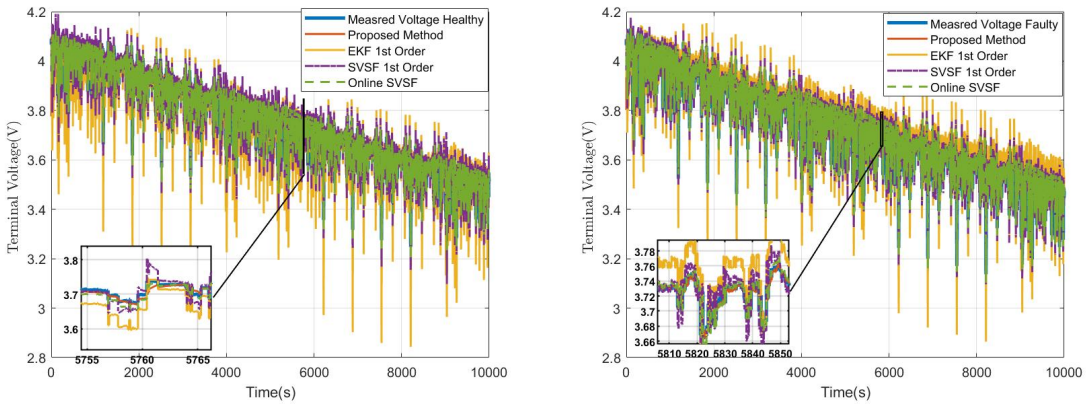

(a) (b)

Figure 5.10: Estimated terminal voltage for a) healthy and b) faulty pack using validation data.

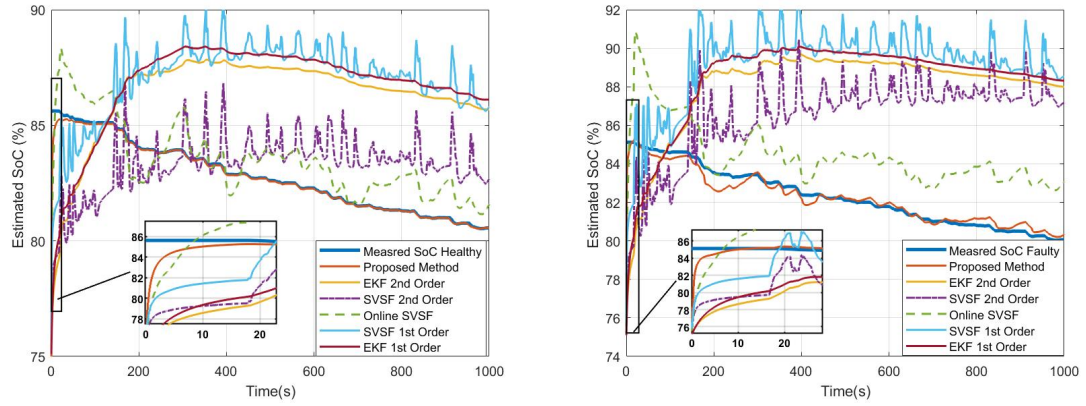

(a) (b)

Figure 5.11: Estimated SoC for a) healthy and b) faulty pack using validation data.

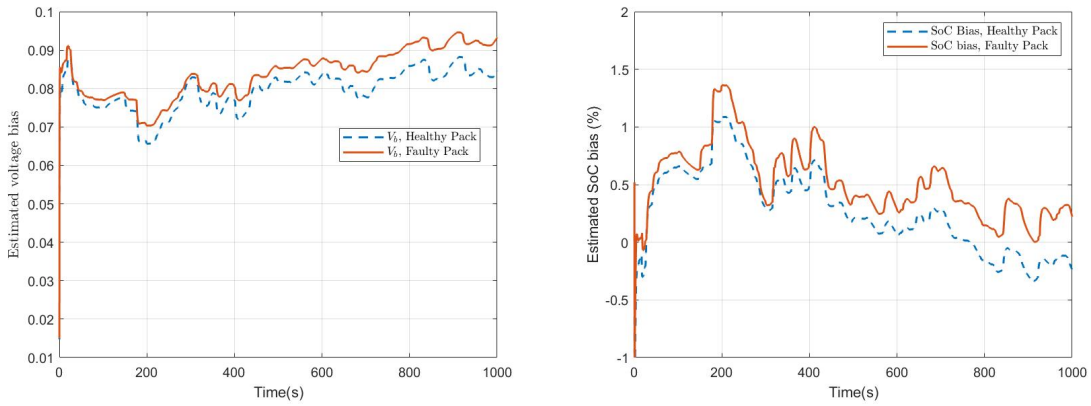

(a) (b)

Figure 5.12: Estimated a) voltage bias, b) SoC bias.

Table 5.5: RMSE for comparison using validation data.

				V_T RMSE		SoC RMSE	
Method	Order of ECM	Parameters Identification	Estimation Level	Healthy	Faulty	Healthy	Faulty
EKF	1	Offline	Cell	0.0443	0.0162	4.9942	7.1041
	2	Offline	Cell	0.0477	0.0328	4.5633	6.2362
SVSF-VBL	1	Offline	Cell	0.0200	0.0102	4.9361	6.5778
	2	Offline	Cell	0.0224	0.0179	2.3662	5.0505
	1	Online	Pack	0.0077	0.0078	1.9354	1.1341
Proposed algorithm	1	Online	Pack	0.0084	0.0090	0.2643	0.6638

5.5 Conclusions

This paper proposes a framework for estimating the SoC, and SoH of a parallel-connected battery pack. A modified first-order ECM model is considered to combine estimation of the SoC, and measurement biases of the SoC and terminal voltage. Using the Recursive Least Square (RLS) with a forgetting factor for online parameter estimation, the parameters of the parallel-connected battery module are tracked and adjusted as the cells age. The estimated internal resistance of the battery module's model is considered as an indicator of its SoH. A robust strategy called the Smooth Variable Structure Filter with Variable Boundary Layer (SVSF-VBL) is then utilized

to estimate the states of the parallel-connected battery cells. The estimated measurement biases are employed to update the measure of SoC obtained by coulomb counting and terminal voltage which lead to a more accurate parameter and SoC estimation. The proposed approach for SoC and SoH estimation is validated with experimental data. Different scenarios are considered to verify the performance of the algorithm. The proposed algorithm reduces the percentage of SoC error significantly compare to previous filters.

Chapter 6: Conclusions

The main findings of this thesis are highlighted in this chapter, and recommendations for future works based on the findings are made.

6.1 Summary of Research

This thesis presents several advances in the field of battery state estimation by developing methods based on the combined use of coulomb counting, Smooth Variable Structure Filter (SVSF), and adaptive filters such as noise adjustment and the Interacting Multiple Model (IMM) concept. Estimating battery State of Charge (SoC), State of Health (SoH), and State of Power (SoP) is critical to Battery Management Systems (BMSs) for Electric Vehicles (EVs). There are numerous methods proposed in the literature, each with its own set of advantages and disadvantages. The main purpose of this thesis is to investigate and develop state estimation techniques by identifying battery dynamic behavior under various operating conditions, as well as to overcome the limitations of existing methods.

In Chapter 2, an online parameter estimation strategy based on the Recursive Least Square (RLS) with a forgetting factor is combined with a robust state estimation strategy based on the SVSF to determine the battery's SoC and terminal voltage. The validation of the proposed strategy revealed that the identified parameters change as SoC and SoH vary. It was demonstrated that online parameter estimation produces more accurate SOC and terminal voltage estimates. Although parameter estimation of a third order model improves the accuracy of state estimation and provides a more

suitable method for BMS, it is computationally intensive. As a result, multiple model strategies should be investigated in order to track changes in dynamic characterization of a battery under various operating conditions. The goal of the technique developed in Chapter 3 is to accomplish this.

Chapter 3 proposes an interacting multiple modeling strategy for estimating a battery's SoC, SoH, and SoP. A proposed third-order ECM model is introduced and used in conjunction with the conventional coulomb counting method. The latter, is commonly used for SoC calculation onboard a BMS due to its simplicity. In this research coulomb counting is treated as an additional measurement for the battery model. This model formulation improves estimation accuracy and enables the estimation of internal resistance, SoC, and SoC bias all at the same time. Chapter 3 further investigates and ensures the model's observability. The observability condition must be met to ensure that system states can be uniquely extracted from measurements. To track and adjust to changes in a battery's characteristics over time, an IMM strategy associated with SVSF with Variable Boundary Layer (SVSF-VBL) is proposed. The estimated SoC bias is used to update the coulomb counting SoC measure, resulting in a more accurate SoC. The proposed technique has the lowest SoC estimation error, which is less than 2% compared to all other published methods.

In addition to multiple model strategies, filter tuning methods such as noise adjustment should be considered in a battery to improve the performance of a BMS. In Chapter 4, an adaptive strategy referred to as the Adaptive SVSF-VBL (ASVSF-VBL) is proposed to estimate the SoC and SoH of a battery. In addition to the SoC and SoH, the state vector was augmented to estimate the bias in current measurement and the battery's internal resistance. Under scenarios involving noise with changing

statistics, the ASVSF-VBL modifies the unknown system and measurement noise covariance matrices to deliver higher performance. The estimation process' stability is still ensured by the adaptation method. The ASVSF-VBL provides an indicator for the battery SoH in addition to its SoC. The proposed methodology is tested on experimental data and performance enhancement is shown. In comparison to the SVSF-VBL and EKF, the proposed ASVSF-VBL reduced the percentage of SoC error to 2%.

For estimating the status of a battery cell, several methods have been presented. These strategies, however, should be expanded to a pack level for use onboard of a BMS. Estimating the states of a battery pack is extremely challenging as cell-to-cell variations must be taken into account. In Chapter 5, different strategies are applied to battery cells connected in parallel where the number of sensors are limited. To estimate the battery SoC, the robust SVSF estimation strategy is used. When compared to the EKF, the technique provides greater robustness and accuracy in the presence of cell-to-cell differences. To improve the performance of state estimation in parallel-connected battery cells, a novel strategy is proposed in Chapter 5 and compared to previous methods. A modified first-order ECM model is considered to combine estimation of the SoC, and measurements bias of the SoC and terminal voltage. The parameters of a parallel-connected battery pack are tracked and adjusted as the cells age using online parameter estimation, which eliminates the need for additional sensors. The terminal voltages and the SoC derived from coulomb counting method can be updated with the estimated biases, thereby providing a more accurate estimate of the state. The estimated voltage bias estimation aims to detect voltage drops caused by aging or cell differences. To validate the algorithm's performance,

various operating scenarios were considered. When compared to previous filters, the proposed algorithm reduces the percentage of SoC error of the parallel-connected battery cells to 2%.

6.2 Future Work Recommendations

There are a number of areas of potential avenues for future research that can improve the performance of a BMS for EVs. This study presented methods for estimating operational states of a battery cell and a battery pack. The methods were validated by using experimental data obtained from tests. The proposed methods are computationally efficient and can be applied in real-time. As a next step, they should be implemented in BMS hardware and operated in real-time.

The IMM-SVSF-VBL can be expanded to a pack level and implemented in a BMS as voltage and current measurements are readily available in a BMS and given that with the proposed method, no additional measurements are needed. The battery's SoH has a slow dynamic and is not required to be estimated continuously if there are constraints associated with the availability of computational resources.

The proposed IMM-SVSF-VBL strategy for estimating a battery's states improves performance across different SoH values. The number of models, however, can be increased to cover a broader range of operation, including different SoH, temperature, and C-rates. More experiments are required to develop models that account for a wide range of functionality which can be an area of research. Furthermore, to ensure the filter's stability, more research is required to develop a switching strategy between these models. Each factor should be evaluated in terms of its impact on the estimation method and its effectiveness in terms of BMS performance.

The proposed strategy for estimating the states of a battery module takes into account parallel-connected cells. Another suggestion for future work is to extend these methods to a pack level with cells connected in parallel and series. As more sensors become available, the number of filters operating in parallel should be increased for series-connected cells.

References

[1] S. Yang, Z. Zhang, R. Cao, M. Wang, H. Cheng, L. Zhang, Y. Jiang, Y. Li, B. Chen, H. Ling, *et al.*, "Implementation for a cloud battery management system based on the chain framework," *Energy and AI*, vol. 5, p. 100088, 2021.

[2] K. W. E. Cheng, B. Divakar, H. Wu, K. Ding, and H. F. Ho, "Battery-management system (bms) and soc development for electrical vehicles," *IEEE transactions on vehicular technology*, vol. 60, no. 1, pp. 76–88, 2010.

[3] M. Hossain Lipu, M. Hannan, T. F. Karim, A. Hussain, M. H. M. Saad, A. Ayob, M. S. Miah, and T. Indra Mahlia, "Intelligent algorithms and control strategies for battery management system in electric vehicles: Progress, challenges and future outlook," *Journal of Cleaner Production*, vol. 292, p. 126044, 2021.

[4] B. Scrosati and J. Garche, "Lithium batteries: Status, prospects and future," *Journal of power sources*, vol. 195, no. 9, pp. 2419–2430, 2010.

[5] A. J. Smiley, *Estimation of battery aging using an interacting multiple model Kalman filter*. University of Colorado at Colorado Springs, 2015.

[6] A. Smith, *A high precision study of li-ion batteries*. PhD thesis, Dalhousie University, 2012.

[7] A. Smith, J. Burns, and J. Dahn, "A high precision study of the coulombic efficiency of li-ion batteries," *Electrochemical and Solid State Letters*, vol. 13, no. 12, p. A177, 2010.

[8] J. Burns, A. Kassam, N. Sinha, L. Downie, L. Solnickova, B. Way, and J. Dahn, "Predicting and extending the lifetime of li-ion batteries," *Journal of the Electrochemical Society*, vol. 160, no. 9, p. A1451, 2013.

[9] R. Hausbrand, G. Cherkashinin, H. Ehrenberg, M. Gröting, K. Albe, C. Hess, and W. Jaegermann, "Fundamental degradation mechanisms of layered oxide li-ion battery cathode materials: Methodology, insights and novel approaches," *Materials Science and Engineering: B*, vol. 192, pp. 3–25, 2015.

[10] A. Wang, S. Kadam, H. Li, S. Shi, and Y. Qi, "Review on modeling of the anode solid electrolyte interphase (sei) for lithium-ion batteries," *npj Computational Materials*, vol. 4, no. 1, pp. 1–26, 2018.

[11] R. Xiong, Y. Pan, W. Shen, H. Li, and F. Sun, "Lithium-ion battery aging mechanisms and diagnosis method for automotive applications: Recent advances and perspectives," *Renewable and Sustainable Energy Reviews*, vol. 131, p. 110048, 2020.

[12] R. Ahmed, *Modeling and state of charge estimation of electric vehicle batteries*. PhD thesis, McMaster University, 2014.

[13] G. Pistoia, *Electric and hybrid vehicles: Power sources, models, sustainability, infrastructure and the market*. Elsevier, 2010.

[14] U. S. A. B. Consortium *et al.*, "Electric vehicle battery test procedures manual," *USABC, Jan*, 1996.

[15] J. Belt, "Battery test manual for plug-in hybrid electric ve," tech. rep., Idaho National Laboratory (INL), 2008.

[16] R. Ahmed, J. Gazzarri, S. Onori, S. Habibi, R. Jackey, K. Rzemien, J. Tjong, and J. LeSage, "Model-based parameter identification of healthy and aged li-ion batteries for electric vehicle applications," *SAE International Journal of Alternative Powertrains*, vol. 4, no. 2, pp. 233–247, 2015.

[17] M. Conte, F. V. Conte, I. D. Bloom, K. Morita, T. Ikeya, and J. R. Belt, "Ageing testing procedures on lithium batteries in an international collaboration context," *World Electric Vehicle Journal*, vol. 4, no. 2, pp. 335–346, 2010.

[18] D. D. Schedules, "U.s. environmental protection agency (epa)."

[19] Y. Zheng, M. Ouyang, X. Han, L. Lu, and J. Li, "Investigating the error sources of the online state of charge estimation methods for lithium-ion batteries in electric vehicles," *Journal of Power Sources*, vol. 377, pp. 161–188, 2018.

[20] R. Yang, R. Xiong, W. Shen, and X. Lin, "Extreme learning machine-based thermal model for lithium-ion batteries of electric vehicles under external short circuit," *Engineering*, vol. 7, no. 3, pp. 395–405, 2021.

[21] E. Chemali, P. J. Kollmeyer, M. Preindl, and A. Emadi, "State-of-charge estimation of li-ion batteries using deep neural networks: A machine learning approach," *Journal of Power Sources*, vol. 400, pp. 242–255, 2018.

[22] M. Berecibar, I. Gandiaga, I. Villarreal, N. Omar, J. Van Mierlo, and P. Van den Bossche, "Critical review of state of health estimation methods of li-ion batteries for real applications," *Renewable and Sustainable Energy Reviews*, vol. 56, pp. 572–587, 2016.

[23] S. E. Samadani, R. A. Fraser, and M. Fowler, "A review study of methods for lithium-ion battery health monitoring and remaining life estimation in hybrid electric vehicles," tech. rep., SAE Technical Paper, 2012.

[24] X. Liu, C. Zheng, J. Wu, J. Meng, D.-I. Stroe, and J. Chen, "An improved state of charge and state of power estimation method based on genetic particle filter for lithium-ion batteries," *Energies*, vol. 13, no. 2, p. 478, 2020.

[25] F. Sun, R. Xiong, and H. He, "Estimation of state-of-charge and state-of-power capability of lithium-ion battery considering varying health conditions," *Journal of Power Sources*, vol. 259, pp. 166–176, 2014.

[26] J. Meng, G. Luo, M. Ricco, M. Swierczynski, D.-I. Stroe, and R. Teodorescu, "Overview of lithium-ion battery modeling methods for state-of-charge estimation in electrical vehicles," *Applied sciences*, vol. 8, no. 5, p. 659, 2018.

[27] M. Farag, *Lithium-Ion Batteries: Modelling and State of Charge Estimation*. PhD thesis, McMaster University, 2013.

[28] R. Ahmed, M. E. Sayed, I. Arasaratnam, J. Tjong, and S. Habibi, "Reduced-order electrochemical model parameters identification and soc estimation for healthy and aged li-ion batteries part i: Parameterization model development for healthy batteries," *IEEE Journal of Emerging and Selected Topics in Power Electronics*, vol. 2, no. 3, pp. 659–677, 2014.

[29] R. Ahmed, M. El Sayed, I. Arasaratnam, J. Tjong, and S. Habibi, "Reduced-order electrochemical model parameters identification and state of charge estimation for healthy and aged li-ion batteries—part ii: Aged battery model and

state of charge estimation," *IEEE Journal of Emerging and Selected Topics in Power Electronics*, vol. 2, no. 3, pp. 678–690, 2014.

[30] A. A.-H. Hussein and I. Batarseh, "An overview of generic battery models," in *2011 IEEE Power and Energy Society General Meeting*, pp. 1–6, IEEE, 2011.

[31] B. Pattipati, C. Sankavaram, and K. Pattipati, "System identification and estimation framework for pivotal automotive battery management system characteristics," *IEEE Transactions on Systems, Man, and Cybernetics, Part C (Applications and Reviews)*, vol. 41, no. 6, pp. 869–884, 2011.

[32] S. Barcellona and L. Piegari, "Lithium ion battery models and parameter identification techniques," *Energies*, vol. 10, no. 12, p. 2007, 2017.

[33] L. De Sutter, Y. Firouz, J. De Hoog, N. Omar, and J. Van Mierlo, "Battery aging assessment and parametric study of lithium-ion batteries by means of a fractional differential model," *Electrochimica Acta*, vol. 305, pp. 24–36, 2019.

[34] Z. Cui, N. Cui, C. Wang, C. Li, and C. Zhang, "A robust online parameter identification method for lithium-ion battery model under asynchronous sampling and noise interference," *IEEE Transactions on Industrial Electronics*, vol. 68, no. 10, pp. 9550–9560, 2020.

[35] Z. Lao, B. Xia, W. Wang, W. Sun, Y. Lai, and M. Wang, "A novel method for lithium-ion battery online parameter identification based on variable forgetting factor recursive least squares," *Energies*, vol. 11, no. 6, p. 1358, 2018.

[36] M. Moonen and J. Vandewalle, "A square root covariance algorithm for constrained recursive least squares estimation," *Journal of VLSI signal processing systems for signal, image and video technology*, vol. 3, no. 3, pp. 163–172, 1991.

[37] M. A. Al-Shabi, *The general toeplitz/observability smooth variable structure filter*. PhD thesis, McMaster University, 2011.

[38] S. S. Haykin, B. Widrow, and B. Widrow, *Least-mean-square adaptive filters*, vol. 31. Wiley Online Library, 2003.

[39] Y. Bar-Shalom, *Estimation with application to tracking and navigation*. John Wiley and Sons, 2001.

[40] A. Gelb, *Applied optimal estimation*. MIT press, 1974.

[41] B. Ristic, S. Arulampalam, and N. Gordon, *Beyond the Kalman filter: Particle filters for tracking applications*. Artech house, 2003.

[42] M. Grewal and A. Andrews, "Kalman filtering: Theory and practice using matlab, wiley," 2001.

[43] H. H. Afshari, S. A. Gadsden, and S. Habibi, "Gaussian filters for parameter and state estimation: A general review of theory and recent trends," *Signal Processing*, vol. 135, pp. 218–238, 2017.

[44] R. E. Kalman and R. S. Bucy, "New results in linear filtering and prediction theory," *Journal of fluid engineering*, 1961.

[45] R. E. Kalman, "A new approach to linear filtering and prediction problems," *Journal of Basic Engineering*, vol. 82, no. 1, pp. 35–45, 1960.

[46] I. Arasaratnam, *Cubature Kalman filtering theory & applications*. PhD thesis, McMAster University, 2009.

[47] S. NAJAR, M. N. ABDELKRIM, M. ABDELHAMID, and A. Mohamed, "Discrete fractional kalman filter," *IFAC Proceedings Volumes*, vol. 42, no. 19, pp. 520–525, 2009.

[48] D. Sierociuk and A. Dzieliński, "Fractional kalman filter algorithm for the states, parameters and order of fractional system estimation," *International Journal of Applied Mathematics and Computer Science*, vol. 16, pp. 129–140, 2006.

[49] V. Utkin, J. Guldner, and J. Shi, *Sliding mode control in electro-mechanical systems*. CRC press, 2017.

[50] S. Qaiser, A. Bhatti, R. Samar, M. Iqbal, and J. Qadir, "Higher order sliding mode observer based estimation of precursor concentration in a research reactor," in *2008 4th International Conference on Emerging Technologies*, pp. 338–343, IEEE, 2008.

[51] S. Habibi and R. Burton, "The variable structure filter," *Journal of dynamic systems, measurement, and control*, vol. 125, no. 3, pp. 287–293, 2003.

[52] M. Avzayesh, M. Abdel-Hafez, M. AlShabi, and S. A. Gadsden, "The smooth variable structure filter: A comprehensive review," *Digital Signal Processing*, vol. 110, p. 102912, 2021.

[53] S. Habibi, "The extended variable structure filter," *Journal of dynamic systems, measurement, and control*, vol. 128, no. 2, pp. 341–351, 2006.

[54] S. Habibi, "The smooth variable structure filter," *Proceedings of the IEEE*, vol. 95, no. 5, pp. 1026–1059, 2007.

[55] S. A. Gadsden and S. R. Habibi, "A new form of the smooth variable structure filter with a covariance derivation," in *49th IEEE Conference on Decision and Control (CDC)*, pp. 7389–7394, IEEE, 2010.

[56] S. A. Gadsden and H. H. Afshari, "A review of smooth variable structure filters: recent advances in theory and applications," in *ASME International Mechanical Engineering Congress and Exposition*, vol. Volume 4A: Dynamics, Vibration, and Control, pp. IMECE2015–50966, American Society of Mechanical Engineers, 2015.

[57] S. Gadsden and S. Habibi, "A new robust filtering strategy for linear systems," *Journal of Dynamic Systems, Measurement, and Control*, vol. 135, no. 1, 2013.

[58] M. Attari, *SVSF Estimation for Target Tracking with Measurement Origin Uncertainty*. PhD thesis, McMaster University, 2016.

[59] S. A. Gadsden, *Smooth variable structure filtering: theory and applications*. PhD thesis, McMaster University, 2011.

[60] S. S. Haykin, *Kalman filtering and neural networks*. Wiley Online Library, 2001.

[61] X. Yang, K. Xing, K. Shi, and Q. Pan, "Joint state and parameter estimation in particle filtering and stochastic optimization," *Journal of Control Theory and Applications*, vol. 6, no. 2, pp. 215–220, 2008.

[62] G. L. Plett, "Dual and joint ekf for simultaneous soc and soh estimation," in

Proceedings of the 21st Electric Vehicle Symposium (EVS21), Monaco, pp. 1–12, 2005.

[63] J. Duník, O. Straka, O. Kost, and J. Havlík, "Noise covariance matrices in state-space models: A survey and comparison of estimation methods—part i," *International Journal of Adaptive Control and Signal Processing*, vol. 31, no. 11, pp. 1505–1543, 2017.

[64] R. Mehra, "Approaches to adaptive filtering," *IEEE Transactions on automatic control*, vol. 17, no. 5, pp. 693–698, 1972.

[65] M. Vidyasagar, *Nonlinear systems analysis*. SIAM, 2002.

[66] A. F. Villaverde, N. Tsiantis, and J. R. Banga, "Full observability and estimation of unknown inputs, states and parameters of nonlinear biological models," *Journal of the Royal Society Interface*, vol. 16, no. 156, p. 20190043, 2019.

[67] G. L. Plett, "Extended kalman filtering for battery management systems of lipb-based hev battery packs: Part 1. background," *Journal of Power Sources*, vol. 134, no. 2, pp. 252–261, 2004.

[68] M. Partovibakhsh and G. Liu, "An adaptive unscented kalman filtering approach for online estimation of model parameters and state-of-charge of lithium-ion batteries for autonomous mobile robots," *IEEE Transactions on Control Systems Technology*, vol. 23, no. 1, pp. 357–363, 2014.

[69] F. Sun, X. Hu, Y. Zou, and S. Li, "Adaptive unscented kalman filtering for state of charge estimation of a lithium-ion battery for electric vehicles," *Energy*, vol. 36, no. 5, pp. 3531–3540, 2011.

[70] S. Gadsden, M. Al-Shabi, and S. Habibi, "Estimation strategies for the condition monitoring of a battery system in a hybrid electric vehicle," *International Scholarly Research Notices*, vol. 2011, 2011.

[71] M. S. Farag, R. Ahmed, S. Gadsden, S. Habibi, and J. Tjong, "A comparative study of li-ion battery models and nonlinear dual estimation strategies," in *2012 IEEE Transportation electrification conference and expo (ITEC)*, pp. 1–8, IEEE, 2012.

[72] H. Rahimi-Eichi, F. Baronti, and M.-Y. Chow, "Modeling and online parameter identification of li-polymer battery cells for soc estimation," in *2012 IEEE International Symposium on Industrial Electronics*, pp. 1336–1341, IEEE, 2012.

[73] P. Kumar and P. Bauer, "Parameter extraction of battery models using multi-objective optimization genetic algorithms," in *Proceedings of 14th International Power Electronics and Motion Control Conference EPE-PEMC 2010*, pp. T9–106, IEEE, 2010.

[74] G. Dong, Z. Chen, J. Wei, C. Zhang, and P. Wang, "An online model-based method for state of energy estimation of lithium-ion batteries using dual filters," *Journal of Power Sources*, vol. 301, pp. 277–286, 2016.

[75] B. Xia, Z. Lao, R. Zhang, Y. Tian, G. Chen, Z. Sun, W. Wang, W. Sun, Y. Lai, M. Wang, *et al.*, "Online parameter identification and state of charge estimation of lithium-ion batteries based on forgetting factor recursive least squares and nonlinear kalman filter," *Energies*, vol. 11, no. 1, p. 3, 2018.

[76] B. Xia, R. Huang, Z. Lao, R. Zhang, Y. Lai, W. Zheng, H. Wang, W. Wang,

and M. Wang, "Online parameter identification of lithium-ion batteries using a novel multiple forgetting factor recursive least square algorithm," *Energies*, vol. 11, no. 11, p. 3180, 2018.

[77] R. Ahmed, S. Rahimifard, and S. Habibi, "Offline parameter identification and soc estimation for new and aged electric vehicles batteries," in *2019 IEEE Transportation Electrification Conference and Expo (ITEC)*, pp. 1–6, IEEE, 2019.

[78] Z. M. Salameh, M. A. Casacca, and W. A. Lynch, "A mathematical model for lead-acid batteries," *IEEE Transactions on Energy Conversion*, vol. 7, no. 1, pp. 93–98, 1992.

[79] X. Hu, S. Li, and H. Peng, "A comparative study of equivalent circuit models for li-ion batteries," *Journal of Power Sources*, vol. 198, pp. 359–367, 2012.

[80] M. Verbrugge and E. Tate, "Adaptive state of charge algorithm for nickel metal hydride batteries including hysteresis phenomena," *Journal of Power Sources*, vol. 126, no. 1-2, pp. 236–249, 2004.

[81] H. Rahimi-Eichi, U. Ojha, F. Baronti, and M.-Y. Chow, "Battery management system: An overview of its application in the smart grid and electric vehicles," *IEEE Industrial Electronics Magazine*, vol. 7, no. 2, pp. 4–16, 2013.

[82] L. Zhang, X. Hu, Z. Wang, J. Ruan, C. Ma, Z. Song, D. G. Dorrell, and M. G. Pecht, "Hybrid electrochemical energy storage systems: An overview for smart grid and electrified vehicle applications," *Renewable and Sustainable Energy Reviews*, p. 110581, 2020.

[83] S. Piller, M. Perrin, and A. Jossen, "Methods for state-of-charge determination and their applications," *Journal of power sources*, vol. 96, no. 1, pp. 113–120, 2001.

[84] I. Baccouche, S. Jemmali, A. Mlayah, B. Manai, and N. E. B. Amara, "Implementation of an improved coulomb-counting algorithm based on a piecewise soc-ocv relationship for soc estimation of li-ionbattery," *arXiv preprint arXiv:1803.10654*, 2018.

[85] L. Zhao, M. Lin, and Y. Chen, "Least-squares based coulomb counting method and its application for state-of-charge (soc) estimation in electric vehicles," *International Journal of Energy Research*, vol. 40, no. 10, pp. 1389–1399, 2016.

[86] J. Xie, J. Ma, and K. Bai, "Enhanced coulomb counting method for state-of-charge estimation of lithium-ion batteries based on peukert's law and coulombic efficiency," *Journal of Power Electronics*, vol. 18, no. 3, pp. 910–922, 2018.

[87] K. S. Ng, C.-S. Moo, Y.-P. Chen, and Y.-C. Hsieh, "Enhanced coulomb counting method for estimating state-of-charge and state-of-health of lithium-ion batteries," *Applied energy*, vol. 86, no. 9, pp. 1506–1511, 2009.

[88] J.-C. Wu, J.-Y. Chuang, W.-Y. Horng, and J. Wang, "Method and apparatus for calibrating coulomb counting based state-of-charge estimation," June 2 2020. US Patent 10,670,662.

[89] X. Lin, "Theoretical analysis of battery soc estimation errors under sensor bias and variance," *IEEE Transactions on Industrial Electronics*, vol. 65, no. 9, pp. 7138–7148, 2018.

[90] M. Messing, T. Shoa, R. Ahmed, and S. Habibi, "Battery soc estimation from eis using neural nets," in *2020 IEEE Transportation Electrification Conference & Expo (ITEC)*, pp. 588–593, IEEE, 2020.

[91] S. Zhao, S. R. Duncan, and D. A. Howey, "Observability analysis and state estimation of lithium-ion batteries in the presence of sensor biases," *IEEE Transactions on Control Systems Technology*, vol. 25, no. 1, pp. 326–333, 2016.

[92] G. L. Plett, "Extended kalman filtering for battery management systems of lipb-based hev battery packs: Part 2. modeling and identification," *Journal of power sources*, vol. 134, no. 2, pp. 262–276, 2004.

[93] A. Smiley and G. L. Plett, "An adaptive physics-based reduced-order model of an aged lithium-ion cell, selected using an interacting multiple-model kalman filter," *Journal of Energy Storage*, vol. 19, pp. 120–134, 2018.

[94] A. J. Smiley, W. K. Harrison, and G. L. Plett, "Postprocessing the outputs of an interacting multiple-model kalman filter using a markovian trellis to estimate parameter values of aged li-ion cells," *Journal of Energy Storage*, vol. 27, p. 101043, 2020.

[95] G. L. Plett, "Extended kalman filtering for battery management systems of lipb-based hev battery packs: Part 3. state and parameter estimation," *Journal of Power sources*, vol. 134, no. 2, pp. 277–292, 2004.

[96] G. L. Plett, "Sigma-point kalman filtering for battery management systems of lipb-based hev battery packs: Part 2: Simultaneous state and parameter estimation," *Journal of power sources*, vol. 161, no. 2, pp. 1369–1384, 2006.

[97] S. Sattarzadeh, S. Dey, A. Colclasure, and K. Smith, "Addressing the observability problem in batteries: Algorithm design for electrode-level charge and health estimation," in *2020 American Control Conference (ACC)*, pp. 1131–1136, IEEE, 2020.

[98] Y. He, X. Liu, C. Zhang, and Z. Chen, "A new model for state-of-charge (soc) estimation for high-power li-ion batteries," *Applied Energy*, vol. 101, pp. 808–814, 2013.

[99] S. Gadsden, D. Dunne, S. Habibi, and T. Kirubarajan, "Comparison of extended and unscented kalman, particle, and smooth variable structure filters on a bearing-only target tracking problem," in *Signal and Data Processing of Small Targets 2009*, vol. 7445, p. 74450B, International Society for Optics and Photonics, 2009.

[100] Y. Bar-Shalom, X. R. Li, and T. Kirubarajan, *Estimation with applications to tracking and navigation: theory algorithms and software*. John Wiley & Sons, 2004.

[101] H. A. Blom and Y. Bar-Shalom, "The interacting multiple model algorithm for systems with markovian switching coefficients," *IEEE transactions on Automatic Control*, vol. 33, no. 8, pp. 780–783, 1988.

[102] H. A. Blom, "An efficient filter for abruptly changing systems," in *The 23rd IEEE Conference on Decision and Control*, pp. 656–658, IEEE, 1984.

[103] S. A. Gadsden, S. R. Habibi, and T. Kirubarajan, "A novel interacting multiple

model method for nonlinear target tracking," in *2010 13th International Conference on Information Fusion*, pp. 1–8, IEEE, 2010.

[104] S. Nejad, D. Gladwin, and D. Stone, "A systematic review of lumped-parameter equivalent circuit models for real-time estimation of lithium-ion battery states," *Journal of Power Sources*, vol. 316, pp. 183–196, 2016.

[105] S. Rahimifard, S. Habibi, and J. Tjong, "Dual estimation strategy for new and aged electric vehicles batteries," in *2020 IEEE Transportation Electrification Conference & Expo (ITEC)*, pp. 579–583, IEEE, 2020.

[106] A. Guha and A. Patra, "State of health estimation of lithium-ion batteries using capacity fade and internal resistance growth models," *IEEE Transactions on Transportation Electrification*, vol. 4, no. 1, pp. 135–146, 2017.

[107] S. A. Gadsden, S. Habibi, and T. Kirubarajan, "Kalman and smooth variable structure filters for robust estimation," *IEEE Transactions on Aerospace and Electronic Systems*, vol. 50, no. 2, pp. 1038–1050, 2014.

[108] S. A. Gadsden, M. El Sayed, and S. R. Habibi, "Derivation of an optimal boundary layer width for the smooth variable structure filter," in *Proceedings of the 2011 American Control Conference*, pp. 4922–4927, IEEE, 2011.

[109] S. B. Sarmah, P. Kalita, A. Garg, X.-d. Niu, X.-W. Zhang, X. Peng, and D. Bhattacharjee, "A review of state of health estimation of energy storage systems: challenges and possible solutions for futuristic applications of li-ion battery packs in electric vehicles," *Journal of Electrochemical Energy Conversion and Storage*, vol. 16, no. 4, 2019.

[110] P. Shen, M. Ouyang, L. Lu, J. Li, and X. Feng, "The co-estimation of state of charge, state of health, and state of function for lithium-ion batteries in electric vehicles," *IEEE Transactions on vehicular technology*, vol. 67, no. 1, pp. 92–103, 2017.

[111] X. Zhang, Y. Wang, J. Wu, and Z. Chen, "A novel method for lithium-ion battery state of energy and state of power estimation based on multi-time-scale filter," *Applied energy*, vol. 216, pp. 442–451, 2018.

[112] Y. Wang, J. Tian, Z. Sun, L. Wang, R. Xu, M. Li, and Z. Chen, "A comprehensive review of battery modeling and state estimation approaches for advanced battery management systems," *Renewable and Sustainable Energy Reviews*, vol. 131, p. 110015, 2020.

[113] S. Park, J. Ahn, T. Kang, S. Park, Y. Kim, I. Cho, and J. Kim, "Review of state-of-the-art battery state estimation technologies for battery management systems of stationary energy storage systems," *Journal of Power Electronics*, pp. 1–15, 2020.

[114] K. Movassagh, A. Raihan, B. Balasingam, and K. Pattipati, "A critical look at coulomb counting approach for state of charge estimation in batteries," *Energies*, vol. 14, no. 14, p. 4074, 2021.

[115] Z. Wei, J. Zhao, H. He, G. Ding, H. Cui, and L. Liu, "Future smart battery and management: Advanced sensing from external to embedded multi-dimensional measurement," *Journal of Power Sources*, vol. 489, p. 229462, 2021.

[116] W. Waag, C. Fleischer, and D. U. Sauer, "Critical review of the methods for

monitoring of lithium-ion batteries in electric and hybrid vehicles," *Journal of Power Sources*, vol. 258, pp. 321–339, 2014.

[117] X. Lin, H. E. Perez, J. B. Siegel, and A. G. Stefanopoulou, "Robust estimation of battery system temperature distribution under sparse sensing and uncertainty," *IEEE Transactions on Control Systems Technology*, vol. 28, no. 3, pp. 753–765, 2019.

[118] Z. Wei, J. Zhao, R. Xiong, G. Dong, J. Pou, and K. J. Tseng, "Online estimation of power capacity with noise effect attenuation for lithium-ion battery," *IEEE Transactions on Industrial Electronics*, vol. 66, no. 7, pp. 5724–5735, 2018.

[119] S. Rahimifard, R. Ahmed, and S. Habibi, "Interacting multiple model strategy for electric vehicle batteries state of charge/health/ power estimation," *IEEE Access*, vol. 9, pp. 109875–109888, 2021.

[120] M. Messing, S. Rahimifard, T. Shoa, and S. Habibi, "Low temperature, current dependent battery state estimation using interacting multiple model strategy," *IEEE Access*, vol. 9, pp. 99876–99889, 2021.

[121] M. Farag, M. Fleckenstein, and S. Habibi, "Continuous piecewise-linear, reduced-order electrochemical model for lithium-ion batteries in real-time applications," *Journal of Power Sources*, vol. 342, pp. 351–362, 2017.

[122] I. Arasaratnam and S. Haykin, "Cubature kalman filters," *IEEE Transactions on automatic control*, vol. 54, no. 6, pp. 1254–1269, 2009.

[123] W. Wang, D. Wang, X. Wang, T. Li, R. Ahmed, S. Habibi, and A. Emadi, "Comparison of kalman filter-based state of charge estimation strategies for

li-ion batteries," in *2016 IEEE Transportation Electrification Conference and Expo (ITEC)*, pp. 1–6, IEEE, 2016.

[124] S. A. Gadsden and A. S. Lee, "Advances of the smooth variable structure filter: square-root and two-pass formulations," *Journal of Applied Remote Sensing*, vol. 11, no. 1, p. 015018, 2017.

[125] H. H. Afshari, S. A. Gadsden, and S. Habibi, "A nonlinear second-order filtering strategy for state estimation of uncertain systems," *Signal Processing*, vol. 155, pp. 182–192, 2019.

[126] Q. Zhang, Y. Yang, Q. Xiang, Q. He, Z. Zhou, and Y. Yao, "Noise adaptive kalman filter for joint polarization tracking and channel equalization using cascaded covariance matching," *IEEE Photonics Journal*, vol. 10, no. 1, pp. 1–11, 2018.

[127] A. Mohamed and K. Schwarz, "Adaptive kalman filtering for ins/gps," *Journal of geodesy*, vol. 73, no. 4, pp. 193–203, 1999.

[128] S. Akhlaghi, N. Zhou, and Z. Huang, "Adaptive adjustment of noise covariance in kalman filter for dynamic state estimation," in *2017 IEEE power & energy society general meeting*, pp. 1–5, IEEE, 2017.

[129] M. Song, R. Astroza, H. Ebrahimian, B. Moaveni, and C. Papadimitriou, "Adaptive kalman filters for nonlinear finite element model updating," *Mechanical Systems and Signal Processing*, vol. 143, p. 106837, 2020.

[130] L. Zhang, D. Sidoti, A. Bienkowski, K. R. Pattipati, Y. Bar-Shalom, and D. L.

Kleinman, "On the identification of noise covariances and adaptive kalman filtering: A new look at a 50 year-old problem," *IEEE Access*, vol. 8, pp. 59362–59388, 2020.

[131] W. Ding, J. Wang, C. Rizos, and D. Kinlyside, "Improving adaptive kalman estimation in gps/ins integration," *The Journal of Navigation*, vol. 60, no. 3, p. 517, 2007.

[132] L. Chen, Z. Lü, W. Lin, J. Li, and H. Pan, "A new state-of-health estimation method for lithium-ion batteries through the intrinsic relationship between ohmic internal resistance and capacity," *Measurement*, vol. 116, pp. 586–595, 2018.

[133] Z. B. Omariba, L. Zhang, and D. Sun, "Review of battery cell balancing methodologies for optimizing battery pack performance in electric vehicles," *IEEE Access*, vol. 7, pp. 129335–129352, 2019.

[134] C.-S. Huang, Z. Cheng, and M.-Y. Chow, "A robust and efficient state-of-charge estimation methodology for serial-connected battery packs: Most significant cell methodology," *IEEE Access*, vol. 9, pp. 74360–74369, 2021.

[135] M. Naguib, P. Kollmeyer, and A. Emadi, "Lithium-ion battery pack robust state of charge estimation, cell inconsistency, and balancing," *IEEE Access*, vol. 9, pp. 50570–50582, 2021.

[136] K. Rumpf, M. Naumann, and A. Jossen, "Experimental investigation of parametric cell-to-cell variation and correlation based on 1100 commercial lithium-ion cells," *Journal of Energy Storage*, vol. 14, pp. 224–243, 2017.

[137] C. Zhang, Y. Jiang, J. Jiang, G. Cheng, W. Diao, and W. Zhang, "Study on battery pack consistency evolutions and equilibrium diagnosis for serial-connected lithium-ion batteries," *Applied Energy*, vol. 207, pp. 510–519, 2017. Transformative Innovations for a Sustainable Future – Part II.

[138] Y.-X. Wang, H. Zhong, J. Li, and W. Zhang, "Adaptive estimation-based hierarchical model predictive control methodology for battery active equalization topologies: Part i–balancing strategy," *Journal of Energy Storage*, vol. 45, p. 103235, 2022.

[139] W. Diao, M. Pecht, and T. Liu, "Management of imbalances in parallel-connected lithium-ion battery packs," *Journal of Energy Storage*, vol. 24, p. 100781, 2019.

[140] W. C. Lee, D. Drury, and P. Mellor, "Comparison of passive cell balancing and active cell balancing for automotive batteries," in *2011 IEEE Vehicle Power and Propulsion Conference*, pp. 1–7, IEEE, 2011.

[141] S. Hemavathi, "Overview of cell balancing methods for li-ion battery technology," *Energy storage*, vol. 3, no. 2, p. e203, 2021.

[142] X. Gong, R. Xiong, and C. C. Mi, "Study of the characteristics of battery packs in electric vehicles with parallel-connected lithium-ion battery cells," *IEEE Transactions on Industry Applications*, vol. 51, no. 2, pp. 1872–1879, 2014.

[143] X. Fan, W. Zhang, Z. Wang, F. An, H. Li, and J. Jiang, "Simplified battery pack modeling considering inconsistency and evolution of current distribution," *IEEE*

Transactions on Intelligent Transportation Systems, vol. 22, no. 1, pp. 630–639, 2020.

[144] S. Rahimifard, S. Habibi, G. Goward, and J. Tjong, "Adaptive smooth variable structure filter strategy for state estimation of electric vehicle batteries," *Energies*, vol. 14, no. 24, 2021.

[145] S. Sepasi, L. R. Roose, and M. M. Matsuura, "Extended kalman filter with a fuzzy method for accurate battery pack state of charge estimation," *Energies*, vol. 8, no. 6, pp. 5217–5233, 2015.

[146] X. Hu, F. Sun, and Y. Zou, "Estimation of state of charge of a lithium-ion battery pack for electric vehicles using an adaptive luenberger observer," *Energies*, vol. 3, no. 9, pp. 1586–1603, 2010.

[147] Y. Hua, A. Cordoba-Arenas, N. Warner, and G. Rizzoni, "A multi time-scale state-of-charge and state-of-health estimation framework using nonlinear predictive filter for lithium-ion battery pack with passive balance control," *Journal of Power Sources*, vol. 280, pp. 293–312, 2015.

[148] F. Sun and R. Xiong, "A novel dual-scale cell state-of-charge estimation approach for series-connected battery pack used in electric vehicles," *Journal of Power Sources*, vol. 274, pp. 582–594, 2015.

[149] S.-L. Wang, C. Fernandez, C.-Y. Zou, C.-M. Yu, L. Chen, and L. Zhang, "A comprehensive working state monitoring method for power battery packs considering state of balance and aging correction," *Energy*, vol. 171, pp. 444–455, 2019.

[150] X. Chen, H. Lei, and R. Xiong, "A bias correction based state-of-charge estimation method for multi-cell battery pack under different working conditions," *IEEE Access*, vol. 6, pp. 78184–78192, 2018.

[151] F. Sun, R. Xiong, and H. He, "A systematic state-of-charge estimation framework for multi-cell battery pack in electric vehicles using bias correction technique," *Applied Energy*, vol. 162, pp. 1399–1409, 2016.

[152] T. R. Jow, S. A. Delp, J. L. Allen, J.-P. Jones, and M. C. Smart, "Factors limiting li+ charge transfer kinetics in li-ion batteries," *Journal of the electrochemical society*, vol. 165, no. 2, p. A361, 2018.

[153] S. Habibi and R. Burton, "Parameter identification for a high-performance hydrostatic actuation system using the variable structure filter concept," *Journal of Dynamic Systems, Measurement, and Control*, vol. 129, no. 2, pp. 229–235, 2007.